Development of a fluorescent quantum dot-mycolic acid probe for use in *Mycobacterium tuberculosis* antibody detection

By

Kapambwe Peter Kabwe

Submitted in partial fulfilment of the requirements for the

degree

Doctor of Philosophy in Chemistry

In the Faculty of Natural & Agricultural Sciences

University of Pretoria

Supervisor: Prof. Patricia B.C. Forbes

Co-supervisors: Prof. Lynne A. Pilcher

Dr. Yolandy Lemmer

18 February 2022

Declaration

I, **Kapambwe Peter Kabwe**, declare that this thesis, which I hereby submit for the degree Doctor of Philosophy in Chemistry at the University of Pretoria, is my own work and has not previously been submitted by me for a degree at this or any other tertiary institution.

Signature: ----------

Date: 18 February 2022

Acknowledgements

I would like to acknowledge the efforts and support from all the people who contributed to the completion of this research project at this prestigious university.

Particularly, I give my heartfelt appreciation to my supervisor; Professor Patricia Forbes, and co-supervisors; Professor Lynne Pilcher and Dr Yolandy Lemmer for their excellent supervision, guidance, encouragement, criticism, and the confidence they built in me. Their major roles from the start up to the end of the research project will be always appreciated. May the Almighty God continue guiding them with more blessings in this wonderful career.

My special thanks go to my entire family for the love, care, and encouragement they gave me whilst doing my research. I am deeply grateful to you all. May the Almighty God prolong your lives.

I am grateful to all my lab mates, office mates, and friends for their help and support. More thanks go to Dr Sifiso Nsibande for his comments and guidance and Alma Truyts from the Next Generation Health Unit at CSIR for assisting with the lateral flow and detection experiments.

Lastly, I would like to outstretch my sincere gratitude to the TWAS-NRF doctoral scholarship and the University of Pretoria postgraduate bursary for financial assistance. Added to the list is Copperbelt University, my employer, for allowing me to further my education.

Abstract

Tuberculosis (TB) is a highly contagious chronic pulmonary disease caused by *Mycobacterium tuberculosis* (M.tb). Early detection of this deadly disease using a simple and effective method at the point of care is not yet available, and this poses a serious challenge, especially in developing countries, because the start of treatment could be delayed allowing the disease to spread. Therefore, rapid, inexpensive, and accurate methods for early detection and diagnosis of TB are required.

In this work, therefore, quantum dots (QDs) were coupled to mycolic acids (MAs) to investigate their potential to serve as water-soluble fluorescent tuberculosis (TB) biosensors (probes). MAs are found in the cell wall of *Mycobacterium tuberculosis*. They are lipids that are antigenic, interacting well with anti-MA antibodies, and are soluble only in chloroform and hexane. QDs are nanomaterials with attractive optical properties such as high fluorescence, good biocompatibility, and good water solubility.

Water-soluble core/shell cadmium selenide/zinc sulphide quantum dots capped with L-cysteine (L-cys-CdSe/ZnS QDs) and amine functionalised graphene quantum dots (GQDs) were synthesized and covalently coupled (linked) to chloroform-soluble MAs via amide linkages to form water-soluble fluorescent probes: mycolic acid-cadmium selenide/zinc sulphide quantum dots (MA-CdSe/ZnS QDs) and mycolic acid-graphene quantum dots (MA-GQDs), respectively. The successful synthesis of these water-soluble fluorescent probes was confirmed by a series of spectroscopic methods including: electronic absorption spectroscopy (UV-Vis), fluorescence spectrophotometry, transmission electron microscopy (TEM), powder X-ray diffraction (XRD) spectroscopy, and Fourier-transform infrared (FT-IR) spectroscopy.

Visual lateral flow of the coupled fluorescent probes was achieved on strips of nitrocellulose membrane using both water and membrane blocking solution as eluents, showing potential for

development of a lateral flow device. To explore the possibility of interaction of the MA-QDs with TB biomarkers, the interaction between water-soluble fluorescent probes and the known synthetic anti-MA antibodies (gallibodies) was monitored by the enzyme-linked immunosorbent assay (ELISA) test, paper-based lateral flow assay, and fluorescence techniques.

The coupled fluorescent probes (biosensors) showed good solubility in water, have high fluorescence, and visually flowed through a nitrocellulose membrane. However, preliminary tests indicated that the interaction between these water-soluble fluorescent probes and the anti-MA antibodies were non-specific.

This work demonstrated that the main objective of improving the solubility of the coupled fluorescent probes was achieved, including that of coupled GQDs which are of lower toxicity than cadmium (Cd)-based QDs, although the specific binding with the anti-MA antibodies was not achieved. Future research recommendations to enhance the specific binding between the coupled fluorescent probes and the anti-MA antibodies include (i) increasing the amount of antigen MAs during the covalent coupling to QDs to improve the antigenic properties of the coupled materials, (ii) developing techniques that will be able to quantify the amount and concentration of MAs coupled to the QDs, and (iii) exploring the possibility of using molecular beacons (MBs) with M.tb DNA covalently attached to MA-QDs as a biosensor (probe) to increase the antigenic properties.

Research outputs

Published article

K. P. Kabwe, S. A. Nsibande, Y. Lemmer, L. A. Pilcher and P. B. C. Forbes, Synthesis and characterisation of quantum dots coupled to mycolic acids as a water-soluble fluorescent probe for potential lateral flow detection of antibodies and diagnosis of tuberculosis, *Luminescence,* 2022, 37(2), 278. **DOI:** https://doi.org/10.1002/bio.4170

Submitted manuscript

Kapambwe P. Kabwe, Sifiso A. Nsibande, Lynne A. Pilcher and Patricia B.C. Forbes, Development of a graphene quantum dot-mycolic acid probe as a potential tuberculosis biosensor, *Luminescence*, 2022.

Conference presentation

Kapambwe Peter Kabwe, Alma Truyts, Jan Verschoor, Yolandy Lemmer, Lynne Pilcher and Patricia Forbes, Synthesis and Characterization of Quantum Dots Coupled with Mycolic Acid as a Fluorescent Probe for Detection of Antibodies and Diagnosis of Tuberculosis, Nanoscience Young Researchers' Symposium, 12 November 2019, Future Africa, University of Pretoria. [**Poster presentation**].

Table of Contents

List of figures

Chapter two

Chapter three

List of tables

List of abbreviations

Abs: Antibodies

Ags: Antigens

AuNPs: Gold nanoparticles

BSA: Bovine serum albumin

CA: Citric acid

CB: Conduction band

CD4: Cluster of differentiation 4

CDs: Carbon dots

CNPs: Carbon nanoparticles

CP: Coat protein

CSIR: Council for Scientific and Industrial Research

CTV: Citrus tristeza virus

DCC: Dicyclohexycarbodiimide

DCM: Dichloromethane

DCR: Dendritic cell receptors

DI: Deionised

DMF: Dimethylformamide

DMSO: Dimethyl sulfoxide

DNA: Deoxyribonucleic acid

EDA: Ethylenediamine

EDC: Ethyl-3-(3-dimethylaminopropyl) carbodiimide

EIS: Electrochemical impedance spectroscopy

ELISA: Enzyme-linked immunosorbent assay

ET: Energy transfer

FRET: Fluorescence resonance energy transfer

FT-IR: Fourier transform infrared

FWHM: Full width at half maximum

Gbs: Gallibodies

GQDs: Graphene quantum dots

HIV: Human immunodeficiency virus

IgG: Immunoglobulin G

IgY: Immunoglobulin Y

LAM: lipoarabinomannan

LFA: lateral-flow assay

M.tb: *Mycobacterium tuberculosis*

MA-CdSe/ZnS: Mycolic acid-cadmium selenide/zinc sulfide

MA-Cl: Mycolic acid chloride

MA-GQDs: Mycolic acid- graphene quantum dots

MARTI: Mycolic Acid Real Time Inhibition

MAs: Mycolic acids

MB: Molecular beacon

MBS: Membrane blocking solution

MCs: Micellar nanocarriers

MMSs: Magnetic microspheres

NHS: N-hydroxy succinimide

NMR: Nuclear Magnetic Resonance

OA: Oleic acid

ODE: Octadecene

PBS: Phosphate-buffered saline

PEG-PPS: Poly (ethylene glycol)-bi-poly propylene sulfide

PIM: Phosphatidylinositol mannoside

PL: Photoluminescence

PLGA: Poly lactic-co-glycolic acid

PNA: Peptide nucleic acid

QDs: Quantum dots

QE: Quantum efficiency

RNA: Ribonucleic acid

Sam: Sample

S-Cl: Stearoyl- chloride

S-G: Stearoyl glycine

SiQDs: Silicon quantum dots

StA: Stearic acid

Std: Standard

TB: Tuberculosis

TEA: Triethylamine

TEM: Transmission electron microscope

THF: Tetrahydrofuran

TMB: Tetramethylbenzidine

TOPO: Trioctylphosphine oxide

VB: Valence band

VOBs: Organic volatile biomarkers

WHO: World Health Organization

XRD: X-Ray diffraction

CHAPTER ONE: Introduction

This chapter gives an overview of the problem that motivated this study. It also includes the aims, objectives, and the structure of the thesis.

1.1 Problem Statement and Motivation

Tuberculosis (TB) is a highly contagious chronic pulmonary disease caused by *Mycobacterium tuberculosis* (M.tb) [1]. The World Health Organization (WHO) Global Tuberculosis series 2020 stated that 10.0 million new cases of TB were reported in 2019, and 1.5 million people died from the disease [2]. Despite considerable improvement in the diagnosis of TB over the past years, a simple and effective method for the early detection of TB at the point of care is not yet available [3]. This poses a serious challenge, especially in developing countries, because the start of treatment could be delayed allowing the disease to spread [3]. Some of the current challenges in TB detection and diagnosis include inaccurate results, low sensitivity, and time taken between detection and initiating treatment. The more accurate TB tests that are currently used, such as chest X-rays, are expensive, especially for developing countries [4]. The occurrence of TB, and the increased risk of TB in human immunodeficiency virus (HIV) infected persons, have boosted the need for rapid, inexpensive, and accurate methods for detection and diagnosis of TB.

Therefore, this project seeks to develop a water-soluble fluorescence probe consisting of fluorescence quantum dots (QDs) and TB antigenic mycolic acids (MAs) that can be used in the point of care detection of anti-MA antibodies and for the diagnosis of tuberculosis. The diagnostic assay is normally performed in aqueous buffer and, therefore, a water-soluble probe is required. Early detection of tuberculosis can assist in preventing the disease from spreading further.

1.2 Aim and objectives of the study

1.2.1 Aim

The main aim of this research was to synthesize water-soluble QDs coupled to mycolic acids (MAs) as TB antigens to form a water-soluble fluorescence probe for potential detection of anti-MA antibodies and diagnosis of TB.

1.2.2 Objectives

Specific objectives of the study were to:

(i) Synthesize and characterize core-shell water-soluble cadmium selenide/zinc sulfide quantum dots capped with L-cysteine (L-cys-CdSe/ZnS QDs); and graphene quantum dots (GQDs).

(ii) Characterize the chemical and optical properties of the synthesized L-cys-CdSe/ZnS QDs and GQDs.

(iii) Devise means to effectively couple MAs to the water-soluble L-cys-CdSe/ZnS QDs and GQDs to form MA-CdSe/ZnS QDs and MA-GQDs.

(iv) Characterize the coupled materials, namely MA-CdSe/ZnS QDs and MA-GQDs.

(v) Investigate the lateral flow of the MA-CdSe/ZnS QDs and MA-GQDs.

(vi) Evaluate the suitability of these coupled materials, namely MA-CdSe/ZnS QDs and MA-GQDs, for TB anti-MA antibody testing.

1.3 Structure of the thesis

Chapter two defines tuberculosis and reviews the methods that have been previously used to detect TB. It also discusses MAs, antibodies, antigen-antibody interaction, core/shell cadmium based QDs, graphene QDs and coupling reactions of water-soluble QDs. Furthermore, fluorescence detection techniques, lateral flow techniques and the enzyme-linked immunosorbent assay (ELISA) are described. Finally, this chapter presents some applications of QDs bonded with biological molecules, and MAs bonded with different fluorophores.

Chapter three highlights the synthesis, characterization, water solubility and visual lateral flow methodologies of L-cys-CdSe/ZnS QDs and the coupled MAs-CdSe/ZnS QDs (**journal**

paper 1). **Chapter four** presents the development of a graphene quantum dot-mycolic acid probe as a potential tuberculosis biosensor (**manuscript submitted**). **Chapter five** discusses the detection of anti-MA antibodies using ELISA, lateral flow assay, and fluorescence techniques. Finally, **chapter six** provides the overall conclusions and suggests future work.

1.4 References

[1] N. Ariffin, N.A. Yusof, J. Abdullah, S.F. Abd Rahman, N.H. Ahmad Raston, N. Kusnin, S. Suraiya, Lateral flow immunoassay for naked eye detection of *Mycobacterium tuberculosis*, *Journal of Sensors* 2020, (2020), 1687.

[2] Russell, D.G., Cardona, P., Kim, M., Allain, S., Altare, F., Foamy macrophages and the progression of the human tuberculosis granuloma. Nat Immunol, 2009. 10: p. 943-948.

[3] S. Sudha, Tuberculosis diagnosis-an overview to the conventional diagnostic methodology and need for nanodiagnosis, *International Journal of Medical Engineering and Informatics* 8, (2016), 27-40.

[4] F.A. Khan, A. Majidulla, G. Tavaziva, A. Nazish, S.K. Abidi, A. Benedetti, D. Menzies, J.C. Johnston, A.J. Khan, S. Saeed, Chest x-ray analysis with deep learning-based software as a triage test for pulmonary tuberculosis: a prospective study of diagnostic accuracy for culture-confirmed disease, *The Lancet Digital Health* 2, (2020), e573-e581.

CHAPTER TWO: Literature review

This chapter defines tuberculosis and reviews the methods that have been previously used to detect TB. It also discusses core/shell cadmium based QDs, graphene QDs, MAs, coupling reactions of water-soluble QDs, application of QDs bonded with biological molecules, and application of MAs bonded with different fluorophores. Furthermore, this chapter defines antibodies and antigen-antibody interactions, whilst fluorescence detection and lateral flow techniques, as well as the Enzyme-linked Immunosorbent Assay (ELISA) are described.

2.1 Tuberculosis

Tuberculosis is a global health problem due to co-infection with human immunodeficiency virus (HIV) and the development of drug-resistant strains. It is a chronic pulmonary disease caused by the *Mycobacterium tuberculosis* (M.tb) bacterium. M.tb is transmitted through sputum droplets released through speaking, coughing, and sneezing, and the bacterium replicates every 18-72 hrs [1]. M.tb can be taken up by alveolar macrophages and inhibits phagosome maturation [2].

TB is a serious challenge in developing countries as well as an increasing scourge in many developed areas of the world. The World Health Organization (WHO) Global Tuberculosis series 2020 stated that 10.0 million new cases of TB were reported in 2019, of which 1.22 million people died [3]. Despite considerable improvement in the diagnosis of TB over the past years, a simple and effective method for the early detection of TB at the point of care is not yet available [4]. As a result, the start of treatment could be delayed allowing the disease to spread. Some of the current challenges in TB detection and diagnosis include inaccurate results, low sensitivity and time taken between detection and initiating treatment. The more accurate TB tests that are currently used, such as chest X-rays, are expensive especially for developing countries [4]. The occurrence of TB and the increased risk of TB in HIV infected persons have boosted the need for rapid, inexpensive, and accurate methods for the detection and diagnosis of TB that can prevent further disease transmission. Some of the methods that have been previously used for the detection and diagnosis of TB is discussed in this section.

Sputum analysis research has been conducted to determine the presence of live M.tb in different ways and is used in TB detection and diagnosis. Such a technique often involves microbial culture, digestion, and concentration of a sputum sample [5]. Even though this technique is very sensitive with a low detection limit for M.tb, it suffers some serious drawbacks, specifically that it takes 6-8 weeks for the completion of the detection and diagnosis of TB. Because of this delayed diagnosis, patient care and TB control can be affected as it gives enough time for the spread of the infection. The other limitation is that the desired

detectable amount of the bacteria from the sputum sample in the lungs for TB detection and diagnosis often cannot be produced due to the weak immune system of HIV-infected patients [6].

The lipoarabinomannan (LAM) urine dipstick test is also used to diagnose TB [7]. The use of this test gained popularity as it is simple, easy to use and is more sensitive than the sputum test, especially for people with high human immunodeficiency virus (HIV) loads. LAM tests work well for people with a very low cluster of differentiation 4 (CD4) counts (high HIV load) [7, 8]. The LAM test has limited sensitivity for non-HIV infected patients and underlines the need for new diagnostic tests.

The colloidal gold test is another method used to detect M.tb deoxyribonucleic acid (DNA) electrochemically. This method involves coupling of rapid isotherm amplification of target DNA that is specific to M.tb with gold nanoparticle electrochemistry on disposable screen-printed carbon electrodes [9]. The method works well because it is sensitive and specific, but the complicated DNA sample preparation method before the detection process and the potential toxicity of gold nanoparticles limit its application [10]. Therefore, a more simplified and user-friendly test is required for TB antibody detection.

2.2 Mycolic acids

Mycolic acids (MAs) are lipids that are the emblem of the cell envelope of *Mycobacterium tuberculosis* and associated species and genera [11]. MAs are the major lipid constituent of the cell walls [12] as shown in **Figure 2.1**. They form a lipid shell around the organism as they are strongly hydrophobic molecules and affect the permeability properties of the cell surface, hence protecting it from attack by oxygen radicals, cationic proteins, and lysozymes from the host cell [13].

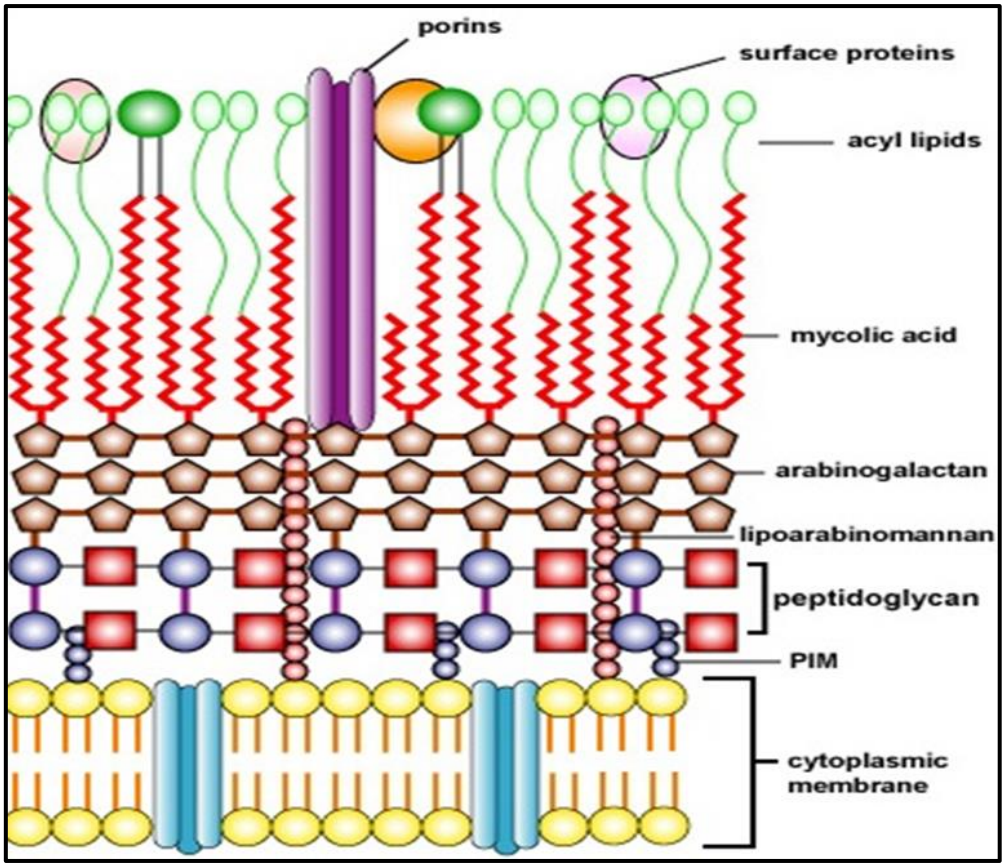

Figure 2.1: Structure of acid-cell wall of *Mycobacterium tuberculosis*. PIM stands for phosphatidylinositol mannoside [14]

MAs are chemically inert and control host-pathogen interactions. They achieve this by identifying and signalling of the host cells during pathogen invasion, intracellular trafficking, and docking [15]. There are three main classes of MAs found in *Mycobacterium tuberculosis*, namely alpha-MAs, methoxy-MAs, and keto-MAs. Around 70% of MAs are alpha-MAs which posses two *cis* cyclopropane groups. 15% of MAs of the organism are methoxy-MAs and the remaining 15% is made up of keto-MAs (**Figure 2.2**). Methoxy-MAs and keto-MAs possess one cyclopropane group that can either be *cis* or *trans* oriented [16].

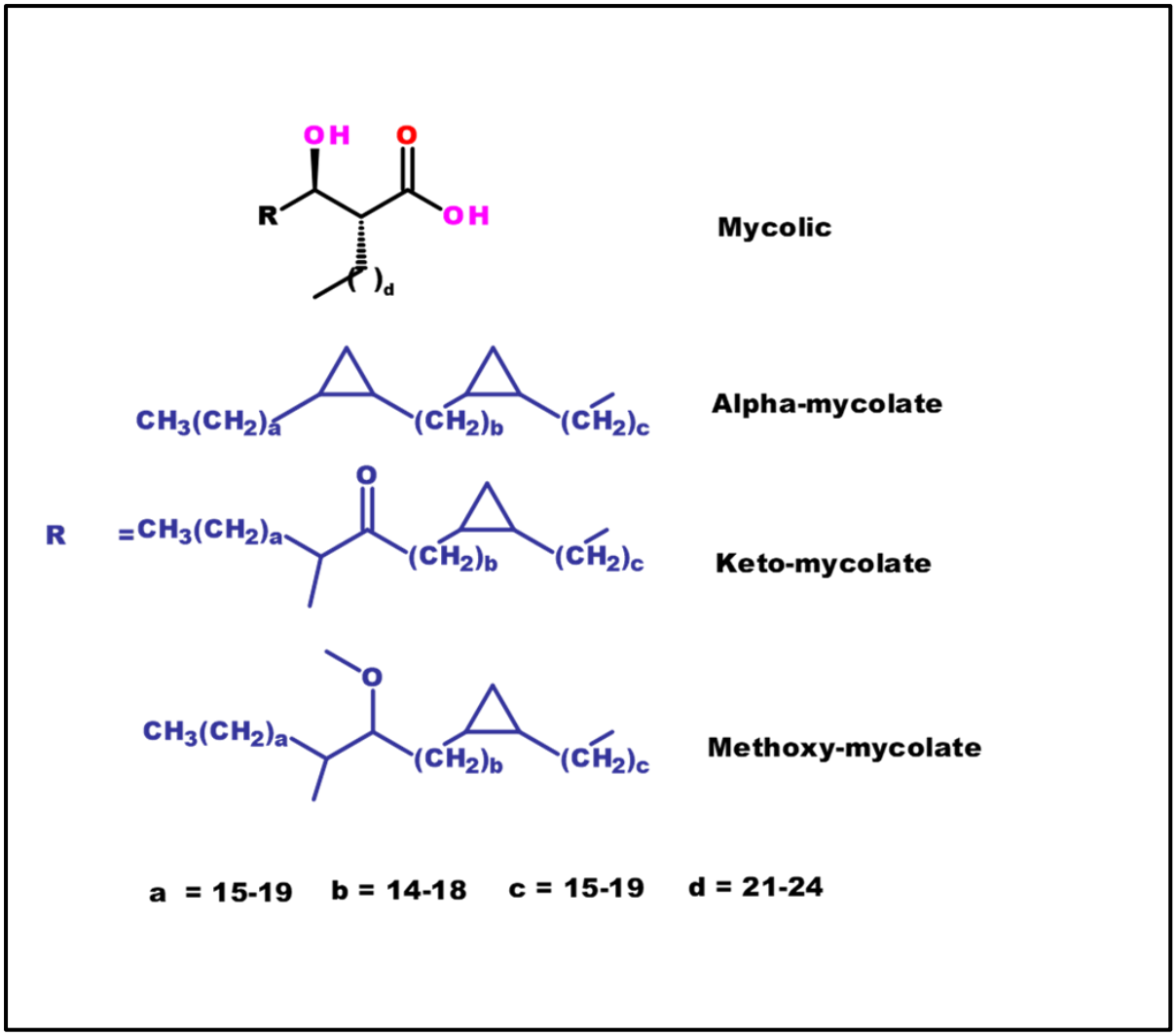

Figure 2.2 Chemical structures of the three main classes of mycolic acids [17].

MAs are also called antigenic cell wall lipids because they elicit an antibody response [18]. Anti-MA antibodies serving as specific TB biomarkers can provide prognostic information about the TB infection status, either for individual patients or study cohorts [19]. Chemical inertness of MAs makes them attractive diagnostic tools to detect anti-MA antibodies for TB. However, the poor solubility of MAs in most solvents (they are only soluble in chloroform and hexane) presents the biggest challenge in their application as biomarkers [20]. Most diagnostic assays are carried out in aqueous buffers and therefore chloroform and hexane are not compatible solvents.

2.3 Gallibodies

Antibodies (Abs) are protein molecules that bind to specific proteins such as antigens to protect the organism against disease [21]. They are generated by the immune process in reaction to infection. They are produced from a single cell division of clones. The region within the antigen that allows the binding of the antibodies is referred to as the epitope. Antibodies are specific and target different antigens without side effects and they are sometimes called antigenic determinants [22]. Abs are mainly used as essential tools for molecular immunology investigations by labeling the target antigens [23]. Due to these unique properties, Abs are normally used for detecting and identifying blood serum analytes, cell markers and also as agents of pathogens [24]. Gallibodies are special engineered antibodies derived from the immunoglobulin genes of the chicken. The name Gallibody comes from the Latin nomenclature for the domestic chicken: *Gallus gallus domesticus* [25]. Selected artificial gallibodies, like human antibodies, specifically bind to mycolic acids as lipid antigens, and hence they are sometimes called anti-mycolic acid gallibodies [26].

2.4 Antigen-antibody interactions

An antigen-antibody interaction is a type of interaction that is specific in nature. It involves the binding of antigens (Ags) and antibodies (Abs) to form an antigen-antibody complex (Ag-Ab complex) [27]. The binding of Ags and Abs occurs at the surface of the cells and in different proportions. During the interaction of Ags and Abs, denaturation does not take place, and they are both involved in the formation of the antigen-antibody complex, as illustrated in the equation below:

$$\text{Antigen} + \text{Antibody} \leftrightarrow \text{Antigen- antibody complex}$$

The formation of the Ag-Ab complex is a reversible reaction, but it has very strong intermolecular attractive forces. The reversibility of the reaction is influenced by the nature of binding of the antigen to the antibody. Antigen-antibody interactions are influenced by many factors, such as temperature, pH, ionic strength, concentration of antigens and antibodies, number of antigen sites per cell (zygosity) and period of incubation [28, 29].

2.5 Core/shell cadmium-based quantum dots

Cadmium-based quantum dots (QDs) are semiconductor nanocrystals with a size range between 1-10 nm [30]. Different cadmium-based QDs have been produced over the past decades and have been applied in various fields because of their electronic and optical properties including: high surface to volume ratio, size-tuneable band gap energy, narrow emission spectra and broad absorption spectra [31]. Cadmium-based QDs also have high fluorescence quantum yields and higher resistance to photo-initiated degradation when compared to organic fluorophores [32]. The functional groups bound on the surface of QDs (**Figure 2.3**) define their solubility and strongly influence their physical and photophysical properties. QDs containing cadmium metal such as cadmium sulfide/zinc selenide (CdS/ZnSe), cadmium tellurium/zinc sulfide (CdTe/ZnS) and cadmium selenide tellurium /zinc sulfide (CdSeTe/ZnS) have been used in biological sensing and imaging applications, due to their bright fluorescence and surface chemistry [32]. The big challenge of using cadmium is its potential cytotoxicity due to the formation of free cadmium ions (Cd^{2+}) [33, 34]. However, the challenge of cytotoxicity can be reduced by surface coating of QDs with other materials that are not toxic to form core-shell quantum dots [31] as shown in **Figure 2.3**. The shell (outer layer material) does not affect the biological function of QDs, instead, it provides stability to the core (inner material) of the QD by protecting it from the surrounding environment and can prevent, for example, oxidation [35]. The shell also improves physical and chemical properties and allows for easy bio functionalization [35]. ZnS or ZnSe are often used as shell materials because they provide efficient confinement of electrons inside the nanocrystals and do not easily form defects [36]. Another method of reducing cytotoxicity of cadmium containing QDs is the use of gelatin or tripeptide glutathione as stabilizers to detoxify cadmium free ions. The tripeptide glutathione binds the cadmium ion and forms a phytochelatin shell that makes cadmium metal inert [33, 37, 38]. Because of these properties, cadmium based QDs have been used extensively in scientific and technological applications that rely on achieving spectral purity at optimum optical flux such as chemical/biological sensing, optoelectronic devices, molecular biology, bioimaging, and photochemistry [37, 39, 40].

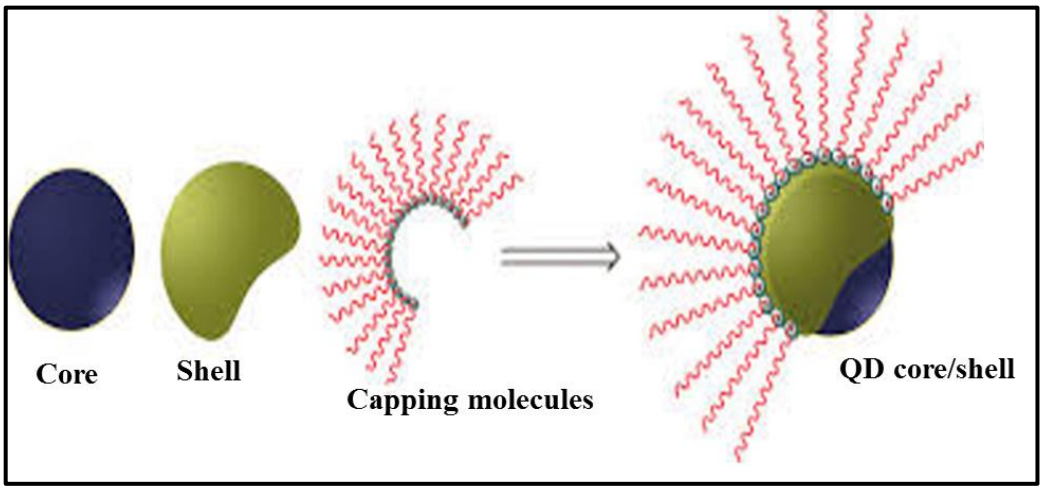

Figure 2.3: Core/shell quantum dot structure [41].

2.6 Graphene quantum dots

Graphene quantum dots (GQDs) are carbon-based nanocrystals with a diameter ranging between 1-20 nm [42]. GQDs have been produced and widely studied in recent years due to their exceptional electronic, optical, and photoelectric properties including; high surface to volume ratio and size-tuneable band gap energy [43]. GQDs possess attractive features such as stable fluorescence properties, simple and cost effective preparation methods, low toxicity that renders them environmentally friendly, have excellent biocompatibility, and good water solubility when compared to semiconductor-based quantum dots [44]. Because of these properties, GQD-based materials have been used extensively in biological imaging, biosensing, drug delivery, optoelectrical detectors, solar cells, filtration devices, and photocatalysis [45]. Additionally, GQDs have emerged as potential fluorophores for biosensing in biological matrices such as human blood, urine, sputum, and saliva, due to their selectivity, sensitivity, and good reproducibility of the results [46]. Furthermore, the presence of π electrons in the GQDs enables them to be easily conjugated or functionalised with other materials such as proteins and lipids via π-π interactions to provide new materials [46].

2.7 Coupling of water-soluble QDs to biological molecules for various applications

Coupling of QDs involves the binding of water-soluble QDs directly to specific biological molecules for different applications such as imaging and fluorescence detection of various biomolecules. Literature

reports that water-soluble QDs are preferred for bio sensing [47], typically of biological molecules such as nucleic acids, peptides, antibodies, proteins, monosaccharides, and liposomes [47]. Both covalent and non-covalent methods are commonly used to couple QDs to biological molecules [37].

Covalent coupling between water-soluble QDs and biological molecules takes place between two functional groups resulting in the formation of a covalent link. Covalent coupling is normally achieved by using a functional cross-linker with a specific length and type of functional group to facilitate cross-binding [48]. For the application of water soluble QDs, carboxylic acid groups are the most used functional group for coupling of QDs with other biological molecules [48]. The carboxylic acid is normally used because it can easily bind with proteins, amino acids, and peptides via an amide link, although the choice of the functional group used depends upon the nature of surface modification of the QDs and the type of coupling [48]. The formation of the covalent amide linkage between QDs and a biological molecule, such as a MA, can be confirmed using FT-IR analysis [49].

Non-covalent coupling involves an association of the QDs and the biological molecules by electrostatic, hydrophobic, and high affinity interactions, for example. Electrostatic interactions take place between negatively charged species and positively charged molecules. It is the most used non-covalent coupling method because it is simple and fast [37]. The surface of QDs is large and therefore the negatively charged carboxylate groups of the surface modified QDs can easily interact with positively charged proteins to form an ionic bond. Although the electrostatic interaction between two molecules is simple and fast, it has some limitations, such as solubility and stability. Ionic bridges only dissolve in polar solvents like water and do not dissolve in organic solvents. Electrostatic interactions require the optimization of some factors that determine the stability of the coupled products, such as charge, size, pH, and ionic strength [37, 48]. Because of these limitations, covalent coupling of QDs and biological molecules is more robust.

2.8 Enzyme-linked Immunosorbent Assay (ELISA)

ELISA is a sensitive technique used to detect and quantify substances, mainly antigens or antibodies [22, 50]. ELISA utilizes the specific interaction between the antigens and antibodies to identify specific

antigens and antibodies in infectious diseases, pregnancy testing, blood type, and many others using a small sample volume. The ELISA test is executed using polystyrene plates, mainly in 96-well plates coated to bind antigens or antibodies strongly. ELISA testing requires a primary or secondary detection antibody depending on the type of assay. The two common ELISA tests are direct and indirect. In the direct ELISA, the primary antibody binds directly to the antigen of interest while in the indirect ELISA, primary and secondary detection antibodies are used. A secondary detection antibody is an enzyme conjugated antibody that binds the primary antibody. During the ELISA test, the detection is carried out with the help of the substrate of the enzyme conjugated to the secondary antibodies. When the enzyme digests its substrate, the product has a different colour. The product is quantified using the absorbance of light at an appropriate wavelength [51]. There are mainly four steps required for the completion of the ELISA test. These are: coating of the plates with the antigens or antibodies, blocking of non-specific binding sites, detection, and final reading. The ELISA test can be affected by some factors such as the shape and quality of the plate assay, the nature of the buffer solution, enzyme conjugates, washes, and the target antigen. In this study, the indirect ELISA test was used. The antigen (MA-QD) was dissolved in volatile solvents such as hexane or phosphate buffered saline (PBS) buffer, etc., and immobilized on a 96-well plate via adsorption. The detection (primary) TB antibody (gallibody) was added to form a complex with the antigen. The secondary antibody labeled with an enzyme was also added to the same plate to covalently link to the detection antibody. The substrate for the reporter enzyme was added thus the enzyme from the secondary antibody catalyzed the reaction of this substrate inducing a colour change from yellow to blue. This was correlated to the amount of antigen present by comparing it to the colour change affected by a concentration series using a standard curve of the reference compounds [51, 52].

2.9 Lateral flow detection technique

The lateral-flow assay (LFA) is a simple platform that is used in medical diagnostics for point of care testing, laboratory use, and home testing to detect the presence of a target analyte, often an antibody in a liquid, based on biochemical interactions such as an antigen-antibody interaction [53]. The LFA format

typically consists of a sample pad, conjugate pad, nitrocellulose membrane, and absorbent pad. The sample pad is the first section where the sample is introduced, which acts as a sponge, and holds the sample fluid. The sample fluid is transported to the conjugate pad using capillary action. The conjugate pad contains the sample and bioconjugate molecules (probe) required for a chemical reaction between the target molecules to form an immune complex. The active site of the LFA is the nitrocellulose membrane which contains the test line and control line for antigen-antibody interaction. The test line recognizes the sample of interest, while the control line captures unbound conjugate antibodies or antigens from the conjugate pad. The absorbent pad acts as a waste drain and prevents the backflow of the liquid [17, 54].The set up of the components of LFA is illustrated in **Figure 2.4.**

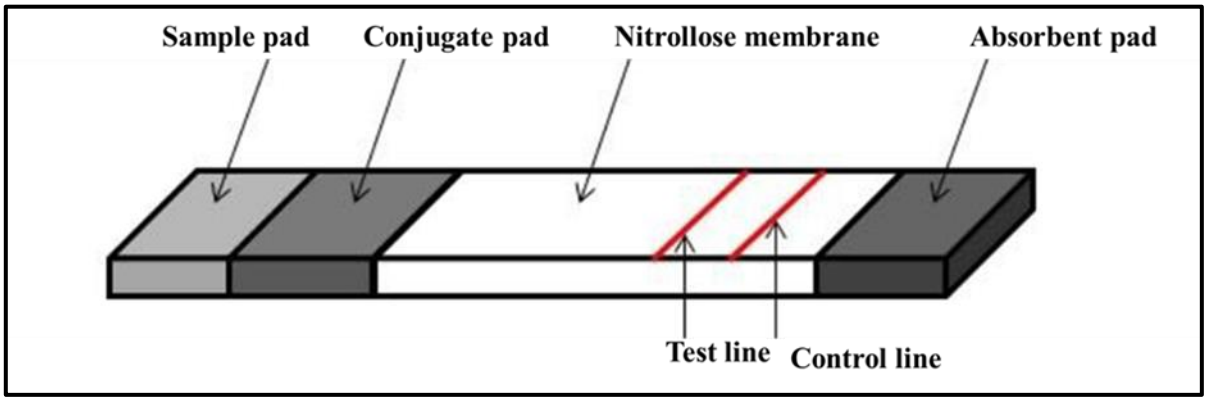

Figure 2.4:Typical lateral flow assay strip set up [55].

There are two common lateral flow assay formats**.** These are competitive and sandwich formats [56]**.** The competitive format is normally used to detect analytes that are too small for multiple bindings or analytes when antibody pairs are not present while the sandwich format is typically used when detecting larger analytes that have two epitopes as shown in **Figure 2.5.**

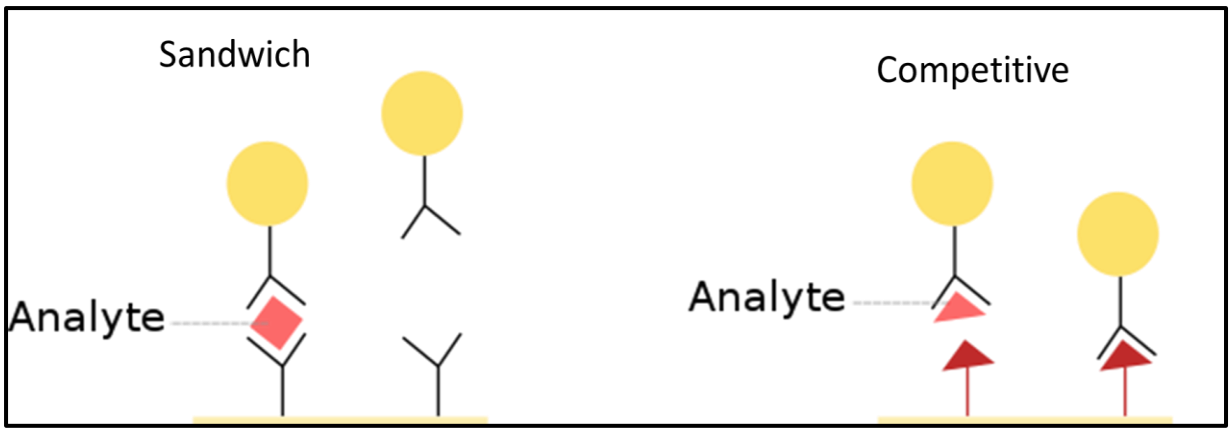

Figure 2.5: Two common lateral flow assay formats namely sandwich and competitive [56].

In this present study, the lateral flow assay strips are composed of three components namely, a sample conjugate release pad, nitrocellulose membrane (test pad), and an absorbent pad. The competitive format was explored in this study to test the binding of TB antibodies to the synthesized fluorophores coupled to mycolic acids as an antigen.

2.10 Fluorescence detection techniques

Fluorescence is a physical property in which fluorophores absorb a photon of energy at a particular wavelength during an initial excitation and then emit a photon of energy with a longer wavelength upon relaxation to the ground state, as illustrated in **Figure 2.6** [57]. After excitation, a fluorophore remains in the excited state for some time before emitting a photon of energy and returning to its original state. The time a fluorophore remains in the excited state is referred to as fluorescence lifetime and it depends on the nature of the fluorophore and the environment which it is interacting with. The difference between the excitation and the emission wavelengths is termed the Stokes shift [58]. The Stokes shift value is very important for fluorescence measurements, as it clearly differentiates the emitted signal from the excitation signal and provides information on the specific molecular features of different fluorophores. The fluorescence technique is applied in different research fields such as biochemistry, biophysics, and biomaterial science for sensing and imaging due to its sensitivity [58] and high spatial resolution [59]. Fluorescence measurements can be obtained in liquid, solid, and gas phases.

Fluorescence emission has three important parameters that can be determined as a function of excitation and emission wavelength. These parameters can be recorded and used for reporting on target interactions in sensing applications. The three parameters are: fluorescence intensity, fluorescence lifetime, and emission anisotropy [60]. Fluorescence intensity, also called the band maximum, is measured at the given wavelength of excitation and emission. The intensity measured over the emission wavelength range provides the fluorescence emission spectrum, and the fluorescence excitation spectrum is achieved in the case of the intensity of emission measured over a range of excitation wavelengths. Fluorescence lifetime, also referred to as fluorescence excited-state lifetime, is the time the fluorophore spends in the excited state and can be directly obtained from the decay curve measured using pulsed excitation. The decay curve does not depend on instrumental factors but is characteristic of the fluorophore. Emission anisotropy is the fluorescence intensity function obtained along the vertical and horizontal axes. It determines how a molecule's spatial orientation changes over time between absorption and emission events. It works on the idea that polarized light excites a fluorophore, resulting in partially polarized emission.

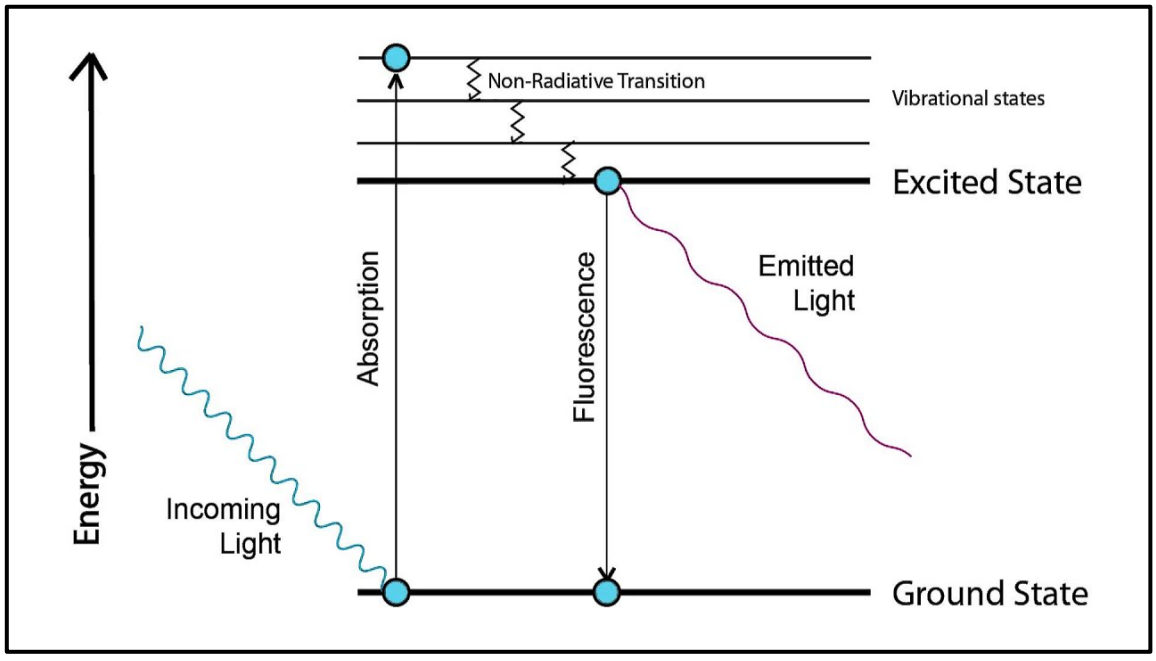

Figure 2.6: Simple Jablonski energy diagram summarizing the fluorescence technique [61].

2.11 Application of QDs bonded with different biological molecules

Fluorescence detection is one of the main applications of QD based probes. This process is achieved by comparing the photophysical properties of the probe alone and after interaction with the target analyte. Once the probe interacts with the target analyte, fluorescence (luminescence) can either be enhanced (turn-on) or quenched (turn-off) or a shift of fluorescence emission wavelength occurs, indicating the detection of the analyte. The enhancement and quenching mechanism involve energy transfer (ET) such as Förster or fluorescence resonance energy transfer (FRET) [62]. FRET takes place between a donor fluorophore in an excited state and a nearby acceptor through a long-range dipole-dipole interaction in a non-radioactive means as illustrated in **Figure 2.7**. FRET decreases the fluorescence intensity and lifetime of the fluorophore donor and enhances the fluorescence intensity of the fluorophore acceptor. FRET only occurs when there is a close distance between the donor and the acceptor, enough fluorescence lifetime, and the overlap of the emission spectrum of the donor molecule and the acceptor absorption spectrum.

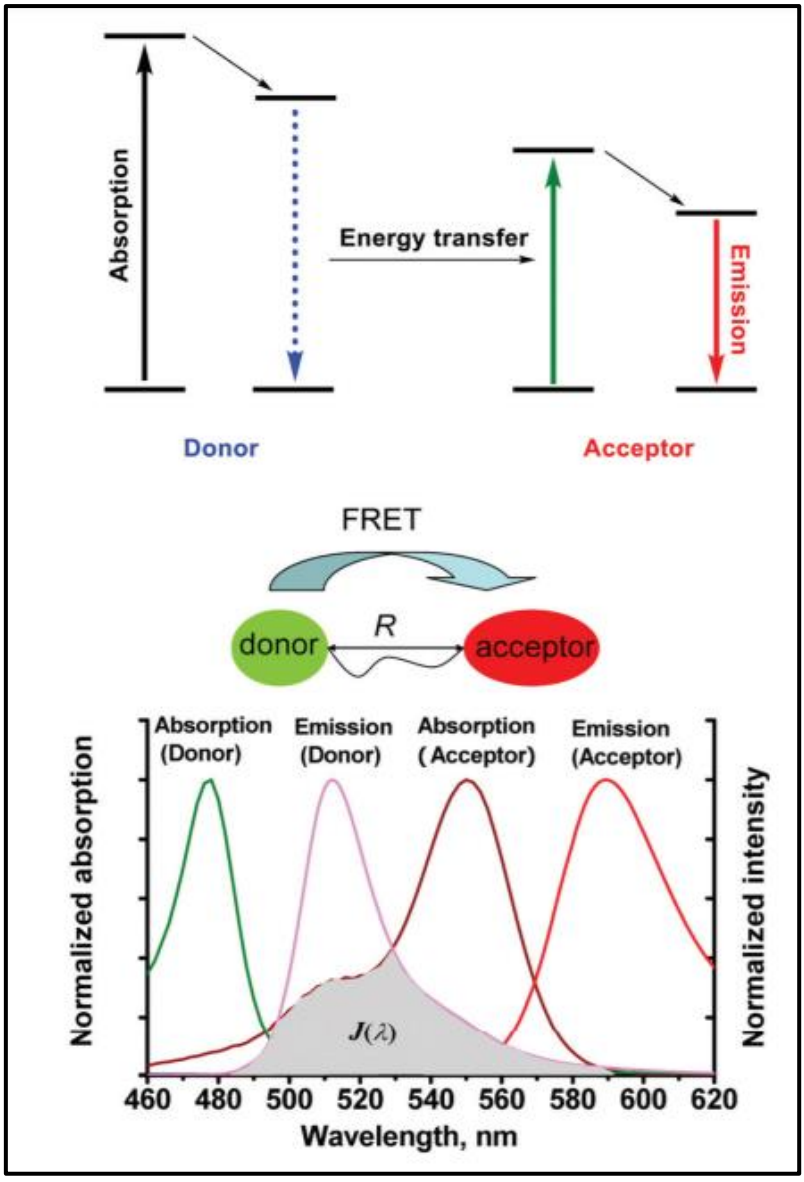

Figure 2.7: Fluorescence resonance energy transfer (FRET) mechanism. R represents the close distance between the donor and the acceptor. ***J*** (λ) indicates the overlap between the donor emission spectrum and the acceptor absorption spectrum [62].

The emission spectrum depends on the bandgap of the donor (fluorophore QDs). Bandgap also called energy gap is the space between the valence band where there is no free electron to move around and the conduction band where there are free electrons to move around [63], as indicated in **Figure 2.8**. In QD fluorophores, the energy gap is very small but not zero. The energy needed to overcome this gap is inversely proportional to the wavelength of the fluorescence emitted. This energy gap increases with a decrease in the size of the QD fluorophore. This implies that the larger the QD fluorophore the smaller the

energy gap and this causes the shift of the emission spectrum towards the red region of the visible region and vice-versa.

Effective fluorescence probes are evaluated by detecting response signals at low concentration of the target analyte, showing high sensitivity, rapidity, and versatility [64-66].

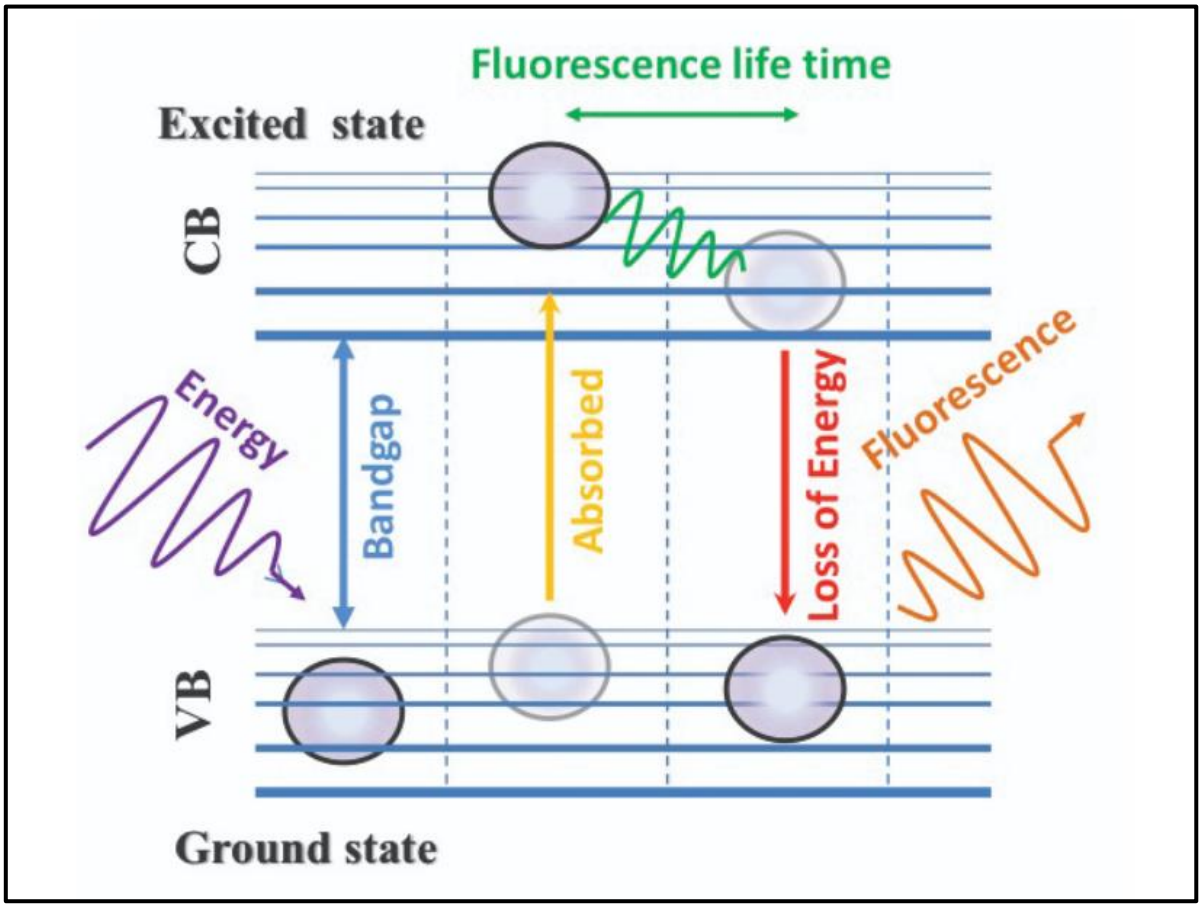

Figure 2.8: Graphical representation of band gap, ground state, excitation state and fluorescence emission. VB stands for valence band and CB for conduction band [63].

To the best of our knowledge, no application of MAs coupled to QDs as a fluorescent probe for detection of TB anti-MA antibodies has been previously reported. However, there are few reports on the applications of QDs bonded with other biological molecules. Examples of these applications of QDs bonded with other biological molecules are discussed in this section.

CdZnSeS QDs coated with SiO_2 conjugated to a molecular beacon (MB) probe have been demonstrated to detect norovirus in human blood serum [64]. MBs are oligonucleotide single-stranded hairpin-shaped molecules with internal fluorophores whose fluorescence is restored

in the presence of the target specific nucleic acid and the fluorescence of the fluorophores is quenched in the absence of the target analyte. MBs are made up of loops of about 15 to 25 nucleotides which serve as probes and the stems of the MB bring the two ends of the molecule (linked to a fluorophore and quencher respectively) closer [67]. MBs are made up of loops about 15 to 25 nucleotides long to serve as probes and stems to bring the two ends of the molecule closer. A CdZnSeS QD-MB probe was synthesized via ethyl-3-(3-dimethylaminopropyl) carbodiimide/N-hydroxy succinimide (EDC/NHS) chemistry. Using this QD-MB, norovirus was analyzed/detected by the steady enhancement of fluorescence emission as the concentration of norovirus increased [64]. In another report, highly sensitive and specific sensors for detecting the *Mycobacterium tuberculosis* Ag85B antigen using CdTeSi-QDs modified with gold nanorods conjugated to the BGP-50B14 antibody were reported [68].The detection process was based on fluorescence resonance energy transfer (FRET) via antigen-antibody interaction as shown in **Figure 2.9.** Silica was used to coat the QDs for easy binding with the GSP-50B14 antibody, while gold nanorods were used as fluorescence quenchers.

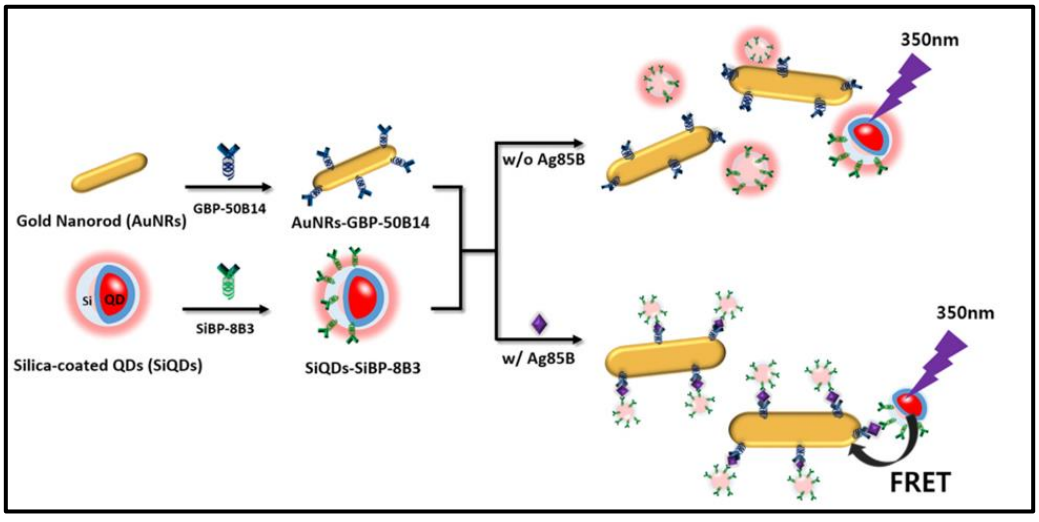

Figure 2.9: Schematic illustration of the detection of secreted antigen from *Mycobacterium tuberculosis* based on a sandwich assay via antigen-antibody interactions using gold nanoparticles (AuNPs) and silicon quantum dots (SiQDs) [68].

CdS QDs have also been used for the detection of *Mycobacterium tuberculosis* DNA using peptide nucleic acid (PNA) [69]. PNA was immobilized on the surface of CdS QDs capped with graphene oxide modified through the EDC/NHS coupling reaction. The CdS-PNA biosensor showed good electrochemical activities towards the detection of *Mycobacterium tuberculosis* DNA.

Brightly fluorescent glutathione functionalized CdSe/ZnSeS core/shell QDs have been synthesized for analysis of dengue virus ribonucleic acid (RNA) [65]. The alloyed shell was used to increase the photoluminescence quantum yields. The biosensor was made in two parts. Firstly, the gold nanoparticles capped with L-cysteine were synthesized via ligand exchange reaction and were conjugated to the CdSe/ZnSeS QDs to form AuNP-QD monohybrids. Then the AuNP-QD monohybrids were conjugated to the end of the molecular beacon (MB) to form a AuNP-QD- MB probe, as shown in **Figure 2.10.** The presence of the dengue virus RNA in solution was detected by a fluorescence enhancement signal which was proportional to the concentration of the dengue virus RNA [65].

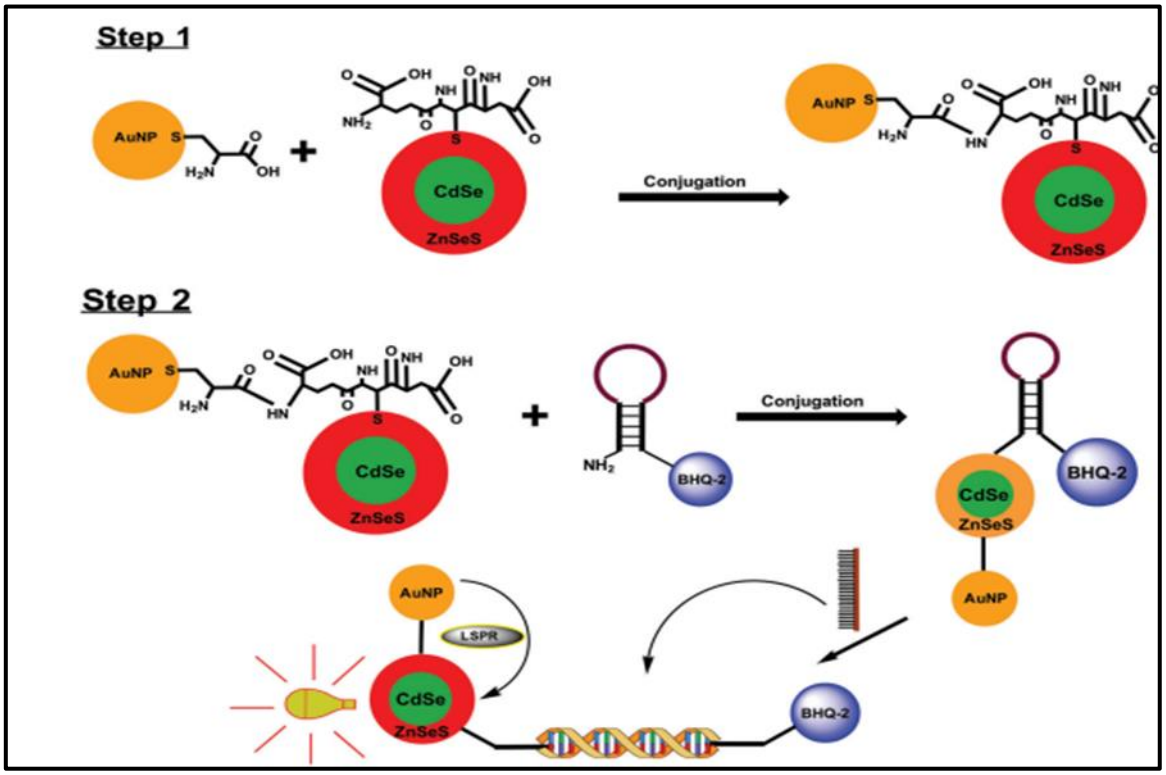

Figure 2.10: Schematic representation of the GSH-CdSe/ZnSeS-MB QD biosensor for the detection of the dengue virus RNA [65].

In another report, CdSe/ZnS QDs capped with diene polyvalent mannose were synthesized via ligand exchange in the presence of sodium hydroxide and methanol [70]. The probe was used successfully to analyze the interaction between the Ebola receptors and the CdSe/ZnS QDs capped with polyvalent mannose in human blood serum, using FRET. This interaction was observed by the strong fluorescence quenching of the CdSe/ZnS QDs indicating the specific binding with the Ebola receptors [70].

The use of stable colloidal suspensions of CdSe QDs as well as carbon dots (CDs) as a viable photoluminescent platform for the detection of TB organic volatile biomarkers (VOBs) have been reported [71]. The CdSe QDs and CDs based fluorescence probes were in solution form, whereas the target VOBs were obtained from exhaled breath. The QDs and CDs were used without further capping or modifications. The emission and absorbance properties of both CdSe QDs and CDs were found to be different from the VOBs mixed with CDs/QDs. When the VOBs were mixed with the QDs and CDs fluorescent probes, there was a shift in the QD emission peak, as shown in **Figure 2.11**, whereas the peak intensity of the CDs reduced with the increase in concentration.

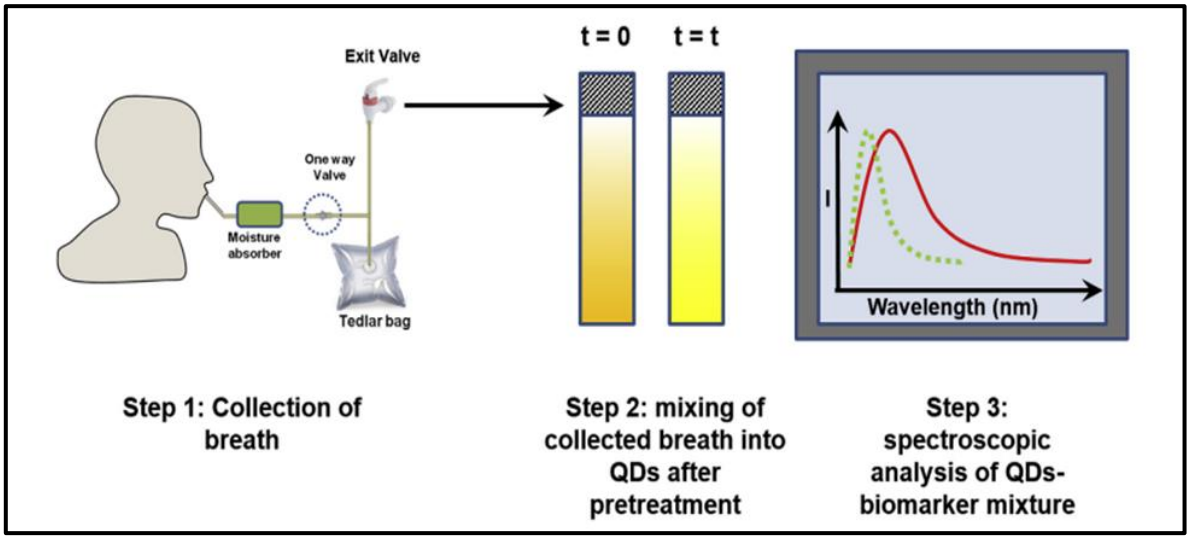

Figure 2.11: Schematic diagram showing the method of TB organic volatile biomarker detection using quantum dots [71].

It is also reported that cadmium-telluride (CdTe) QDs were synthesized and conjugated to an antibody (Ab) that was used to detect citrus tristeza virus (CTV) in plants. The coat protein (CP) of the CTV was

immobilized onto the surface of carbon nanoparticles (CNPs). After mixing, the QD-Ab and CTV bonded to CNPs, and the CNPs quenched the fluorescence of the CdTe QDs [72].

Similarly, a sandwich complex composed of CdTe QDs, coupled with surface functionalized magnetic microspheres (MMSs), conjugated with antibodies and phase-display-derived peptides have been developed [73]. The probe (complex) was used to detect *Mycobacterium tuberculosis* $H_{37}R_V$ binding peptides in sputum. QDs were used to provide a fluorescent signal and MMSs to provide magnetic separations. The phase display derived peptides came from *Mycobacterium tuberculosis* cells. When the probe (complex) mixed with the sputum solution contained TB, there was specific ligand-receptor interaction which resulted in the enhancement of fluorescence signal and thereby detection of *Mycobacterium tuberculosis* as illustrated in **Figure 2.12**.

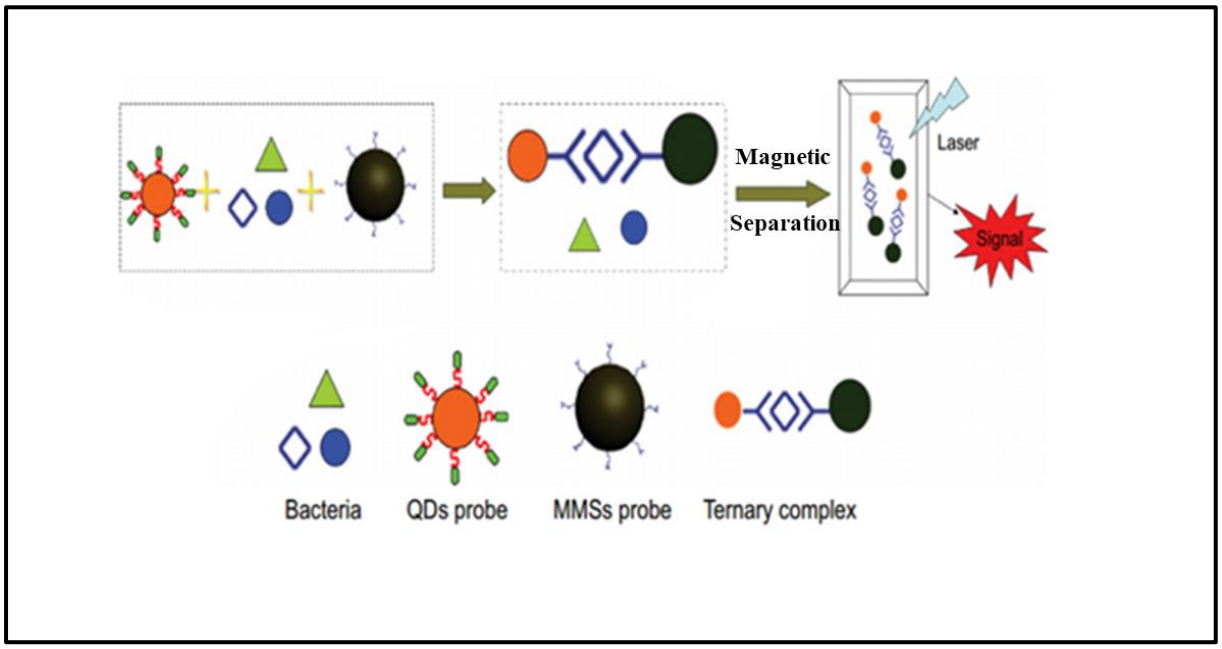

Figure 2.12: Schematic diagram showing the formation of a ternary complex, magnetic separation of bacteria cells and the detection of *Mycobacterium tuberculosis* [73].

Table 2.1: Summary of some reported applications of QDs in the detection of biomolecules

QDs	**Molecules bonded to QDs**	**Detection method**	**Target**	**Reference**
CdZnSeS	Molecular Beacon	Fluorescence	Noroviruses	[64]
CdTeSi	Gold nanorods	Fluorescence	TB Ag85B	[68]
CdS	Graphene Oxide	Cyclic voltammetry	TB	[69]
CdSe	Endonuclease	Impedance spectroscopy	mtbDNA	[74]
CdSe/AuNP	Molecular Beacon	Fluorescence	Dengue virus	[65]
CdSe/ZnS	Dihydrolipoic acid	Fluorescence	HIV/Ebola receptors	[70]
CdSe	Carbon dots	Fluorescence	TB biomarker	[71]
CdTe	Antibody	Fluorescence	Citrus tristeza	[72]
CdTe	Magnetic microspheres	Fluorescence	*Mycobacterium tuberculosis*	[73]
CDs	Antibody IgG	Fluorescence	Human IgG	[75]
GQDs	tTG antigen	Electrochemical	Anti-tTG antibodies	[76]
GQDs	Molecular Beacon	Fluorescence	MicroRNA	[77]

2.12 Application of MAs bonded to different fluorophores

It is reported that three different classes of MAs were synthesized to compare the structure-function relationship of the antigenicity of mycolic acid for detecting TB anti-MA antibodies [78]. The three synthetic classes of MAs are: methoxy-MAs, keto-MAs, and alpha-MAs. These synthetic classes of MA were analyzed separately using enzyme linked immunosorbent assay (ELISA) in phosphate buffered saline (PBS). The results revealed that methoxy-MA bound strongly to the TB anti-MA antibodies in the patient serum by hydroxy-MA, then keto-MA and alpha-MA was the least strongly bound.

MA as a targeting ligand was incorporated into a drug encapsulating polylactic-co-glycolic acid polymer (PLGA) to improve the efficiency of an anti-TB drug delivery system [19]. The MA-PLGA probe was prepared via a double emulsion solvent evaporation technique. The infected mycobacteria strains derived from mouse macrophage were exposed to encapsulated isoniazid-PLGA nanoparticles via MA as a target ligand. The fate of the nanoparticles was monitored by electron microscopy. Analysis of mycobacteria infected macrophages showed a strong and significant increase in phagocytic uptake of MAs coated with nanoparticles. The increase was as a result of the binding between the MAs coated with nanoparticles and the cell surface receptors involved in phagocytic uptake of *Mycobacterium tuberculosis* [19].

In another related report, MA-loaded micellar nanocarriers (MA-MCs) made up of poly(ethylene glycol)-bi-poly(propylene sulfide, PEG-PPS) was developed [20]. The MA-MCs are made up of PEG-PPS whose terminal ends were covalently attached to an acid-sensitive fluorophore to give the signal and also increased intracellular delivery of MAs to phagocytic immune cells in the lungs due to the limited solubility of MAs in water. It was reported that these nanobiomaterials (MA-MCs) were taken up by the alveolar macrophages in the lungs more than free MAs and induced the activation of T cells.

2.13 Conclusion

Much work has been done in the recent past on the application of QDs conjugated with biological molecules on the one hand, and the application of MAs bonded to different fluorophores to detect antibodies and diagnosis of TB in blood serum or sputum on the other, but no work has been previously

reported on the application of QDs coupled to MAs to detect anti-MA antibodies and the diagnosis of TB. Although much progress has been made, many of the sensors (probes) have poor stability, low sensitivity, are not user friendly, are time consuming and some require expensive equipment. Therefore, there is need for a robust method that can produce rapid detection and diagnostic results with high sensitivity and selectivity but that is also user friendly and of reasonable cost.

2.14 References

[1] T.R. Lerner, S. Borel, D.J. Greenwood, U. Repnik, M.R. Russell, S. Herbst, M.L. Jones, L.M. Collinson, G. Griffiths, M.G. Gutierrez, *Mycobacterium tuberculosis* replicates within necrotic human macrophages, *Journal of Cell Biology* 216, (2017), 583-594.

[2] A. Welin, J. Raffetseder, D. Eklund, O. Stendahl, M. Lerm, Importance of phagosomal functionality for growth restriction of *Mycobacterium tuberculosis* in primary human macrophages, *Journal of Innate Immunity* 3, (2011), 508-518.

[3] D.R. Silva, F.C.d.Q. Mello, G.B. Migliori, Tuberculosis series 2020, *Jornal Brasileiro de Pneumologia* 46, (2020), 1806-3756.

[4] S. Sudha, Tuberculosis diagnosis-an overview to the conventional diagnostic methodology and need for nanodiagnosis, *International Journal of Medical Engineering and Informatics* 8, (2016), 27-40.

[5] K.M. Samanich, M.A. Keen, V.D. Vissa, J.D. Harder, J.S. Spencer, J.T. Belisle, S. Zolla-Pazner, S. Laal, Serodiagnostic potential of culture filtrate antigens of *Mycobacterium tuberculosis*, *Clinical and Diagnostic Laboratory Immunology* 7, (2000), 662-668.

[6] T.R. Frieden, T.R. Sterling, S.S. Munsiff, C.J. Watt, C. Dye, Tuberculosis, *The Lancet* 362, (2003), 887-899.

[7] J. Peter, C. Green, M. Hoelscher, P. Mwaba, A. Zumla, K. Dheda, Urine for the diagnosis of tuberculosis: current approaches, clinical applicability, and new developments, *Current Opinion in Pulmonary Medicine* 16, (2010), 262-270.

[8] S.T. Thanyani, V. Roberts, D.G.R. Siko, P. Vrey, J.A. Verschoor, A novel application of affinity biosensor technology to detect antibodies to mycolic acid in tuberculosis patients, *Journal of Immunological Methods* 332, (2008), 61-72.

[9] B.Y. Ng, W. Xiao, N.P. West, E.J. Wee, Y. Wang, M. Trau, Rapid, single-cell electrochemical detection of Mycobacterium tuberculosis using colloidal gold nanoparticles, *Analytical chemistry* 87, (2015), 10613-10618.

[10] A. Mansour, S. Tammam, A. Althani, H.M.E. Azzazy, A single tube system for the detection of *Mycobacterium tuberculosis* DNA using gold nanoparticles-based FRET assay, *Journal of Microbiological Methods* 139, (2017), 165-167.

[11] E.J. North, M. Jackson, R.E. Lee, New approaches to target the mycolic acid biosynthesis pathway for the development of tuberculosis therapeutics, *Current Pharmaceutical Design* 20, (2014), 4357-4378.

[12] N. Fogel, Tuberculosis: A disease without boundaries, *Tuberculosis* 95, (2015), 527-531.

[13] M. Watanabe, Y. Aoyagi, M. Ridell, D.E. Minnikin, Separation and characterization of individual mycolic acids in representative mycobacteria, *Microbiology* 147, (2001), 1825-1837.

[14] K. Gokulan, K.I. Varughese, Drug resistance in *Mycobacterium tuberculosis* and targeting the l, d-transpeptidase enzyme, *Drug Development Research* 80, (2019), 11-18.

[15] J. Madacki, F. Laval, A. Grzegorzewicz, A. Lemassu, M. Záhorszká, M. Arand, M. McNeil, M. Daffé, M. Jackson, M.-A. Lanéelle, Impact of the epoxide hydrolase EphD on the metabolism of mycolic acids in mycobacteria, *Journal of Biological Chemistry* 293, (2018), 5172-5184.

[16] W. Groenewald, M.S. Baird, J.A. Verschoor, D.E. Minnikin, A.K. Croft, Differential spontaneous folding of mycolic acids from *Mycobacterium tuberculosis*, *Chemistry and Physics of Lipids* 180, (2014), 15-22.

[17] M. Sajid, A.-N. Kawde, M. Daud, Designs, formats, and applications of lateral flow assay: A literature review, *Journal of Saudi Chemical Society* 19, (2015), 689-705.

[18] F.L. Ndlandla, V. Ejoh, A.C. Stoltz, B. Naicker, A.D. Cromarty, S. van Wyngaardt, M. Khati, L.S. Rotherham, Y. Lemmer, J. Niebuhr, C.R. Baumeister, J.R. Al Dulayymi, H. Swai, M.S. Baird, J.A. Verschoor, Standardization of natural mycolic acid antigen composition and production for use in biomarker antibody detection to diagnose active tuberculosis, *Journal of Immunological Methods* 435, (2016), 50-59.

[19] Y. Lemmer, L. Kalombo, R.-D. Pietersen, A.T. Jones, B. Semete-Makokotlela, S. Van Wyngaardt, B. Ramalapa, A.C. Stoltz, B. Baker, J.A. Verschoor, Mycolic acids, a promising mycobacterial ligand for targeting of nanoencapsulated drugs in tuberculosis, *Journal of Controlled Release* 211, (2015), 94-104.

[20] S. Shang, D. Kats, L. Cao, E. Morgun, D. Velluto, Y. He, Q. Xu, C.-R. Wang, E.A. Scott, Induction of *Mycobacterium tuberculosis* lipid-specific T cell responses by pulmonary delivery of mycolic acid-loaded polymeric micellar Nanocarriers, *Frontiers in Immunology* 9, (2018), 2709.

[21] A.T. Lucas, A. Moody, A.N. Schorzman, W.C. Zamboni, Importance, and considerations of antibody engineering in antibody-conjugates development from a clinical pharmacologist's perspective, *Antibodies* 10, (2021), 30.

[22] A.J. Jacobs, J. Mongkolsapaya, G.R. Screaton, H. McShane, R.J. Wilkinson, Antibodies and tuberculosis, *Tuberculosis* 101, (2016), 102-113.

[23] Y. Gao, X. Huang, Y. Zhu, Z. Lv, A brief review of monoclonal antibody technology and its representative applications in immunoassays, *Journal of Immunoassay and Immunochemistry* 39, (2018), 351-364.

[24] P. Nelson, G. Reynolds, E. Waldron, E. Ward, K. Giannopoulos, P. Murray, Demystified…: monoclonal antibodies, *Molecular Pathology* 53, (2000), 111.

[25] S. Wemmer, C. Mashau, J. Fehrsen, W. Van Wyngaardt, D.H. Du Plessis, Chicken scFvs and bivalent scFv-CH fusions directed against HSP65 of Mycobacterium bovis, *Biologicals* 38, (2010), 407-414.

[26] H. Ranchod, F. Ndlandla, Y. Lemmer, M. Beukes, J. Niebuhr, J. Al-Dulayymi, S. Wemmer, J. Fehrsen, M. Baird, J. Verschoor, The antigenicity and cholesteroid nature of mycolic acids determined by recombinant chicken antibodies, *PloS One* 13, (2018), e0200298.

[27] J.V. Kringelum, M. Nielsen, S.B. Padkjær, O. Lund, Structural analysis of B-cell epitopes in antibody: protein complexes, *Molecular Immunology* 53, (2013), 24-34.

[28] R. Reverberi, L. Reverberi, Factors affecting the antigen-antibody reaction, *Blood transfusion* 5, (2007), 227.

[29] W.L. Then, H. McLiesh, M.-I. Aguilar, G. Garnier, Duffy blood group (Fya & Fyb) analysis using surface plasmon resonance, *Biomedical Microdevices* 18, (2016), 101.

[30] A. Cheepsattayakorn, R. Cheepsattayakorn, Roles of nanotechnology in diagnosis and treatment of tuberculosis, *Journal of Nanotechnology in Diagnosis and Treatment* 1, (2013), 19-25.

[31] D. Mo, L. Hu, G. Zeng, G. Chen, J. Wan, Z. Yu, Z. Huang, K. He, C. Zhang, M. Cheng, Cadmium-containing quantum dots: properties, applications, and toxicity, *Applied Microbiology and Biotechnology* 101, (2017), 2713-2733.

[32] B. Ferrari, P. Bergquist, Quantum dots as alternatives to organic fluorophores for Cryptosporidium detection using conventional flow cytometry and specific monoclonal antibodies: lessons learned, *Cytometry Part A: The Journal of the International Society for Analytical Cytology* 71, (2007), 265-271.

[33] S.A. Gomes, C.S. Vieira, D.B. Almeida, J.R. Santos-Mallet, R.F. Menna-Barreto, C.L. Cesar, D. Feder,CdTe and CdSe quantum dots cytotoxicity: a comparative study on microorganisms, *Sensors* 11, (2011), 11664-11678.

[34] W.J. Parak, T. Pellegrino, C. Plank, Labelling of cells with quantum dots, *Nanotechnology* 16, (2005), R9.

[35] E.A. Jenrette, M.J. Farrell, J.A. Flowers, A.K. Pradhan, CdSe-ZnO Core–Shell quantum dots for protein detection: A potential sensing platform, *Nanomanufacturing* 1, (2021), 3-13.

[36] B. Ji, S. Koley, I. Slobodkin, S. Remennik, U. Banin, ZnSe/ZnS core/shell quantum dots with superior optical properties through thermodynamic shell growth, *Nano letters* 20, (2020), 2387-2395.

[37] I. Martynenko, A. Litvin, F. Purcell-Milton, A. Baranov, A. Fedorov, Y. Gun'ko, Application of semiconductor quantum dots in bioimaging and biosensing, *Journal of Materials Chemistry B* 5, (2017), 6701-6727.

[38] D. Vasudevan, R.R. Gaddam, A. Trinchi, I. Cole, Core–shell quantum dots: Properties and applications, *Journal of Alloys and Compounds* 636, (2015), 395-404.

[39] O. Adegoke, T. Nyokong, P.B. Forbes, Structural and optical properties of alloyed quaternary CdSeTeS core and CdSeTeS/ZnS core–shell quantum dots, *Journal of Alloys and Compounds* 645, (2015), 443-449.

[40] O. Adegoke, P. Mashazi, T. Nyokong, P.B. Forbes, Fluorescence properties of alloyed ZnSeS quantum dots overcoated with ZnTe and ZnTe/ZnS shells, *Optical Materials* 54, (2016), 104-110.

[41] C.M. Bonilla, V.V. Kouznetsov, Green'quantum dots: basics, Green synthesis, and nanotechnological applications, *Green Nanotechnology-Overview and Further Prospects* (2016), 174-192.

[42] S. Chung, R.A. Revia, M. Zhang, Graphene quantum dots and their applications in bioimaging, biosensing, and therapy, *Advanced Materials* (2019), 1904362.

[43] C. Zhao, X. Song, Y. Liu, Y. Fu, L. Ye, N. Wang, F. Wang, L. Li, M. Mohammadniaei, M. Zhang, Synthesis of graphene quantum dots and their applications in drug delivery, *Journal of Nanobiotechnology* 18, (2020), 1-32.

[44] P. Tian, L. Tang, K. Teng, S. Lau, Graphene quantum dots from chemistry to applications, *Materials Today Chemistry* 10, (2018), 221-258.

[45] W. Chen, G. Lv, W. Hu, D. Li, S. Chen, Z. Dai, Synthesis, and applications of graphene quantum dots: a review, *Nanotechnology Reviews* 7, (2018), 157-185.

[46] B.D. Mansuriya, Z. Altintas, Applications of graphene quantum dots in biomedical sensors, *Sensors* 20, (2020), 1072.

[47] J. Drbohlavova, V. Adam, R. Kizek, J. Hubalek, Quantum dots-characterization, preparation and usage in biological systems, *International Journal of Molecular Sciences* 10, (2009), 656-673.

[48] R. Bilan, F. Fleury, I. Nabiev, A. Sukhanova, Quantum Dot Surface Chemistry and Functionalization for Cell Targeting and Imaging, *Bioconjugate Chemistry* 26, (2015), 609-624.

[49] A. Maleki, R. Taheri-Ledari, J. Rahimi, M. Soroushnejad, Z. Hajizadeh, Facile peptide bond formation: effective interplay between isothiazolone rings and silanol groups at silver/iron oxide nanocomposite surfaces, *American Chemical Sociaty Omega* 4, (2019), 10629-10639.

[50] M. Alhajj, A. Farhana, Enzyme linked immunosorbent assay, *StatPearls [Internet]* (2021).

[51] S. Sakamoto, W. Putalun, S. Vimolmangkang, W. Phoolcharoen, Y. Shoyama, H. Tanaka, S. Morimoto, Enzyme-linked immunosorbent assay for the quantitative/qualitative analysis of plant secondary metabolites, *Journal of Natural Medicines* 72, (2018), 32-42.

[52] B. Pongkitwitoon, S. Sakamoto, H. Tanaka, R. Tsuchihashi, J. Kinjo, S. Morimoto, W. Putalun, Enzyme-linked immunosorbent assay for total isoflavonoids in Pueraria candollei using anti-puerarin and anti-daidzin polyclonal antibodies, *Planta Medica* 76, (2010), 831-836.

[53] E.B. Bahadır, M.K. Sezgintürk, Lateral flow assays: Principles, designs and labels, *TrAC Trends in Analytical Chemistry* 82, (2016), 286-306.

[54] L. Anfossi, F. Di Nardo, S. Cavalera, C. Giovannoli, G. Spano, E.S. Speranskaya, I.Y. Goryacheva, C. Baggiani, A lateral flow immunoassay for straightforward determination of fumonisin mycotoxins based on the quenching of the fluorescence of CdSe/ZnS quantum dots by gold and silver nanoparticles, *Microchimica Acta* 185, (2018), 94.

[55] K. Surasak, S.M. JA, N. Nam-Trung, Challenges and perspectives in the development of paper-based lateral flow assays, *Microfluidics and Nanofluidics* 24, (2020), 17.

[56] J. Li, L. Jing, Y. Song, J. Zhang, Q. Chen, B. Wang, X. Xia, Q. Han, Rapid detection of rongalite via a sandwich lateral flow strip assay using a pair of aptamers, *Nanoscale Research Letters* 13, (2018), 1-7.

[57] S.-W. Lin, C.-H. Chang, C.-H. Lin, High-throughput fluorescence detections in microfluidic systems, *Genomic Medicine, Biomarkers, and Health Sciences* 3, (2011), 27-38.

[58] S. Shaikh, C. O'Donnell, Applications of fluorescence spectroscopy in dairy processing: A review, *Current Opinion in Food Science* 17, (2017), 16-24.

[59] A. Boreham, R. Brodwolf, K. Walker, R. Haag, U. Alexiev, Time-resolved fluorescence spectroscopy and fluorescence lifetime imaging microscopy for characterization of dendritic polymer nanoparticles and applications in nanomedicine, *Molecules* 22, (2017), 17.

[60] A.P. Demchenko, The concept of λ-ratiometry in fluorescence sensing and imaging, *Journal of Fluorescence* 20, (2010), 1099-1128.

[61] J. Zimmermann, A. Zeug, B. Röder, A generalization of the Jablonski diagram to account for polarization and anisotropy effects in time-resolved experiments, *Physical Chemistry Chemical Physics* 5, (2003), 2964-2969.

[62] L. Wu, C. Huang, B.P. Emery, A.C. Sedgwick, S.D. Bull, X.-P. He, H. Tian, J. Yoon, J.L. Sessler, T.D. James, Förster resonance energy transfer (FRET)-based small-molecule sensors and imaging agents, *Chemical Society Reviews* 49, (2020), 5110-5139.

[63] I.P. Kaur, J. Singh, J.V. Yakhmi, G. Singh, C. Dejous, A. Bhatia, A. Sattee, U. Soni, Bioconjugated quantum dots in rapid detection of water microbial load: An emerging technology, Advanced Research in Nanosciences for Water Technology, Springer 2019, 25-38.

[64] O. Adegoke, M.-W. Seo, T. Kato, S. Kawahito, E.Y. Park, An ultrasensitive SiO2-encapsulated alloyed CdZnSeS quantum dot-molecular beacon nanobiosensor for norovirus, *Biosensors and Bioelectronics* 86, (2016), 135-142.

[65] O. Adegoke, E.Y. Park, Bright luminescent optically engineered core/alloyed shell quantum dots: an ultrasensitive signal transducer for dengue virus RNA via localized surface plasmon resonance-induced hairpin hybridization, *Journal of Materials Chemistry B* 5, (2017), 3047-3058.

[66] C. Mi, T. Wang, P. Zeng, S. Zhao, N. Wang, S. Xu, Determination of ascorbic acid via luminescence quenching of LaF3:Ce,Tb nanoparticles synthesized through a microwave-assisted solvothermal method, *Analytical Methods* 5, (2013), 1463-1468.

[67] S. Tyagi, F.R. Kramer, Molecular beacons in diagnostics, *F1000 Medicine Reports* 4, (2012), 10.

[68] E.J. Kim, E.B. Kim, S.W. Lee, S.A. Cheon, H.-J. Kim, J. Lee, M.-K. Lee, S. Ko, T.J. Park,An easy and sensitive sandwich assay for detection of mycobacterium tuberculosis Ag85B antigen using quantum dots and gold nanorods, *Biosensors and Bioelectronics* 87, (2017), 150-156.

[69] M.H. Mat Zaid, J. Abdullah, N.A. Yusof, Y. Sulaiman, H. Wasoh, M.F. Md Noh, R. Issa,PNA biosensor based on reduced graphene oxide/water soluble quantum dots for the detection of mycobacterium tuberculosis, *Sensors and Actuators B: Chemical* 241, (2017), 1024-1034.

[70] Y. Guo, C. Sakonsinsiri, I. Nehlmeier, M.A. Fascione, H. Zhang, W. Wang, S. Pöhlmann, W.B. Turnbull, D. Zhou, Compact, polyvalent mannose quantum dots as sensitive, ratiometric FRET probes for multivalent protein–ligand interactions, *Angewandte Chemie International Edition* 55, (2016), 4738-4742.

[71] D. Bhattacharyya, P.K. Sarswat, M.L. Free, Quantum dots and carbon dots based fluorescent sensors for TB biomarkers detection, *Vacuum* 146, (2017), 606-613.

[72] T.R. Shojaei, M.A.M. Salleh, K. Sijam, R.A. Rahim, A. Mohsenifar, R. Safarnejad, M. Tabatabaei, Fluorometric immunoassay for detecting the plant virus citrus tristeza using carbon nanoparticles acting as quenchers and antibodies labeled with CdTe quantum dots, *Microchimica Acta* 183, (2016), 2277-2287.

[73] H. Yang, L. Qin, Y. Wang, B. Zhang, Z. Liu, H. Ma, J. Lu, X. Huang, D. Shi, Z. Hu, Detection of mycobacterium tuberculosis based on H37R(v) binding peptides using surface functionalized magnetic

microspheres coupled with quantum dots – a nano detection method for *Mycobacterium tuberculosis*, *International Journal of Nanomedicine* 10, (2014), 77-88.

[74] C. Zhang, J. Lou, W. Tu, J. Bao, Z. Dai, Ultrasensitive electrochemical biosensing for DNA using quantum dots combined with restriction endonuclease, *Analyst* 140, (2015), 506-511.

[75] L. Zhu, X. Cui, J. Wu, Z. Wang, P. Wang, Y. Hou, M. Yang, Fluorescence immunoassay based on carbon dots as labels for the detection of human immunoglobulin G, *Analytical Methods* 6, (2014), 4430-4436.

[76] S. Gupta, A. Kaushal, A. Kumar, D. Kumar, Ultrasensitive transglutaminase based nanosensor for early detection of celiac disease in human, *International Journal of Biological Macromolecules* 105, (2017), 905-911.

[77] N. Li, R. Li, Z. Li, Y. Yang, G. Wang, Z. Gu, Pentaethylenehexamine and histidine-functionalized graphene quantum dots for ultrasensitive fluorescence detection of microRNA with target and molecular beacon double cycle amplification strategy, *Sensors and Actuators B: Chemical* 283, (2019), 666-676.

[78] M. Beukes, Y. Lemmer, M. Deysel, J.a.R. Al Dulayymi, M.S. Baird, G. Koza, M.M. Iglesias, R.R. Rowles, C. Theunissen, J. Grooten, G. Toschi, V.V. Roberts, L. Pilcher, S. Van Wyngaardt, N. Mathebula, M. Balogun, A.C. Stoltz, J.A. Verschoor, Structure–function relationships of the antigenicity of mycolic acids in tuberculosis patients, *Chemistry and Physics of Lipids* 163, (2010), 800-808.

CHAPTER THREE: Synthesis and characterisation of quantum dots coupled to mycolic acids as a water-soluble fluorescent probe for potential lateral flow detection of antibodies and diagnosis of tuberculosis

This chapter deals with the synthesis and characterisation of a water-soluble quantum dots-mycolic acid probe for detection of tuberculosis antibodies and is presented in the form of the final published paper in *Luminescence*.

Paper

K. P. Kabwe, S. A. Nsibande, Y. Lemmer, L. A. Pilcher, P. B. C. Forbes, Synthesis, and characterisation of quantum dots coupled to mycolic acids as a water-soluble fluorescent probe for potential lateral flow detection of antibodies and diagnosis of tuberculosis, *Luminescence*, 2022, 37(2), 278-289. DOI: *https://doi.org/10.1002/bio.4170*

Author contributions

Kapambwe. P. Kabwe: Methodology, Validation, Investigation, Data curation, Formal analysis, Writing-Original draft**. Sifiso A. Nsibande:** Visualization, Validation, Writing-Review & Editing**. Yolandy Lemmer:** Supervision, Conceptualization, Resources, Writing-Review & Editing. **Lynne A. Pilcher:** Supervision, Conceptualization, Funding acquisition, Resources, Writing-Review & Editing**. Patricia B.C. Forbes:** Supervision, Conceptualization, Funding acquisition, Resources, Writing-Review & Editing.

Received: 27 August 2021 | Revised: 3 November 2021 | Accepted: 6 November 2021
DOI: 10.1002/bio.4170

RESEARCH ARTICLE

LUMINESCENCE The Journal of Biological and Chemical Luminescence WILEY

Synthesis and characterisation of quantum dots coupled to mycolic acids as a water-soluble fluorescent probe for potential lateral flow detection of antibodies and diagnosis of tuberculosis

Kapambwe P. Kabwe[1] | Sifiso A. Nsibande[1] | Yolandy Lemmer[2] | Lynne A. Pilcher[1] | Patricia B. C. Forbes[1]

[1]Department of Chemistry, Faculty of Natural and Agricultural Sciences, University of Pretoria, Pretoria, South Africa

[2]CSIR-Next Generation Health, Pretoria, South Africa

Correspondence
Patricia B.C. Forbes, Department of Chemistry, Faculty of Natural and Agricultural Sciences, University of Pretoria, Pretoria, South Africa.
Email: patricia.forbes@up.ac.za

Funding information
TWAS-NRF doctoral scholarship; University of Pretoria

Abstract

This work explores the potential use of cadmium-based quantum dots (QDs) coupled to mycolic acids (MAs) as a fluorescent probe to detect anti-MA antibodies which are biomarkers for tuberculosis (TB). The use of free MAs as antigens for the serodiagnosis of TB is known but has not been developed into a point of care test. This study focuses on the synthesis, solubility, and lateral flow of QDs coupled to MAs. Water-soluble CdSe/ZnS QDs capped with L-cysteine were synthesised and covalently coupled to MAs via amide linkages to form a water-soluble fluorescent probe: MA-CdSe/ZnS QDs. The MA-CdSe/ZnS QDs showed broad absorption bands and coupling, confirmed by the presence of amide bonds in the Fourier-transform infrared (FTIR) spectrum, resulting in a blue shift in fluorescence. Powder X-ray diffraction (XRD) revealed a shift and increase in the number of peaks for MA-CdSe/ZnS QDs relative to the L-cys-CdSe/ZnS QDs, suggesting that coupling changed the crystal structure. The average particle size of MA-CdSe/ZnS QDs was ~3.0 nm. Visual paper-based lateral flow of MA-CdSe/ZnS QDs was achieved on strips of nitrocellulose membrane with both water and membrane blocking solution eluents. The highly fluorescent MA-CdSe/ZnS QDs showed good water solubility and lateral flow, which are important properties for fluorescence sensing applications.

KEYWORDS
biomarkers, fluorescence, mycolic acids, quantum dots, tuberculosis

1 | INTRODUCTION

Tuberculosis (TB) is a global health problem due to co-infection with HIV (human immunodeficiency virus) and the development of drug-resistant strains. It is a chronic pulmonary disease caused by the *Mycobacterium tuberculosis* (M.tb) bacterium.[1] M.tb is transmitted through sputum droplets released through speaking, coughing, and sneezing, and the bacterium replicates every 18–72 h.[2] M.tb can be taken up by alveolar macrophages and forms a protective granuloma to sustain a long-term infection.[3] TB is a serious challenge in developing countries as well as an increasing scourge in many developed areas of the world. The World Health Organisation (WHO) Global Tuberculosis Series 2020 reported that 10.0 million new cases of TB in 2019, and 1.5 million TB deaths among HIV-positive people were recorded.[4]

Despite considerable improvement in the diagnosis of TB over the past years, a simple and effective method for the early detection of TB at the point of care is not yet available.[5] As a result, the start

of treatment could be delayed, allowing the disease to spread. Some of the current challenges in TB detection and diagnosis include inaccurate results, low sensitivity and time taken between detection and the correct diagnosis. The more accurate TB tests that are currently used, such as chest X-rays, are expensive particularly for developing countries.[5] The occurrence of TB and the increased risk of TB in HIV infected persons have boosted the need for rapid, inexpensive, and accurate methods for the detection and diagnosis of TB.

Sputum analysis research has been conducted to determine the presence of live M.tb in different ways and is used in TB detection and diagnosis. This technique is very sensitive with a low detection limit for M.tb, but it takes 6–8 weeks to give a diagnosis. Because of this delayed diagnosis, patient care and TB control can be affected as it gives enough time for the spread of the infection. The other limitation is that HIV infected patients do not produce the desired quality sputum sample for TB detection due to their weak immune systems.[6] The lipoarabinomannan (LAM) urine dipstick test is also used to diagnose TB.[7] The use of this test has gained popularity as it is simple, easy to use and is more sensitive than the sputum test for people with HIV. Although the LAM test has worked well for people with very low CD4 counts, false negatives are common and other confirmatory TB tests need to be conducted.[7,8] The colloidal gold test is another method used to detect antibodies to TB in blood serum. This involves marking of antigens on gold nanoparticles to establish an antigen colloidal gold immunochromatographic assay.[9] In this test, the antibodies from TB patients bind to the antigens marked on the colloidal gold nanoparticles to form antibody–antigen gold nanoparticle complexes. These complexes then produce a colour to indicate that the antibodies have been detected. The method works well because it is sensitive and specific, but the detection process is time-consuming as it involves a longer period of incubation, and the potential toxicity of gold nanoparticles limits its application.[9,10] Therefore, a more simplified and user-friendly test is required for TB antibody detection.

Mycolic acids (MAs) are the most abundant lipids found in the cell walls of M.tb.[11] These long chain waxes with chain lengths of 60 to 90 carbons form a hydrophobic shell around the organism, protecting it from attack by oxygen radicals, cationic proteins, and lysozymes that are found in the phagocytic granule.[12] It has been determined that MAs are antigenic, eliciting an immune response even in immune compromised HIV positive individuals.[13] The antibodies to MAs can be used as surrogate markers for active TB. However, the poor solubility of MAs in most solvents (they are only soluble in chloroform and hexane) presents the biggest challenge in their application.[14] The Mycolic Acid Real Time Inhibition (MARTI) test that has good accuracy and sensitivity in both HIV− and HIV+ patients has been developed based on the detection of anti-MA antibodies in human serum using surface plasmon resonance,[15] or electrochemical impedance spectroscopy (EIS).[16] The MARTI EIS technology has been adapted to the use of screen-printed electrodes with the aim of developing a reliable point of care diagnostic,[17] but the technology is proving challenging.

Cadmium-based quantum dots (QDs) are nanocrystals with the size range between 1 and 10 nm.[18] Different cadmium-based QDs have been produced over the past decades and have been applied in various fields because of their electronic and optical properties including; high surface to volume ratio, size-tuneable band gap energy, narrow emission spectra and broad absorption spectra. Cadmium-based QDs also have high fluorescence quantum yields and higher resistance to photo-initiated degradation as compared to organic fluorophores. The functional groups bound on the surface of QDs define their solubility and strongly influence their physical and photophysical properties. The shell protects material inside the core against photo-oxidation degradation and provides another way for surface functionalisation with different ligands. Because of these properties, cadmium-based QDs have been used extensively in scientific and technological applications that rely on achieving spectral purity at optimum optical flux such as chemical/biological sensing, optoelectronic devices, molecular biology, bioimaging, and photochemistry.[19–21]

The paper-based lateral-flow assay is a simple, low-cost test that is used to detect the presence of a target analyte; usually an antibody in a solution. The assay is used for biological applications including rapid detection of diseases based on the biochemical interactions, such as antigen–antibody interaction without much sample processing, making it ideal for a point of care diagnostic tool.[22] The lateral flow device consists of four sections mounted on the cardboard support for easy handling and stability. The sample pad is the first section where the sample is introduced. The conjugation pad is the region where the biomarker antibodies in the sample and pre-loaded labelled antigen combine to form an immune complex. The immune complex flows through the nitrocellulose membrane towards the test line for further antigen–antibody interaction between the immune complex and immobilised antibody. Attached at the end of the strip is an absorbent pad used as a reservoir for waste and preventing the backflow of the liquid.[23,24] To develop such a test based on the MA–anti-MA (antigen–antibody) interaction one could make use of anti-MA antibodies that have been developed,[25] but it would be necessary to add a fluorescent tag to the MAs in order to visualise the antibody–antigen–antibody aggregate and it would be necessary to solubilize the hydrophobic MAs in order for it to interact with the aqueous serum.

To the best of our knowledge, the use of MAs coupled to water-soluble CdSe/ZnS QDs capped with L-cysteine has not been previously reported as a water-soluble fluorescent TB probe. It is anticipated that the coupling of MAs to water-soluble fluorescent CdSe/ZnS QDs would improve its solubility and open doors for it to be used as a fluorescent probe that can be used for detection of anti-MA antibodies in serum for the diagnosis of TB. Here we report on the coupling of MAs to water-soluble core/shell CdSe/ZnS QDs capped with L-cysteine for the first time, and we show that this improves the solubility of MAs. We show for the first time the visual paper-based lateral flow of MA-CdSe/ZnS QDs through a nitrocellulose membrane. This work demonstrates the potential application of MA-CdSe/ZnS QDs as a fluorescent TB biomarker.

2 | EXPERIMENTAL

2.1 | Materials and reagents

Cadmium oxide (CdO, 99.5%), oleic acid (OA, 90%), octadecene (ODE, 90%), selenium (Se, 99%), trioctylphosphine oxide (TOPO, 90%), sulphur (S, 99.5%), zinc oxide (ZnO, 99%) L-cysteine (96%), L-cystine (98%), 1-ethyl-3-(3-dimethylaminopropyl)carbodiimide (EDC, 98%), *N*-hydroxysuccinimide (NHS, 98%), dicyclohexycarbodiimide (DCC, 98%), thionyl chloride (98%), oxalyl chloride (98%) and MA (98%) were purchased from Sigma-Aldrich (Baden-Württemberg, Germany) and were used without further purification. The solvents: methanol (99%), acetone (99.5%), dichloromethane (DCM, 99.8%), tetrahydrofuran (THF), dimethylformamide (DMF, 99%), ethyl acetate (98%), dimethyl sulphoxide (DMSO, 99%), and chloroform (99%) were purchased from Associated Chemical Enterprises, Johannesburg, South Africa and were also used as received. Other solid materials that were purchased from Associated Chemical Enterprises include sodium chloride (99%), potassium chloride (99%), disodium phosphate (Na_2HPO_4, 98%), potassium dihydrogen phosphate (KH_2PO_4, 98%), Potassium hydroxide (KOH, 85%), sodium sulphate (99%), sodium hydrogen carbonate (98%) and sodium hydroxide (97%). Stearic acid (99%), glycine (99%), hydrochloric acid (98%), pyridine (99.5%), and triethylamine (TEA, 99%) were purchased from Radchem Laboratory Chemicals and Consumables (Alberton, South Africa). Argon was supplied by African Oxygen Limited (Afrox, South Africa) while deionised water was obtained from an in-house laboratory water purification system (Drawell Scientific Instrument Co, Ltd, Shanghai, China). Macherey-Nagel Whatman filter papers (MN 615 diameter 125 mm) were purchased from Altmann Analytik (Munich, Germany).

2.2 | Equipment

The ground state electronic absorption of CdSe/ZnS QDs, L-cys-CdSe/ZnS QDs, MA-CdSe/ZnS QDs and 4MA-CdSe/ZnS QDs were recorded on a Cary Eclipse ultraviolet (UV)-visible spectrophotometer (Varian Pty Ltd, Belrose, Australia) with the wavelength range 200 to 800 nm. Fluorescence emission results were achieved using a Horiba Jobin Yvon Fluoromax-4 spectrofluorometer (Horiba Instruments Inc., Edison, NJ, USA). Infrared spectra in the range 4000–400 cm^{-1} were recorded on an Alpha (II) Bruker spectrometer (Bruker Optik, Ettlingen, Germany), equipped with Opus open-source software. The size and morphology of the materials were studied with transmission electron microscopy (TEM) (JEOL JEM 2100F; JOEL Ltd, Tokyo, Japan) with emission at 200 kV, and particle size distribution was determined with ImageJ software. Powder X-ray diffraction (XRD) patterns were recorded on a Bruker D2 phaser (Bruker, Karlsruhe, Germany) using Cu (Kα) radiation (wavelength of the X-ray source is 1.54184 Å). Proton (^1H) and carbon-13 (^{13}C) nuclear magnetic resonance (NMR) spectra were obtained using a Brucker Avance III 300 MHz NMR spectrometer (Bruker Biospin, Rheinstetten, Germany) in DMSO.

2.3 | Synthesis

2.3.1 | Synthesis of water-soluble core/shell CdSe/ZnS quantum dots capped with L-cysteine (L-cys-CdSe/ZnS QDs)

Before the CdSe/ZnS QDs were synthesised, three different precursors, namely Se, S and zinc precursors were prepared as sources of Se, S, and Zn, respectively, following a previously reported procedure,[26] with some modifications. For the Se precursor, 1.54 g of TOPO, which serves as a surfactant was dissolved in 20 ml of ODE and heated to ensure complete dissolution. After that, 0.24 g of Se powder was added and the mixture was sonicated for 10 min followed by stirring at room temperature overnight at 750 rpm. The S precursor was prepared by dissolving 1.54 g of TOPO in 24 ml of ODE and 16 ml of OA. The mixture was heated for a few minutes to ensure complete dissolution. Next, 0.13 g of S was added, and the mixture was heated for a few minutes and later sonicated for 15 to 20 min to speed up the dissolution of the S. The solution was kept stirring overnight at room temperature. The Zn precursor was prepared by adding 0.30 g of ZnO to the solution of 24 ml of ODE and 15 ml of OA at room temperature and stirred. The mixture was sonicated for 15 to 20 min to ensure complete dissolution and was stirred at room temperature overnight at 750 rpm.

After the preparation of the precursors, core/shell CdSe/ZnS QDs capped with L-cysteine were synthesised according to a previously reported method,[26,27] with minor modifications. Briefly, 1.00 g CdO as a source of cadmium (Cd) was added into a solution of 38 ml ODE and 23 ml OA. The reaction mixture was rapidly stirred for 30 min at 280°C under an inert environment (using argon) to form a colourless solution of Cd-ODE-OA. To this solution, 15 ml of the Se precursor was added to allow for nucleation and growth of the CdSe core. After 5 min, 15 ml of Zn and S precursors were added to the solution to passivate the core with a ZnS shell and reduce surface defects. The shell was allowed to grow at a reduced temperature of 200°C for 40 min and the colour changed from yellow to orange to red before the reaction was stopped. To obtain hydrophobic CdSe/ZnS QDs, methanol was added, and the mixture was allowed to stand overnight. The hydrophobic core/shell CdSe/ZnS QDs were then purified by washing with methanol and acetone with centrifuging at 6000 rpm.

The hydrophobic CdSe/ZnS QDs were made water-soluble by the addition of hydrophilic L-cysteine as follows: in 33 ml of methanol, 2.50 g of KOH and 1.70 g of L-cysteine were added and dissolved via ultra-sonication to form a solution of the methanolic-KOH-L-cysteine. After 10 min of ultra-sonication, hydrophobic CdSe/ZnS QDs dissolved in chloroform and deionised water was added until the mixture became clear. The solution was stirred for a few minutes and allowed to stand overnight at room temperature to allow for ligand exchange (Figure 1). The resulting water-soluble CdSe/ZnS QDs capped with L-cysteine (denoted as L-cys-CdSe/ZnS QDs) were purified by washing with acetone, chloroform, then with a mixture of acetone and chloroform, chloroform alone and finally with acetone through centrifugation at a speed of 6000 rpm.

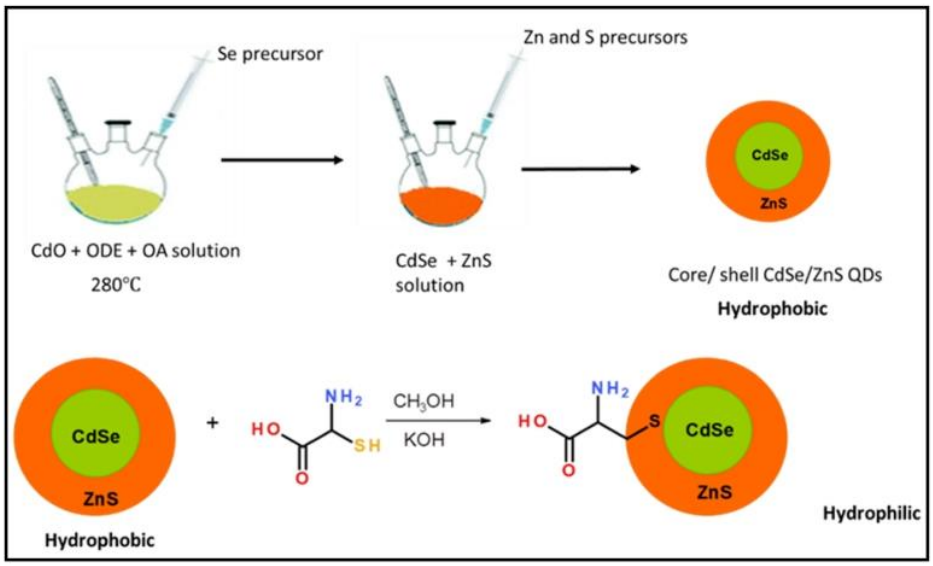

FIGURE 1 Schematic diagram illustrating the synthesis of water-soluble core/shell CdSe/ZnS QDs capped with L-cysteine

2.3.2 | Development of coupling reaction method

Several approaches had to be explored for the coupling of MAs to QDs. MAs are hydrophobic and soluble only in chloroform and hexane, whereas the QDs capped with L-cysteine are water soluble. This posed a challenge to synthesis: how to bring the compounds together for covalent coupling. Due to the high cost of MA, we set out to develop appropriate coupling chemistry using model compounds. Stearic acid was chosen as the model for MA due to its carboxylic acid group and 18-carbon hydrophobic chain, giving it similar solubility properties to MA. Glycine and the dipeptide cystine were selected as possible models for the surface capping on the QDs to allow for structural characterisation of the amide products by NMR analysis. Many different synthetic approaches have been developed for the formation of amide bonds, such as coupling acid chlorides to amines and carbodiimide chemistry. Attempts to use carbodiimide chemistry in the reaction of stearic acid with dipeptide L-cystine and stearic acid with glycine using EDC and NHS in acetone/water or DCC and NHS in water/THF were not successful. Stearic acid was successfully converted to stearic acid chloride using either thionyl chloride or oxalyl chloride in DCM, but the subsequent reaction with glycine refluxing in anhydrous DMF did not yield the amide. After a number of attempts, we achieved the coupling of the stearic acid chloride and glycine in dry chloroform or DCM using DMF as a catalyst. The coupling yield was improved by replacing DMF with triethylamine and adding a catalytic amount of pyridine. The structure of the stearoyl-glycine amide was confirmed using ^{1}H- and ^{13}C-NMR and Fourier-transform infrared (FTIR) analysis.

These reaction conditions were successfully employed for the coupling of stearic acid to L-cys-CdSe/ZnS QDs to form stearoyl-CdSe/ZnS QDs amide. The formation of stearoyl-CdSe/ZnS QDs amide was confirmed by FTIR to be similar to that of the stearic-glycine amide. A blue shift in the fluorescence emission wavelengths indicated a change in the surface structure of the QDs, and evidence of the successful coupling of stearic acid to the L-cys-CdSe/ZnS QDs.

2.3.3 | Coupling of stearic acid to glycine

In 10 ml of dry DCM, stearic acid (1.44 g) and 1 drop of DMF were mixed. The reaction mixture was stirred at room temperature for 5 min, then oxalyl chloride (1.00 ml) was added to the mixture. The mixture was left stirring at 750 rpm for 12 h at room temperature. The excess solvent was removed using a rotary evaporator to obtain a yellow oil product called stearoyl-chloride, which was used directly in the next step without purification.

To couple stearoyl-chloride to glycine, 0.78 g of glycine was dissolved in 16.2 ml of dry DCM with continuous stirring while purging with argon at 750 rpm. Two drops of pyridine were added to the reaction mixture as a catalyst. The mixture was stirred in the bath of acetone and dry ice to a temperate between −15°C to 0°C. Then, 1.2 ml of stearoyl chloride was added dropwise while cooling the mixture. Immediately after all the stearoyl-chloride was added, trimethylamine was added as a base. The mixture was kept stirred at 750 rpm for 12 h at room temperature. The reaction mixture was then filtered using Macherey-Nagel Whatman filter paper (MN 615 diameter 125 mm) to remove excess stearoyl-chloride. The filtrate was dried using a rotary evaporator to obtain orange crystals of stearoyl glycine amide, as illustrated in Figure 2.

Results: ^{1}H-NMR: δ_H (300 MHz; DMSO), 0.89 (3H, t, CH_3), 1.31 (30 H, m, 15 × CH_2), 2.16 (2H, t, CH_2), 3.86 (2H, d, CH_2), 8.11 (1H, t, NH), 10.07 (1H, s, COOH). ^{13}C-NMR: δ_C (300 MHz; DMSO), 15.13, 23.14, 25.31, 30.56, 32.63, 173.61,174.56. IR [(KBr) ν_{max}]: –C=O, 1700 cm $^{-1}$; –C–H, 3000 cm $^{-1}$; –N–H, 3320 cm $^{-1}$; –N–C=O, 2500–2650 cm $^{-1}$.

2.3.4 | Covalent coupling of mycolic acid to water-soluble core/shell CdSe/ZnS QDs capped with L-cysteine

In a 50 ml round bottomed flask, 3 ml of dry chloroform, 1.00 mg of MA and 1 drop of DMF were mixed. The reaction mixture was stirred

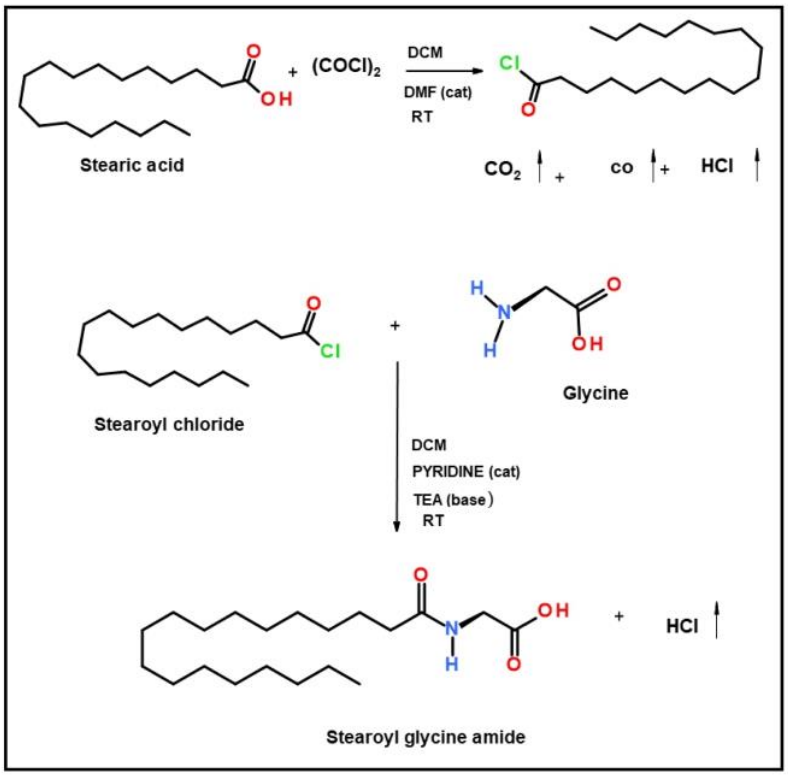

FIGURE 2 Schematic illustration of the covalent coupling of stearic acid to glycine to form stearoyl glycine amide

at room temperature for 5 min and then 0.50 ml of oxalyl chloride was added to the reaction mixture which was kept stirring at room temperature for 12 h at 750 rpm. After this, excess solvent was removed using a rotary evaporator to obtain mycolic acid chloride (MA-Cl) as a yellow oily product. MA-Cl was used directly in the next step without further purification.

To couple MA-Cl to hydrophilic CdSe/ZnS QDs, 0.06 g of the hydrophilic QDs were suspended in 3 ml of dry DCM in a 100 ml round bottomed flask and the suspension was purged with argon while stirring at 750 rpm for 5 min. Two drops of pyridine were added to the reaction mixture as a catalyst to replace chloride with pyridine. The mixture was placed in a bath of acetone and dry ice while stirring at a temperature between −15°C and 0°C. MA-Cl was added drop by drop while cooling the mixture. Immediately after MA-Cl, five drops of TEA were added as a base. The reaction mixture was left stirring at room temperature for 12 h at 750 rpm (Figure 3). The reaction mixture was then filtered (Macherey-Nagel Whatman filter paper MN 615 diameter 125 mm) to remove excess L-cys-CdSe/ZnS QDs. The filtrate was concentrated *in vacuo* to obtain orange crystals of MA-CdSe/ZnS QDs capped with L-cysteine denoted as MA-CdSe/ZnS QDs.

Covalent coupling of MA to water-soluble core/shell CdSe/ZnS QDs capped with L-cysteine was repeated using 4.00 mg of MAs, 9 ml of chloroform, and 1.5 ml of oxalyl chloride, following the same procedure as earlier. This was done to increase the amount of MAs on the coupled material. The new product was denoted as 4MA-CdSe/ZnS QDs.

2.4 | Determination of fluorescence quantum efficiency

The fluorescence quantum efficiency of QDs is measured in relation to fluorescence quantum yields (Φ_f) as previously reported.[28] In this study, the fluorescence quantum efficiency was measured by determining the fluorescence quantum yields of the QDs using equation (1), which compares the fluorescence intensities of the sample (I_{sam}) to Rhodamine 6G as a reference standard in ethanol (I_{std}) with respective absorbances of A_{sam} and $A_{std.}$ The fluorescence quantum yield of Rhodamine 6G was used as a standard denoted as Φ_{std}. The refractive index of water for L-cys-CdSe/ZnS QDs (n_{sam}), chloroform for CdSe/ZnS QDs (n_{sam}) and ethanol for Rhodamine 6G were used as standards (n_{std}), respectively.[29] The excitation wavelength (390 nm) was the same for all the measurements, while the absorbance values were kept at less than 0.05 to reduce inner filter effects.

$$\Phi_f = \Phi_{std} * \frac{I_{sam} * A_{std} * n_{sam}^2}{I_{std} * A_{sam} * n_{std}^2} \quad (1)$$

2.5 | Paper-based lateral flow of L-cys-CdSe/ZnS QDs, MA-CdSe/ZnS QDs and 4MA-CdSe/ZnS QDs

In small vials, 0.01 mg of L-cys-CdSe/ZnS QDs, MA-CdSe/ZnS QDs and 4MA-CdSe/ZnS QDs, respectively, were each dissolved in 100 µl

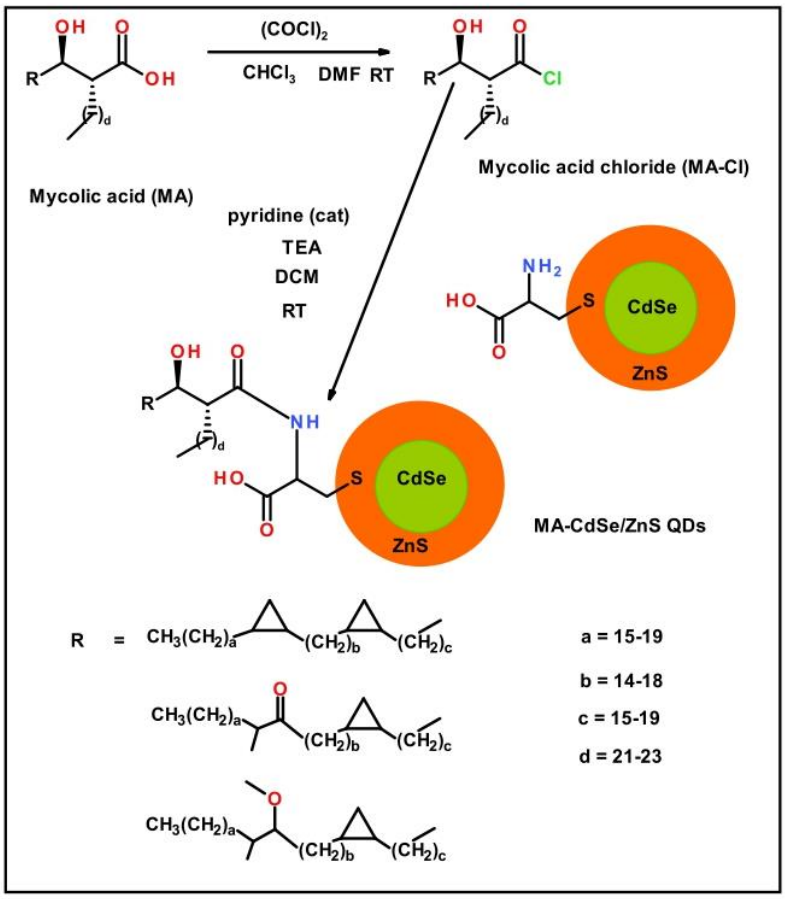

FIGURE 3 Schematic illustration of the covalent coupling of water-soluble CdSe/ZnS QDs capped with L-cysteine to MAs to form a water-soluble fluorescent probe for TB biomarkers: MA-CdSe/ZnS QDs. As natural MA isolated from *Mycobacterium tuberculosis* bovine strain was used, R represents a range of similar side chains of which the most common are shown

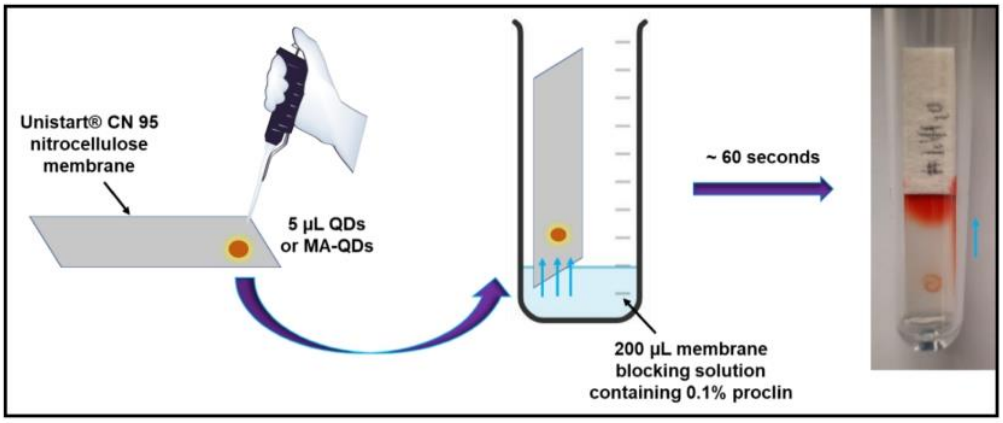

FIGURE 4 Schematic illustration of the procedure for the paper-based lateral flow test for L-cys-CdSe/ZnS QDs, MA-CdSe/ZnS QDs and 4MA-CdSe/ZnS QDs with membrane blocking solution as an eluent

of deionised water to form 0.1 g/L solutions. Two experiments were done in triplicate as follows: in the first experiment, water was used as an eluent with each of the materials (fluorophores) to determine if their flow on the strip of nitrocellulose membrane in water was visually noticeable. To do this, 5 µl aliquot of each of the 0.1 g/L solutions of the fluorophores was spotted onto the strips of nitrocellulose membrane using a 5 µl Eppendorf pipette. The strips were then placed vertically in individual test tubes containing 200 µl of water as an eluent as shown in Figure 4. In the second experiment, a membrane blocking solution containing 0.1% proclin was used as an eluent

instead of water with each of the fluorophores, following the same procedure. The resulting nitrocellulose membrane strips were then scanned using a light HP Scanjet 2400 flatbed scanner for visual analysis.

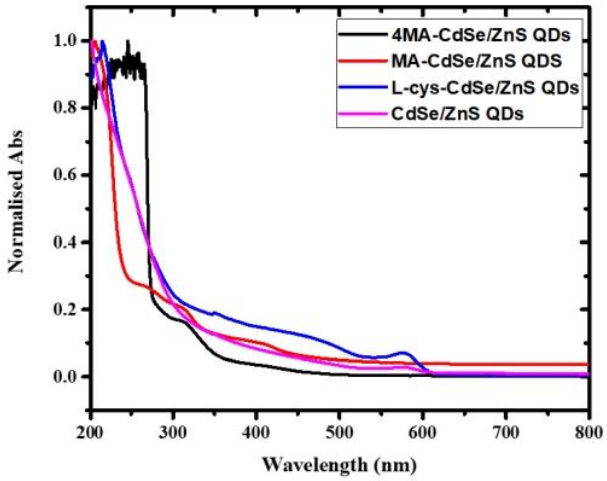

FIGURE 5 Normalised UV-visible absorption spectra of CdSe/ZnS QDs (dissolved in chloroform), L-cys-CdSe/ZnS QDs, MA-CdSe/ZnS QDs and 4MA-CdSe/ZnS QDs dissolved in water

3 | RESULTS AND DISCUSSION

3.1 | Absorption properties of CdSe/ZnS QDs, L-cys-CdSe/ZnS QDs, MA-CdSe/ZnS QDs and 4MA-CdSe/ZnS QDs

The optical properties of CdSe/ZnS QDs, L-cys-CdSe/ZnS QDs, MA-CdSe/ZnS QDs and 4MA-CdSe/ZnS QDs were investigated using UV-visible spectroscopy (Figure 5). The UV-visible spectra for all QD products show broad absorption bands from 200 to 300 nm which is a useful property, as it allows for varying excitation wavelengths to be employed in fluorescence sensing applications. These results show that the amount of MAs does not significantly affect the absorption bands of coupled material, although 4MA-CdSe/ZnS QDs had a strong absorption band in the region 220–260 nm.

3.2 | Effect of excitation wavelength on fluorescence emission spectra of L-cys-CdSe/ZnS QDs, MA-CdSe/ZnS QDs and 4MA-CdSe/ZnS QDs

The effect of excitation wavelength on the fluorescence emission wavelengths of L-cys-CdSe/ZnS QDs, MA-CdSe/ZnS QDs and 4MA-CdSe/ZnS QDs were investigated. Figure 6 shows that the excitation

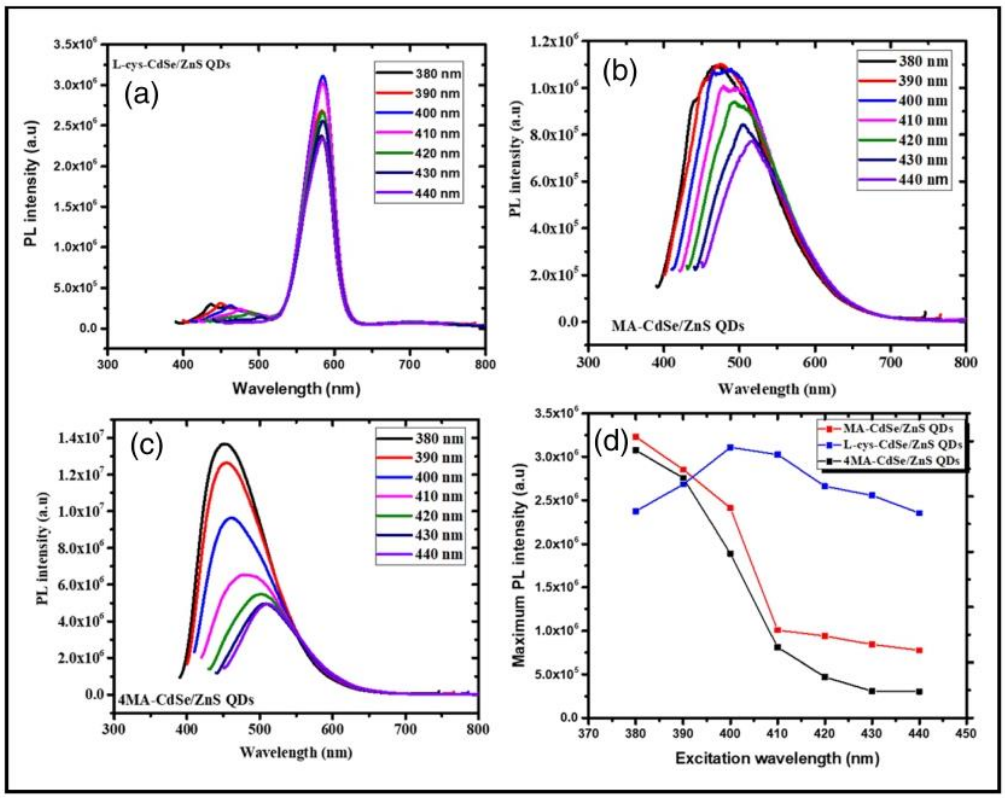

FIGURE 6 The effects of excitation wavelengths on the emission spectra of (a) L-cys-CdSe/ZnS QDs, (b) MA-CdSe/ZnS QDs and (c) 4MA-CdSe/ZnS QDs. (d) The effect of excitation wavelength on the maximum photoluminescence (PL) intensity of (a), (b) and (c)

wavelength that gave the highest emission wavelength intensity for L-cys-CdSe/ZnS QDs was 400 nm while for the MA-CdSe/ZnS QDs and for 4MA-CdSe/ZnS QDs it was 380 nm. It was noticed that changing the excitation wavelength did not affect the emission wavelength of L-cys-CdSe/ZnS QDs, but an increase in emission wavelength (red-shifting) was observed for MA-CdSe/ZnS QDs and 4MA-CdSe/ZnS QDs when the excitation wavelength was increased. The fluorescence emission intensity of L-cys-CdSe/ZnS QDs initially increased to the maximum and thereafter decreased while increasing the excitation wavelength (Figure 6a,d). For MA-CdSe/ZnS QDs and 4MA-CdSe/ZnS QDs, the fluorescence emission intensity continued to decrease while the excitation wavelength increased (Figure 6b,c,d).

3.3 | Fluorescent properties of CdSe/ZnS QDs, L-cys-CdSe/ZnS QDs, MA-CdSe/ZnS QDs and 4MA-CdSe/ZnS QDs

The fluorescent properties of CdSe/ZnS QDs, L-cys-CdSe/ZnS QDs, MA-CdSe/ZnS QDs and 4MA-CdSe/ZnS QDs were investigated using fluorescence spectrophotometry (Figure 7). Hydrophilic CdSe/ZnS QDs were used in this study in preference to other hydrophilic QDs, such as $CsPbX_3$ QDs, because of their excellent stability. CdSe/ZnS QDs bind capping agents, such as L-cysteine, via ligand exchange. This serves as a stabiliser and refines the surface of CdSe/ZnS QDs, maintaining the photoluminescence (PL) properties of the QDs. In the case of $CsPbX_3$ QDs, these are made up of an ionic crystal structure and bind capping agents through surface ions. When these surface ions are exposed to water, light and high temperatures, they may degrade which affects the PL properties and stability of the QDs.[30,31]

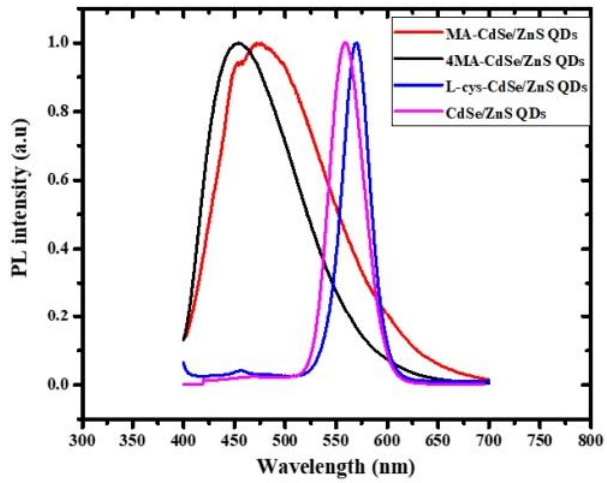

FIGURE 7 Normalised PL emission of CdSe/ZnS QDs (dissolved in chloroform), L-cys-CdSe/ZnS QDs, MA-CdSe/ZnS QDs and 4MA-CdSe/ZnS QDs dissolved in water. All samples were excited at 390 nm

The fluorescence emission spectra of CdSe/ZnS QDs and L-cys-CdSe/ZnS QDs prepared in this work were narrow having the same full width at half maximum (FWHM) of 40 nm with maximum emission wavelengths at 560 nm and 584 nm, respectively, when excited at 390 nm (Table 1). The attachment of L-cysteine ligands to the CdSe/ZnS QDs induced a red shift of the emission spectrum with

TABLE 1 Summary of photophysical properties of CdSe/ZnS QDs, L-cys-CdSe/ZnS QDs, MA-CdSe/ZnS QDs and 4MA-CdSe/ZnS QDs

	λ_{em} (nm)	FWHM (nm)	Φ_f (%)
CdSe/ZnS QDs	560	40	71.2
L-cys-CdSe/ZnS QDs	584	40	89.9
MA-CdSe/ZnS QDs	474	94	23.2
4MA-CdSe/ZnS QDs	454	81	22.8

Note: λ_{em} = wavelength at maximum emission, FWHM = full width at half maximum, and Φ_f = fluorescence quantum yield.

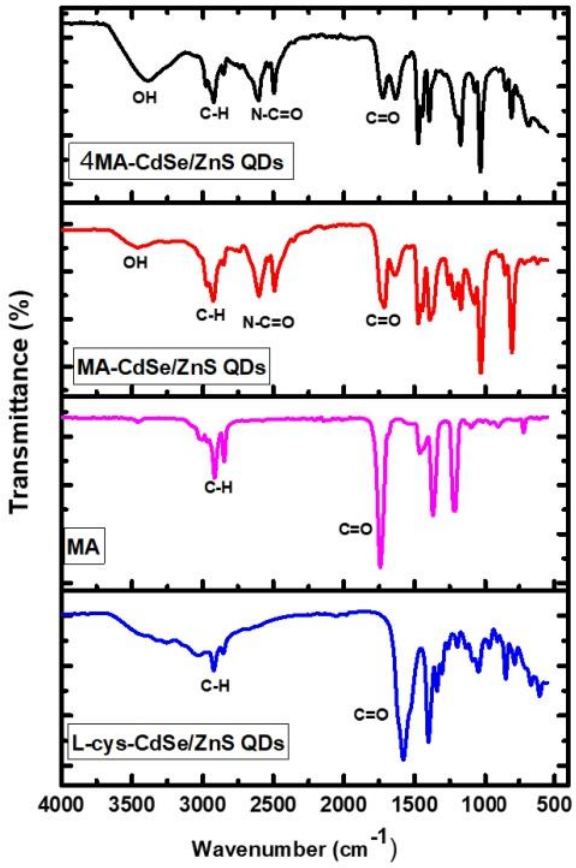

FIGURE 8 FTIR spectra of L-cys-CdSe/ZnS QDs, MA, MA-CdSe/ZnS QDs and 4MA-CdSe/ZnS QDs analysed in powder form

an increase in fluorescence quantum efficiency or quantum yield from 71.2% of CdSe/ZnS QDs to 89.9% of L-cys-CdSe/ZnS QDs likely due to surface passivation effects. Upon coupling 1.00 mg and 4.00 mg of MAs to L-cys-CdSe/ZnS QDs, the emission spectra became broader than that of the L-cys-CdSe/ZnS QDs and were slightly blue shifted with the maximum emission wavelength at 474 nm (FWHM = 94 nm) and 454 nm (FWHM = 81 nm), respectively. The coupling of MAs to L-cys-CdSe/ZnS QDs also caused a decrease in PL quantum yield. This remarkable blue shift and change in quantum yield can be attributed to a change in the surface states of the QDs and is an indication of the successful coupling of MAs to the L-cys-CdSe/ZnS QDs. Despite the emission maxima of these two MA-CdSe/ZnS QDs being broad, and blue shifted, it is notable that they have different emission wavelengths indicating that the amount of MAs used in coupling is responsible for the shift in emission wavelengths. The PL quantum yield, although reduced in the coupled product, was still sufficiently high to be fit for purpose.

3.4 | FTIR spectra of L-cys-CdSe/ZnS QDs, MAs, MA-CdSe/ZnS QDs and 4MA-CdSe/ZnS QDs

The FTIR spectrum of the L-cys-CdSe/ZnS QDs in Figure 8 shows characteristic peaks, i.e. –N–H, –C–H, and –C=O which confirms their

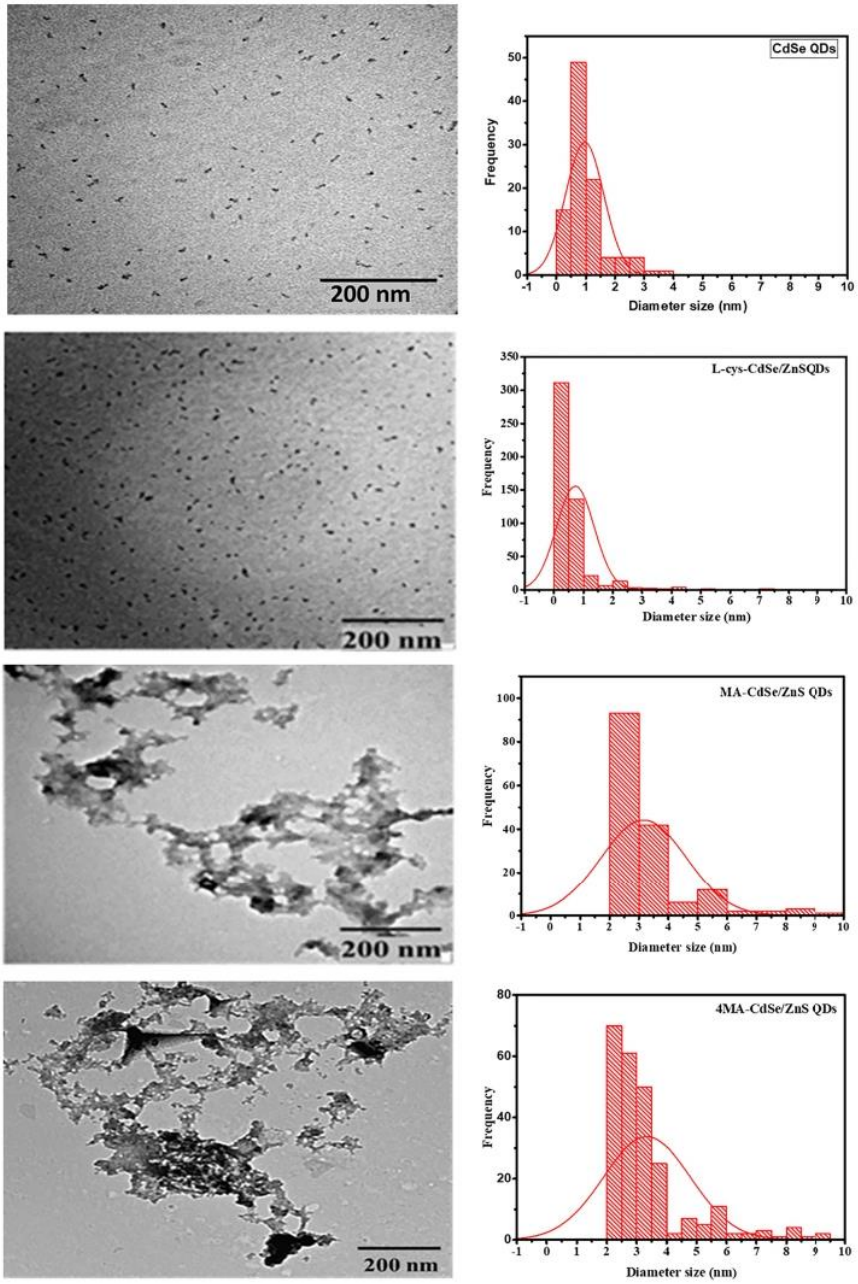

FIGURE 9 TEM micrographs of CdSe QDs (dissolved in chloroform), L-cys-CdSe/ZnS QDs, MA-CdSe/ZnS QDs and 4MA-CdSe/ZnS QDs dissolved in water

successful functionalisation with L-cysteine, while the spectrum for pure MA shows the expected –C–H and –C=O peaks in addition to the –O–H band. After the coupling of 1.00 mg of MA to L-cys-CdSe/ZnS QDs, two new bands that can be attributed to –N–C=O modes were observed between 2490 and 2602 cm^{-1}. These peaks in the MA-CdSe/ZnS QD spectrum indicate the presence of amide bonds, which confirms the successful coupling of MAs to L-cys-CdSe/ZnS QDs.[32,33] Similar results were observed when 4.00 mg of MA was used to prepare 4MA-CdSe/ZnS QDs. These results indicate that changing the amount of MAs does not affect the functional groups of the coupled material.

3.5 | TEM analysis of CdSe QDs, L-cys-CdSe/ZnS QDs, MA-CdSe/ZnS QDs and 4MA-CdSe/ZnS QDs

The morphology and particle size of CdSe QDs, L-cys-CdSe/ZnS QDs, MA-CdSe/ZnS QDs and 4MA-CdSe/ZnS QDs are shown in Figure 9. It is observed that core CdSe QDs dispersed well in chloroform while L-cys-CdSe/ZnS QDs dispersed well in water and had an average estimated particle size of 1.0 ± 0.1 nm and 1.0 ± 0.2 nm, respectively. The morphology of MA-CdSe/ZnS QDs and 4MA-CdSe/ZnS QDs show some particle aggregation. The average estimated particle size of MA-CdSe/ZnS QDs was 3.1 ± 0.8 nm, while 4MA-CdSe/ZnS QDs, was 3.3 ± 0.2 nm. This aggregation could be due to the presence of attractive forces between both hydrophilic and hydrophobic groups of the MA-QD particles and this leads to an increase in average particle size of MA-CdSe/ZnS QDs and 4MA-CdSe/ZnS QDs.[34] Changes in the environmental conditions of aggregated particles in porous media slightly affects the size of the coupled material.[34] As a result of this, different average particle sizes were observed when the amount of MAs was increased during the coupling reaction.

3.6 | Powder XRD analysis of L-cys-CdSe/ZnS QDs, MA-CdSe/ZnS QDs and 4MA-CdSe/ZnS QD

Figure 10 shows broad peaks for L-cys-CdSe/ZnS QDs at 25.5° (111), 43.3° (200) and 50.6° (311) corresponding to the Zn blende crystal structure as reported previously for this material.[26] MA-CdSe/ZnS QDs have sharper peaks with a significant shift to the left at 7.4° (100), 12.6° (111), 16.4° (210), 20.2° (220), 22.9° (310), 28.2° (321), and 30.0° (322). This shift and the increase in the number of peaks suggests that the coupling of MAs to L-cys-CdSe/ZnS QDs resulted in a change in the crystal phase, which is expected due to the non-crystalline MA moieties present in the MA-CdSe/ZnS QDs. Sharp peak positions of MA-CdSe/ZnS QDs show the crystal structure of the resulting material.

Similarly, sharp peak positions were observed for 4MA-CdSe/ZnS QDs at different positions. The peak positions were at 9.7° (110), 19.7° (211), 23.0° (310), 25.9° (320), 27.9° (321), 35.3° (332) and 38.2° (333). These results suggest that increasing the amount of MAs during the synthesis of MA-CdSe/ZnS QDs slightly changes the crystal structure of the coupled material.

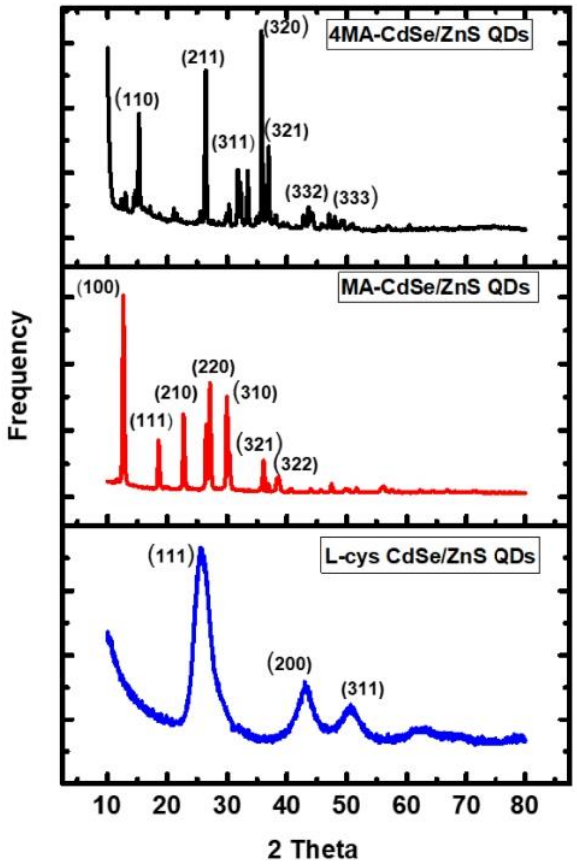

FIGURE 10 Powder XRD spectra of L-cys-CdSe/ZnS QDs, MA-CdSe/ZnS QDs and 4MA-CdSe/ZnS QDs

3.7 | Paper-based lateral flow of L-cys-CdSe/ZnS QDs, MA-CdSe/ZnS QDs and 4MA-CdSe/ZnS QDs

Paper-based lateral flow tests for L-cys-CdSe/ZnS QDs, MA-CdSe/ZnS QDs and 4MA-CdSe/ZnS QDs were conducted to investigate their potential application in TB detection and diagnosis. Figure 11 shows that L-cys-CdSe/ZnS QDs, MA-CdSe/ZnS QDs and 4MA-CdSe/ZnS QDs were able to visually flow through the strips of nitrocellulose membrane in both eluents, that is water and membrane blocking solution. Membrane blocking solution is a buffer solution used to block non-specific sites on the nitrocellulose membrane and made up of 0.1% proclin, water, bovine serum albumin (BSA), goat immunoglobulin G (IgG) and Tween® 20. The rate flow of the fluorophores through the strips of nitrocellulose membrane was fast enough to be seen with the naked eye.

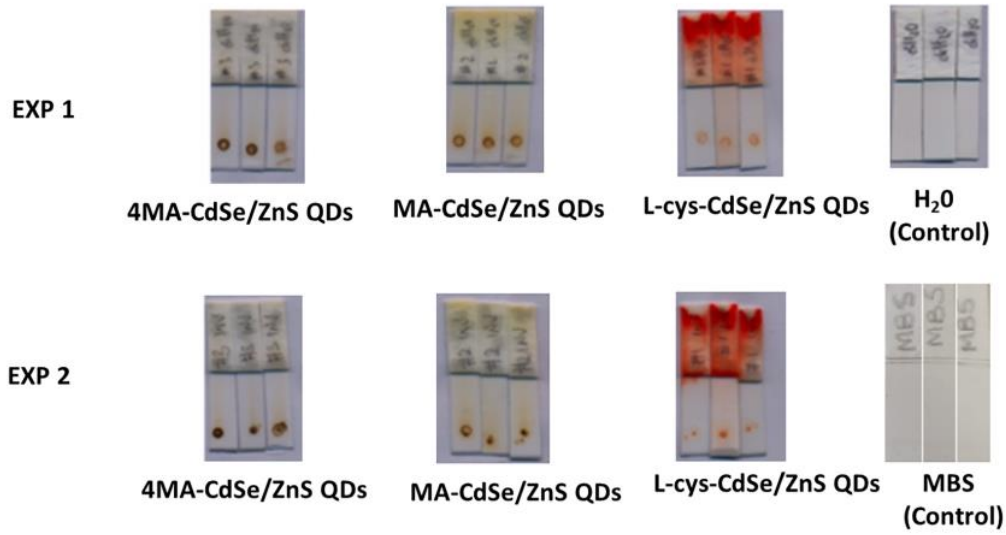

FIGURE 11 Images of the strips of nitrocellulose membrane taken after each of the two lateral flow experiments of L-cys-CdSe/ZnS QDs, MA-CdSe/ZnS QDs and 4MA-CdSe/ZnS QDs with water (experiment 1) and membrane blocking solution (MBS) (experiment 2) as eluents

4 | CONCLUSION

Water-soluble core/shell CdSe/ZnS QDs capped with L-cysteine were successfully synthesised and coupled to MAs to form MA-CdSe/ZnS QDs with potential prospects as a water-soluble fluorescent TB probe. The coupled MA-CdSe/ZnS QDs and synthesised L-cys-CdSe/ZnS QDs were characterised by absorption and fluorescence spectroscopy, TEM analysis, FTIR and XRD spectroscopy. The absorption results indicated that both CdSe/ZnS QDs and MA-CdSe/ZnS QDs show broad absorption bands ranging from 200 to 420 nm which allows for variation of excitation wavelengths in fluorescence sensing applications. It is also noted that the amount of MAs in the coupled material affected the emission wavelength thereof. Fluorescence results showed that CdSe/ZnS QDs and L-cys-CdSe/ZnS QDs had narrow emission spectra with maximum emission wavelengths at 560 nm and 584 nm, when exciting at 390 nm, while MA-CdSe/ZnS QDs and 4MA-CdSe/ZnS QDs had broader spectra with a maximum emission at 474 nm and at 454 nm, respectively. The presence of –N–C=O peaks in MA-CdSe/ZnS QDs and 4MA-CdSe/ZnS QDs FTIR spectra indicated the presence of amide bonds, which confirms the successful coupling of MAs to L-cys-CdSe/ZnS QDs. TEM analysis results showed average estimated size particle distribution of CdSe QDs to be 1.0 ± 0.1 nm, 1.0 ± 0.2 nm for L-cys-CdSe/ZnS QDs, 3.1 ± 0.8 nm for MA-CdSe/ZnS QDs and 3.3 ± 0.2 nm for 4MA-CdSe/ZnS QDs. The powder XRD results showed a shift and an increase in the number of peaks for MA-CdSe/ZnS QDs and 4MA-CdSe/ZnS QDs relative to the L-cys-CdSe/ZnS QDs. This suggests that the coupling of MAs to L-cys-CdSe/ZnS QDs changed the crystal structure of the MA-CdSe/ZnS QDs. Sharp peak positions observed in MA-CdSe/ZnS QDs and 4MA-CdSe/ZnS QDs confirms that changing the amount of MAs does not negatively affect the crystallinity of the material, but the crystal structure did change from the Zn blende of the uncoupled QDs. Paper-based lateral-flow experiments confirmed visually the flow of L-cys-CdSe/ZnS QDs, MA-CdSe/ZnS QDs and 4MA-CdSe/ZnS QDs through the nitrocellulose membrane with water and membrane blocking solution as eluents. Due to their good solubility in water (0.1 mg/ml), and high fluorescence, MA-QDs have the potential to be used as a point of care fluorescent probe for the lateral flow detection of antibodies and the diagnosis of TB.

ACKNOWLEDGEMENTS

TWAS-NRF doctoral scholarship funding and a University of Pretoria postgraduate student bursary is gratefully acknowledged (KK). The Next Generation Health unit of the CSIR, specifically Alma Truyts, is acknowledged for assisting with lateral flow experiments and the Microscopy and Microanalysis Laboratory of the University of Pretoria for assistance with microscopy measurements.

ORCID

Patricia B. C. Forbes https://orcid.org/0000-0003-3453-9162

REFERENCES

[1] N. Fogel, *Tuberculosis* **2015**, *95*, 527.
[2] T. R. Lerner, S. Borel, D. J. Greenwood, U. Repnik, M. R. Russell, S. Herbst, M. L. Jones, L. M. Collinson, G. Griffiths, M. G. Gutierrez, *J. Cell Biol.* **2017**, *216*, 583.
[3] A. Welin, J. Raffetseder, D. Eklund, O. Stendahl, M. Lerm, *J. Innate Immun.* **2011**, *3*, 508.
[4] D. R. Silva, F. C.d. Q. Mello, G. B. Migliori, *J. Bras. Pneumol.* **2020**, *46*, 1806.
[5] S. Sudha, *Int. J. Med. Eng. Inform.* **2016**, *8*, 27.
[6] T. R. Frieden, T. R. Sterling, S. S. Munsiff, C. J. Watt, C. Dye, *Lancet* **2003**, *362*, 887.

[7] J. Peter, C. Green, M. Hoelscher, P. Mwaba, A. Zumla, K. Dheda, *Curr. Opin. Pulm. Med.* **2010**, *16*, 262.
[8] S. T. Thanyani, V. Roberts, D. G. R. Siko, P. Vrey, J. A. Verschoor, *J. Immunol. Methods* **2008**, *332*, 61.
[9] M. S. Verma, J. L. Rogowski, L. Jones, F. X. Gu, *Biotechnol. Adv.* **2015**, *33*, 666.
[10] A. Mansour, S. Tammam, A. Althani, H. M. E. Azzazy, *J. Microbiol. Methods* **2017**, *139*, 165.
[11] E. J. North, M. Jackson, R. E. Lee, *Curr. Pharm. Des.* **2014**, *20*, 4357.
[12] M. Watanabe, Y. Aoyagi, M. Ridell, D. E. Minnikin, *Microbiology* **1825**, *2001*, 147.
[13] F. L. Ndlandla, V. Ejoh, A. C. Stoltz, B. Naicker, A. D. Cromarty, S. van Wyngaardt, M. Khati, L. S. Rotherham, Y. Lemmer, J. Niebuhr, C. R. Baumeister, J. R. Al Dulayymi, H. Swai, M. S. Baird, J. A. Verschoor, *J. Immunol. Methods* **2016**, *435*, 50.
[14] S. Shang, D. Kats, L. Cao, E. Morgun, D. Velluto, Y. He, Q. Xu, C.-R. Wang, E. A. Scott, *Front. Immunol.* **2018**, *9*, 2709.
[15] J. Verschoor, *Trop. Med. Int. Health* **2010**, *15*, 1360.
[16] J. A. Verschoor, C. Baumeister, A method of diagnosing tuberculosis, Google Patents, **2016**.
[17] J. A. Verschoor, I. E. Okeke, L. Kalombo, Y. Lemmer, Core elements for point of care diagnosis of tuberculosis, Google Patents, **2017**.
[18] A. Cheepsattayakorn, R. Cheepsattayakorn, *J. Nanotech. Diagn. Treat.* **2013**, *1*, 19.
[19] O. Adegoke, T. Nyokong, P. B. Forbes, *J. Alloys Compd.* **2015**, *645*, 443.
[20] O. Adegoke, P. Mashazi, T. Nyokong, P. B. Forbes, *Opt. Mater.* **2016**, *54*, 104.
[21] I. Martynenko, A. Litvin, F. Purcell-Milton, A. Baranov, A. Fedorov, Y. Gun'ko, *J. Mater. Chem. B* **2017**, *5*, 6701.
[22] E. B. Bahadır, M. K. Sezgintürk, *TrAC-Trends Anal. Chem.* **2016**, *82*, 286.
[23] L. Anfossi, F. Di Nardo, S. Cavalera, C. Giovannoli, G. Spano, E. S. Speranskaya, I. Y. Goryacheva, C. Baggiani, *Microchim. Acta* **2018**, *185*, 94.
[24] M. Sajid, A.-N. Kawde, M. Daud, *J. Saudi Chem. Soc.* **2015**, *19*, 689.
[25] H. Ranchod, F. Ndlandla, Y. Lemmer, M. Beukes, J. Niebuhr, J. Al-Dulayymi, S. Wemmer, J. Fehrsen, M. Baird, J. Verschoor, *PLoS ONE* **2018**, *13*, e0200298.
[26] H. Montaseri, P. B. Forbes, *Mater. Today Commun.* **2018**, *17*, 480.
[27] O. Adegoke, H. Montaseri, S. A. Nsibande, P. B. C. Forbes, *J. Alloys Compd.* **2017**, *720*, 70.
[28] Y. Chen, W. Xing, Y. Liu, X. Zhang, Y. Xie, C. Shen, J. G. Liu, C. Geng, S. Xu, *Nanomaterials* **2020**, *10*, 317.
[29] D. Magde, R. Wong, P. G. Seybold, *Photochem. Photobiol.* **2002**, *75*, 327.
[30] Y. Zhao, C. Xie, X. Zhang, P. Yang, *ACS Appl. Nano Mater.* **2021**, *4*, 5478.
[31] W. Shi, X. Zhang, H. S. Chen, K. Matras-Postolek, P. Yang, *J. Mater. Chem. C* **2021**, *9*, 5732.
[32] Y. Zhang, Y. Sun, T. Wang, J. Liu, B. Spingler, S. Duttwyler, *Molecules* **2018**, *23*, 3137.
[33] L. H. Chan-Chan, G. González-García, R. F. Vargas-Coronado, J. M. Cervantes-Uc, F. Hernández-Sánchez, A. Marcos-Fernandez, J. V. Cauich-Rodríguez, *Eur. Polym. J.* **2017**, *92*, 27.
[34] P. Babakhani, *Sci. Rep.* **2019**, *9*, 1.

How to cite this article: K. P. Kabwe, S. A. Nsibande, Y. Lemmer, L. A. Pilcher, P. B. C. Forbes, *Luminescence* **2022**, *37*(2), 278. https://doi.org/10.1002/bio.4170

CHAPTER FOUR: Development of a graphene quantum dot-mycolic acid probe as a potential tuberculosis biosensor

This chapter presents the development of a graphene quantum dot-mycolic acid probe as a potential tuberculosis biosensor. It is presented in the format as submitted to *Luminescence.*

Submitted manuscript

Kapambwe P. Kabwe, Sifiso A. Nsibande, Lynne A. Pilcher, Patricia B.C. Forbes, Development of a graphene quantum dot-mycolic acid probe as a potential tuberculosis biosensor, *Luminescence*, 2022.

Authorship contributions

Kapambwe. P. Kabwe: Methodology, Validation, Investigation, Data curation, Formal analysis, Writing-Original draft**. Sifiso A. Nsibande:** Visualization, Validation, Writing-Review & Editing**. Lynne A. Pilcher:** Supervision, Conceptualization, Funding acquisition, Resources, Writing-Review & Editing**. Patricia B.C. Forbes:** Supervision, Conceptualization, Funding acquisition, Resources, Writing-Review & Editing.

Development of a graphene quantum dot-mycolic acid probe as a potential tuberculosis biosensor

Kapambwe P. Kabwe, Sifiso A. Nsibande, Lynne A. Pilcher, Patricia B.C. Forbes*

Department of Chemistry, Faculty of Natural and Agricultural Sciences, University of Pretoria, Pretoria, South Africa

*Corresponding author: patricia.forbes@up.ac.za

Abstract

The development of amine-functionalized graphene quantum dots (GQDs) linked to mycolic acids (MAs) as a potential fluorescent biosensor to detect tuberculosis (TB) biomarkers (namely anti-MA antibodies) is described. GQDs are nanomaterials with attractive properties such as high fluorescence, excellent biocompatibility, good water solubility, and they are environmentally friendly because of their low toxicity. MAs are lipids that are found in the cell wall of *Mycobacterium tuberculosis* that are antigenic, however, they are soluble only in chloroform and hexane. Chloroform-soluble MAs were covalently linked to synthesized water-soluble GQDs using an amide connection to create a potential fluorescent water-soluble TB biosensor: MA-GQDs. Fluorescence results showed that GQDs had a narrow emission spectrum with the highest emission wavelength at 440 nm, while MA-GQDs had a broader spectrum with the highest emission at 470 nm, after exciting at 360 nm. The appearance of the peptide bond (amide linkage) in the FT-IR spectrum of MA-GQDs confirmed the successful linking of MAs to GQDs. Powder X-ray diffraction (XRD) exhibited an increase in the number of peaks for MA- GQDs relative to GQDs, suggesting that linking MAs to GQDs changed the crystal structure thereof. The linked MA-GQDs showed good solubility in water, high fluorescence, and visual flow through a nitrocellulose membrane. These properties are promising for biomedical fluorescence sensing applications.

Keywords: graphene quantum dots; mycolic acid; tuberculosis; lateral flow; fluorescence

1. Introduction

Graphene quantum dots (GQDs) are zero-dimensional carbon based nanocrystals with a diameter between 1-20 nm.[1] GQDs have been produced and widely studied in recent years due to their exceptional electronic, optical, and photoelectric attributes including: size-tunable bandgap energy and high surface to volume ratio.[2] Compared to semiconductor based quantum dots, GQDs possess attractive features such as stable fluorescence properties, simple and cost effective preparation methods, low toxicity, excellent biocompatibility, and good water solubility.[3] As a result of these exceptional attributes, GQD-based materials have been used in biological imaging, biosensing, drug delivery, optoelectrical detectors, solar cells, filtration devices, and photocatalysis.[4] Additionally, GQDS have emerged as potential fluorophores for biosensing in biological matrices such as human blood, urine, sputum, and saliva, due to the selectivity, sensitivity, and reproducibility of the results.[5]

Mycolic acids (MAs), also called 2-alkyl-3-hydroxy-long-chain fatty acids, are lipids that are located in the cell walls of *Mycobacterium tuberculosis* (M.tb), the agent that causes the disease tuberculosis (TB).[6] MAs are made up of a long beta-hydroxy chain and a long alpha-alkyl side chain.[7] Depending on the size and nature of the functional groups in the long hydroxy chain, MAs are divided into three main classes, namely alpha-MAs, methoxy-MAs, and keto-MAs.[8] MAs are sometimes referred to as antigenic cell wall lipids because they elicit an antibody response.[9] MAs are strongly hydrophobic molecules that create a lipid shell over the organism. This affects the permeability properties of the cell surface, hence protecting the organism against lysozymes, oxygen radicals, and cationic proteins. [10]

Anti-MA antibodies serve as specific TB biomarkers that can provide prognostic information about health status and can advance knowledge of disease pathogenesis in predicting reactivation, cure, and induced vaccine protection either for individual patients or study cohorts.[11] Detection of the anti-MA TB biomarker via its association with chemically inert

MAs is an attractive proposition. Nevertheless, the insolubility of MAs in bulk solvents apart from chloroform and hexane presents a big challenge to their application as biosensors and in TB diagnosis,[12] as the diagnostic assay is commonly achieved in aqueous buffer therefore a water-soluble probe is necessary.

The nitrocellulose membrane lateral flow assay is a technique used in medical diagnostics for point of care testing, laboratory use, and home testing to detect the target analyte, often an antibody in a liquid centered on an antigen-antibody interaction.[13] The nitrocellulose membrane lateral flow assay is typically comprised of four components, namely, the sample pad, conjugate pad, nitrocellulose membrane, and absorbent pad. The sample pad is where the sample is introduced first, acting as a sponge, and holding the sample fluid. The sample fluid is then transported to the conjugate pad through capillary action. The conjugate pad contains the sample and bioconjugate molecules (probe) required for a strong attraction via intermolecular forces between the target molecules to form an immune complex. The reactive area of lateral flow assay is the nitrocellulose membrane, which contains the control and test lines for antigen-antibody interaction. The test line recognizes the sample of interest, while the control line captures unbound conjugate antibodies or antigens from the conjugate pad. The absorbent pad acts as a waste drain and stops the liquid from flowing backwards.[14-15] In this present study, the lateral flow assay strips were composed of three components namely, sample conjugate release pad, nitrocellulose membrane (test pad), and absorbent pad used for a visual flow test.

Tuberculosis is a highly contagious chronic pulmonary disease caused by the *M.tb bacterium*.[16] Early detection of this disease at the point of care is a serious obstacle worldwide, more especially in less developed countries.[17] About ten million cases of TB were reported in 2020, and about 1.5 million people died from TB.[18] Therefore, this work focuses on progress towards providing a solution to meet the need for facile TB detection. The linking of chloroform-soluble

lipid MAs to water-soluble GQDs to provide a water-soluble fluorescent biosensor to detect TB anti-MA antibodies has not been reported previously to the best of our knowledge. The linking of MAs to water-soluble fluorescent GQDs is expected to improve the water solubility of the MAs and thus enable them to be used as a fluorescent TB biosensor. In this study, we present for the first time the linking of chloroform-soluble MAs to water-soluble GQDs to form MA-GQDs and show that this enhances the solubility of MAs and enables their lateral flow and reduces the potential toxicity of the sensor material as compared to semiconductor-based QDs, which we have reported on previously.[19]

2. Experimental

2.1 Materials and reagents

Citric acid (CA, 98%), ethylenediamine (EDA, 99.5%), mycolic acid (MA, 98%), and oxalyl chloride ($(COCl)_2$, 97.5%) were procured from Germany (Sigma-Aldrich) and used as received. The solvents chloroform ($CHCl_3$, 99%), dimethylformamide (DMF, 98.5%), acetone (99.5%), and dichloromethane (DCM, 99.8%) were procured from Associated Chemical Enterprises (South Africa) and used without further purification. Triethylamine (TEA, 99%), and pyridine (99.5%) were purchased from Radchem Laboratory Chemicals and Consumables, South Africa. SnakeSkin dialysis tubing (3.5 kDa MWCO, 22 mm) was procured from Thermo Fisher Scientific, South Africa and filter paper (Whatman Macherey-Nagel, 125 mm, MN 615 D) from Altmann Analytik GmbH & Co, Germany. Deionised (DI) water (9.2 $\mu S/cm^3$) was acquired using a Drawell water purification laboratory in-house system (Drawell Scientific Instrument Co, Ltd, USA) while argon was provided by African Oxygen Limited (Afrox, South Africa). Nitrocellulose membranes (Sartorius Stedim Biotech, Germany) were provided by the Council for Scientific and Industrial Research (CSIR), South Africa.

2.2 Instrumentation

The electronic absorption spectra of GQDs and MA-GQDs were obtained using a UV-visible Cary Eclipse spectrophotometer (Varian Pty Ltd, Australia). Fluorescence was analysed by a Yvon Jobin Horiba Fluoromax-4 spectrofluorometer (Horiba Instruments Inc., Edison, NJ, USA) at 360 nm excitation, with slit widths set at 5 nm. The infra-red investigations were done using a Bruker Alpha (II) spectrometer (Bruker Optik GMBh, Ettlingen, Germany) over 4000-400 cm^{-1} furnished with the Opus software. The morphology and size of the GQDs and MA-GQDs were measured using transmission electron microscopy (TEM) with a JEOL JEM 2100F (JOEL Ltd, Tokyo, Japan), and the software ImageJ was used to analyse the particle size distribution. XRD spectra were studied using a D2 Bruker phaser (Bruker AXS GmbH, Karlsruhe, Germany) using Cu Kα radiation. The data obtained were collected in the range from $2\theta = 10°$ to 90°. A Teflon™ lined stainless steel autoclave (100 ml, 200 ºC maximum working temperature) was purchased from Systec, Germany.

2.3 Synthesis of amine functionalised graphene quantum dots

Citric acid (0.022 moles) and ethylenediamine (0.022 moles) were mixed and dispersed in 40 ml of deionised water in a 100 cm^3 flask, following a reported method.[20] The reaction mixture was transferred to a Teflon™ lined stainless-steel autoclave and heated at 150 ˚C for 6 hr. The autoclave was left to cool down to room temperature. The obtained yellowish solution was dialysed for 3.5 hr, after which it was frozen and then freeze dried for 48 hr to obtain yellow crystals of amine functionalised graphene quantum dots (GQDs). A schematic representation of the synthesis is provided in **Figure 1**.

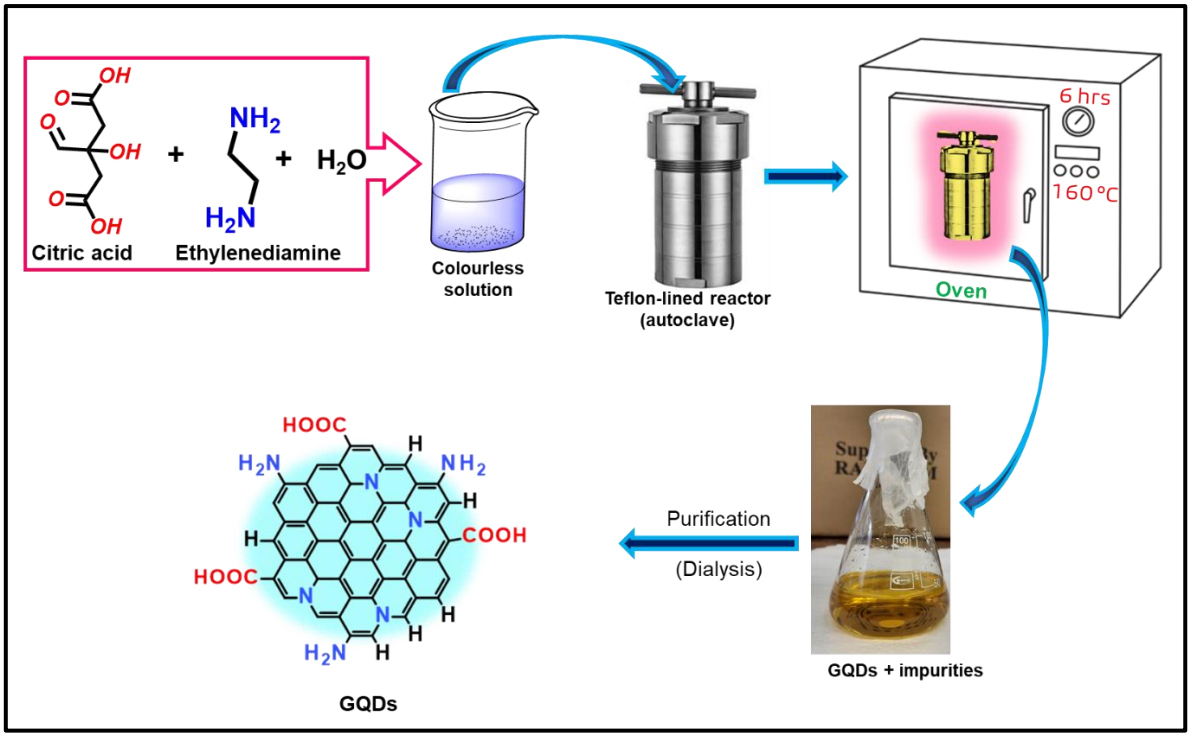

Figure 1: Schematic of the hydrothermal synthesis of GQDs from citric acid and ethylenediamine as sources of carbon and nitrogen respectively.

2.4 Covalent linking of mycolic acid to amine functionalised graphene quantum dots

Using a round bottomed flask (50 cm^3), 4.00 mg of MA, 9 cm^3 of dry $CHCl_3$, and DMF (1 drop) were combined. The combination was stirred at 750 rpm for 5 min and soon after, oxalyl chloride (1 cm^3) was added with continued stirring at 750 rpm at room temperature for 12 hr. Immediately after that, excess $CHCl_3$ was removed via a rotary evaporator to secure a yellow oily mycolic acid chloride, which was then used directly without further purification in the next step.

To link amine-functionalized GQDs to the mycolic acid chloride, 1.50 mg of amine-functionalized GQDs and 9 cm^3 of dry DCM were combined in a round bottomed flask (100 cm^3). The suspension was purged with argon while stirring for 5 min, after which pyridine (two drops) was added to the suspension as a catalyst. The suspension was placed in a dry ice and acetone bath at the temperature range between 0 ^oC and -15 ^oC whilst stirring. Thereafter,

mycolic acid chloride was added drop by drop whilst cooling. Triethylamine (five drops) were slowly added to neutralize the acid combination. The reaction mixture was stirred at 750 rpm at room temperature for 12 hr and later filtered through filter paper (Whatman Macherey-Nagel, 125 mm, MN 615 D) to remove excess amine-functionalized GQDs. Excess DCM was evaporated under vacuum to secure crystals of mycolic acid-amine functionalized graphene quantum dots (MA-GQDs). A summary of the linking reaction scheme is shown in **Figure 2**.

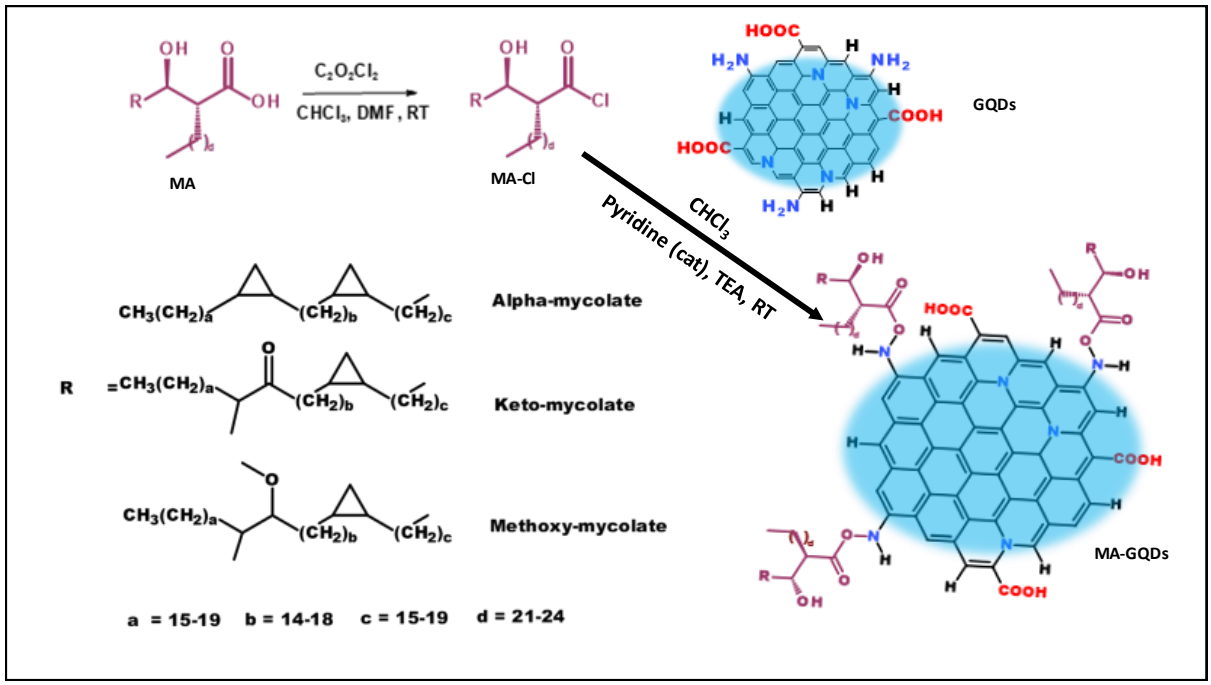

Figure 2: Schematic of the covalent linking of chloroform-soluble MAs to water-soluble GQDs to obtain a water-soluble fluorescent TB biosensor: MA-GQDs.

2.5 Calculation of fluorescence quantum yield (Φ_f)

In this study, the fluorescence quantum yield was calculated using Equation 1, which used Rhodamine 6G as a standard fluorescence quantum yield ($\Phi_{std,}$). The sample fluorescence intensities (I_{sam}) and Rhodamine 6G in ethanol as standard (I_{std}) were compared with the corresponding absorbances of the sample (A_{sam}) and the standard (A_{std}). The refractive index of water for GQDs (n_{sam}) and the refractive index of ethanol for Rhodamine 6G (n_{std}) were

used.[21] The absorbances were less than 0.05 to minimize internal filter effects, while 360 nm excitation wavelength was used for all the measurements.

$$\Phi_f = \Phi_{std} * \frac{I_{sam} * A_{std} * n^2{}_{sam}}{I_{std} * A_{sam} * n^2{}_{std}} \quad (1)$$

2.6 GQDs and MA-GQDs lateral flow tests

Using 5 cm^3 vials, 0.01 mg/cm^3 solutions of GQDs or MA-GQDs were made, by dispersing 0.01 mg in 1 cm^3 of deionized water. Thereafter, 5 µL aliquots of each of the 0.01 mg/mL solution of the GQDs or MA-GQDs were spotted onto 1 cm × 5 cm pieces of nitrocellulose membrane, 5 mm above the bottom edge, using an Eppendorf micropipette. The pieces were dried under ambient laboratory conditions for 1 hr and then dipped vertically into individual test tubes holding 200 µL of deionized water until the water reached the top part of the membrane strips. A blank piece of the nitrocellulose membrane was similarly eluted as a control. The pieces were removed from the water and dried under ambient laboratory conditions for 2 hr. Thereafter, fluorescence analysis was conducted using a Horiba Jobin Yvon Fluoromax-4 spectrofluorometer on two portions of the nitrocellulose membrane strips. The first portion was where the sample was initially deposited (5 mm above the bottom edge), and the second portion was the upper part (5 mm below the upper edge). All the fluorescence spectra were obtained using an excitation wavelength of 360 nm and fluorescence emission was recorded from 370 to 750 nm, with slit widths set at 5 nm.

3 Results and discussion

3.1 UV-vis absorption properties of GQDs and MA-GQDs

The absorption properties of GQDs and MA-GQDs were explored by UV-vis spectroscopy. The absorption spectra for both GQDs and MA-GQDs exhibit wide absorption bands extending

from 200 to 420 nm with one prominent peak at 344 nm for GQDs, while MA-GQDs have prominent peaks at 255, 315, and 408 nm (**Figure 3**). These wide absorption bands are an excellent property in sensing applications using the fluorescence technique, as they facilitate the use of a range of excitation wavelengths.

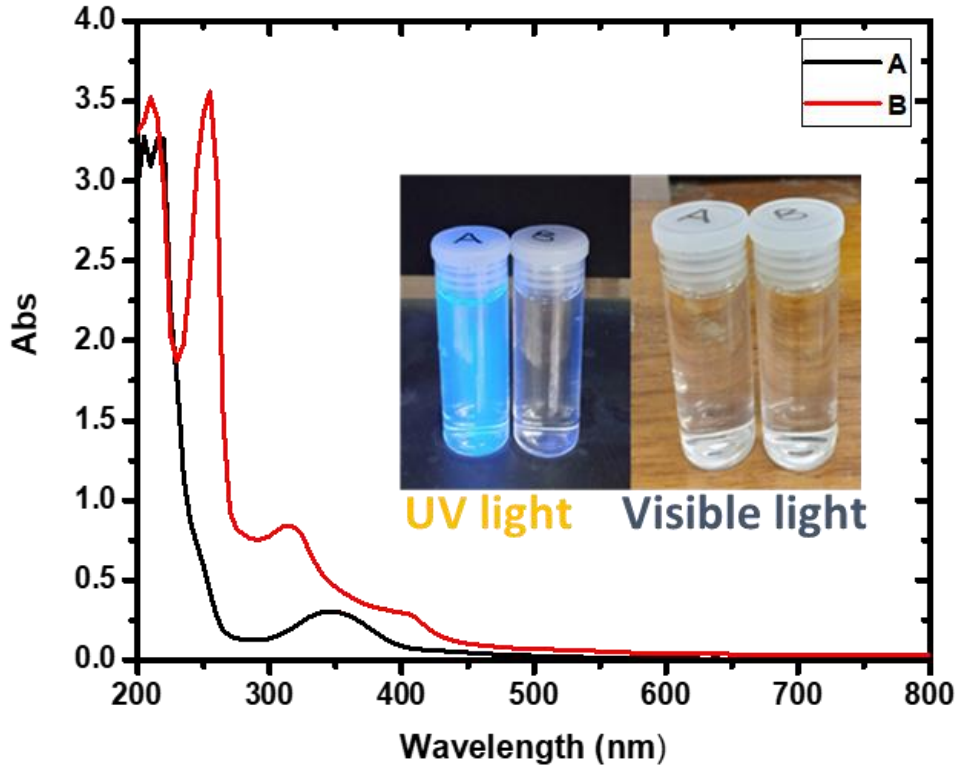

Figure 3: UV-vis absorption spectra of GQDs (A) and MA-GQDs (B) dissolved in water (0.01 mg/ml). Insert: GQDs (A) and MA-GQDS (B) under UV light and visible light.

3.2 Fluorescence emission optimisation

The optimisation of fluorescence emission of GQDs and MA-GQDs were explored by varying the excitation wavelength**.** It was found that the maximum emission intensity for GQDs was with 360 nm excitation, and 380 nm for MA-GQDs (**Figure 4).** The results also indicated that varying the excitation wavelength did not change the fluorescence emission wavelength of the GQDs, suggesting a pure product with a narrow size distribution, but red-shifting was noticed for the emission wavelength of MA-GQDs with an increase in excitation wavelength. This

could be due to a variation in the amount of MA coupled to individual GQDs. The intensity of fluorescence emission of GQDs and MA-GQDs was found to increase to a maximum and thereafter decreased as the wavelength of excitation increased further (**Figure 4c**).

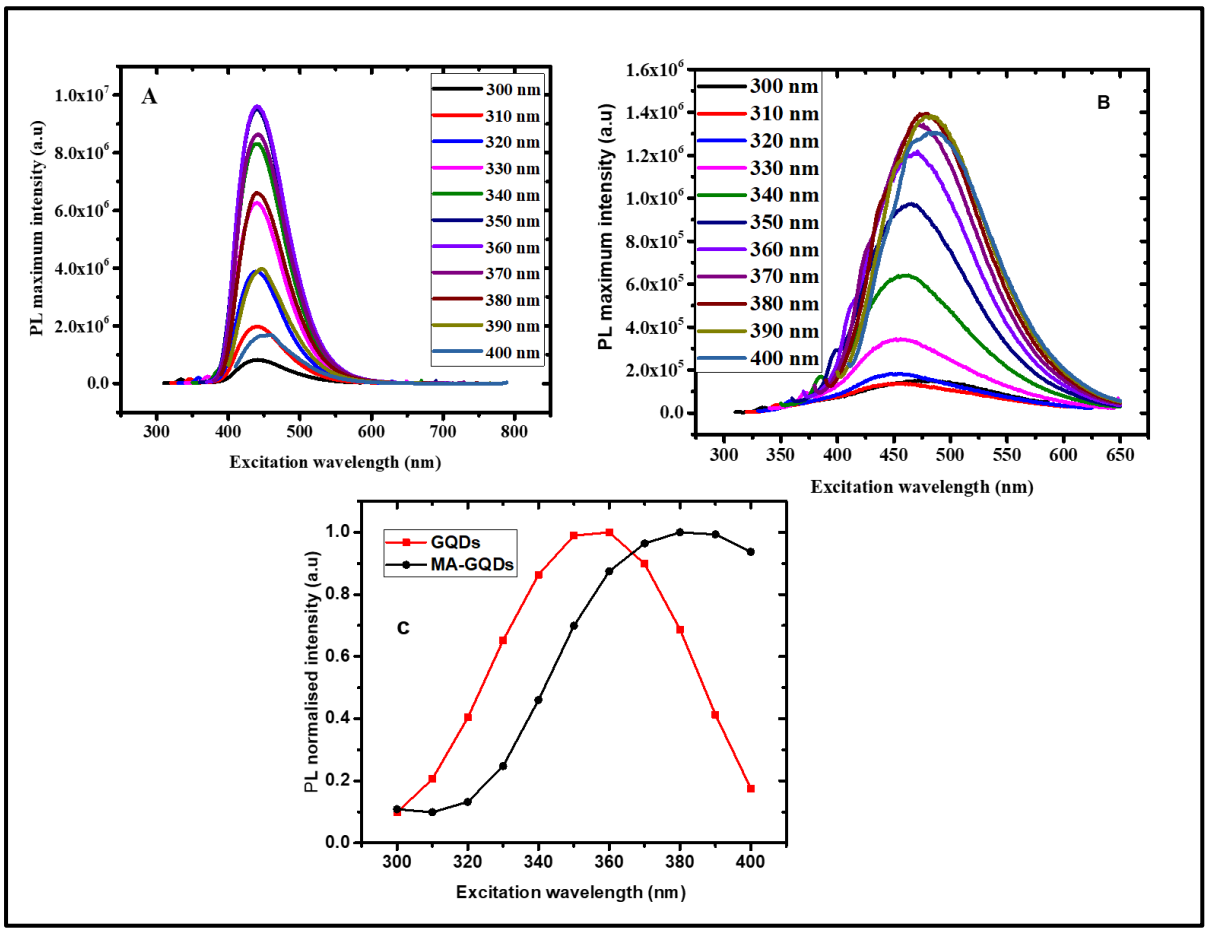

Figure 4: Fluorescence spectra of GQDs (A) and MA-GQDs (B) with varying excitation wavelengths. (C) Shows the effect of the excitation wavelength on the maximum photoluminescence (PL) intensity.

3.3 Fluorescent properties of GQDs and MA-GQDs

The fluorescence properties of the synthesized GQDs and MA-GQDs were studied using photoluminescence (PL) spectroscopy (**Table 1**). The fluorescence emission spectrum of GQDs was narrow, having full width at half maximum (FWHM) of 57.67 nm with the highest emission wavelength at 440 nm and a fluorescence quantum yield of 69.0% when exciting at 360 nm (**Figure 5**). Upon the linking of MA to GQDs, the fluorescence quantum yield

decreased to 21.6% while the emission spectrum became somewhat broader (FWHM of 97.17 nm) than that of the GQDs and was moderately red shifted with the highest fluorescence emission wavelength at 470 nm. This decrease in the fluorescence quantum yield and the red shift may be attributed to the change in the size and surface properties of MA-GQDs, suggesting the successful linking of MA to the GQDs. The fluorescence quantum yield of the GQDs and MA-GQDs is somewhat lower than the fluorescence quantum yield of semiconductor-based QDs and the corresponding MA-QDs reported in our previous work.[19]

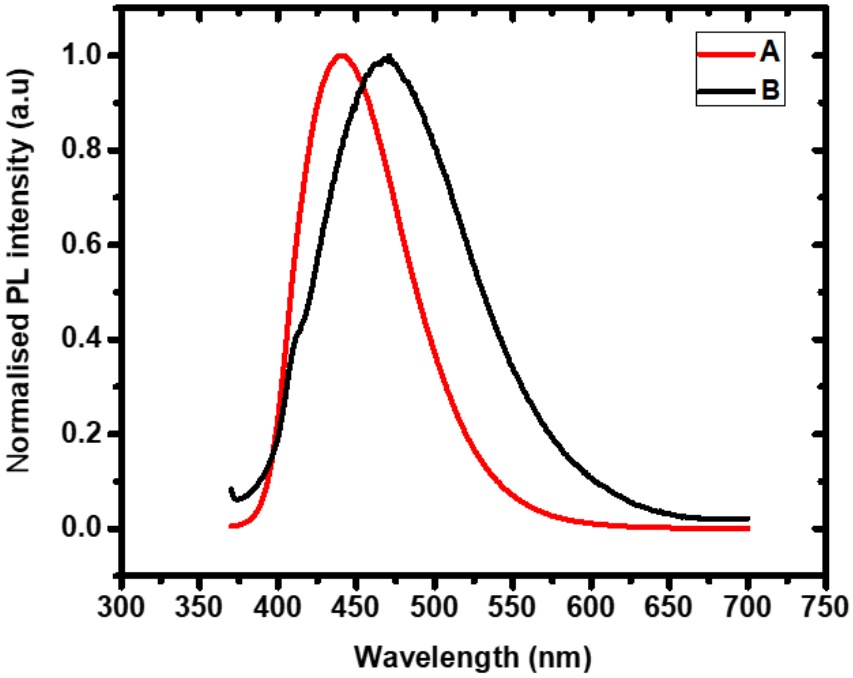

Figure 5: Normalized PL emission of GQDs (A) and MA-GQDs (B) dispersed in water when exciting at 360 nm, with slit widths set at 5 nm.

Table 1 Summary of fluorescent properties of GQDs and MA-GQDs

	GQDs	**MA-GQDs**
Wavelength at highest fluorescence emission (λ_{em}, nm)	440	470
Full width at half maximum (FWHM, nm)	57.7	97.2
Fluorescence quantum yield (Φ_f, %)	69.0	21.6

3.4 FT-IR analysis of MA, GQDs and MA-GQDs

Figure 6 shows the FT-IR spectra of MAs, GQD, and MA-GQDs. The spectra of MAs and GQDs indicate expected characteristic peaks resulting from the presence of -C-H; -O-H and -C=O functional groups. The additional peaks between 2450 cm^{-1} and 2790 cm^{-1} in MA-GQDs can be due to -N-C=O modes. The presence of these peaks in MA-GQDs indicates the appearance of the peptide bond, which confirms the covalent linking of GQDs to MAs.

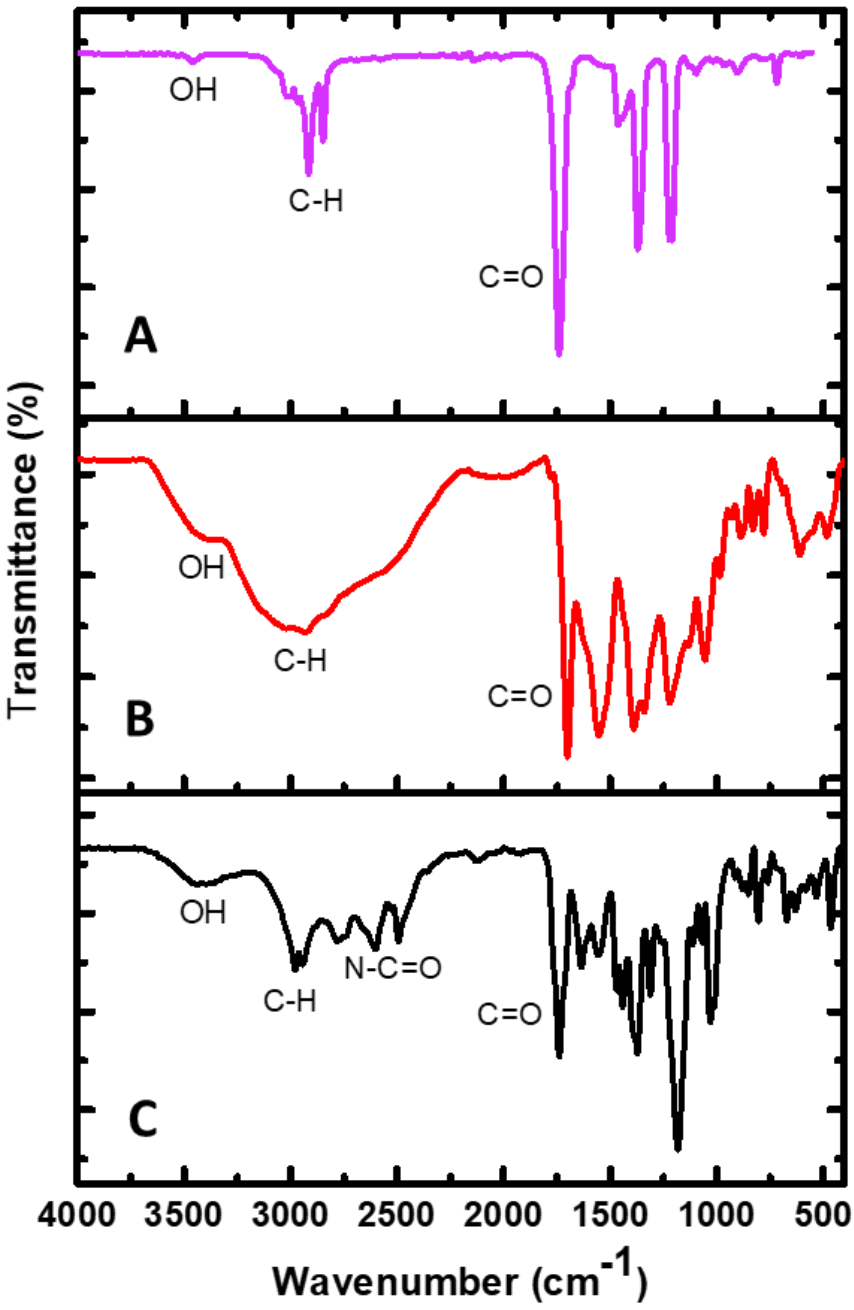

Figure 6: FT-IR spectra of MAs (A), GQDs (B), and MA-GQDs (C) in solid form.

3.5 TEM analysis of GQDs and MA-GQDs

The particle size and morphology of GQDs and MA-GQDs are shown in **Figure 7.** It was noticed that GQDs distributed well in water with a mean approximate particle size of 0.8 ± 0.3 nm while the MA-GQDs showed some particle aggregation with a mean approximate particle

size of 1.6 ± 0.8 nm. The aggregation observed could be a result of interactions between hydrophobic and hydrophilic groups in the linked MA-GQDs, respectively.

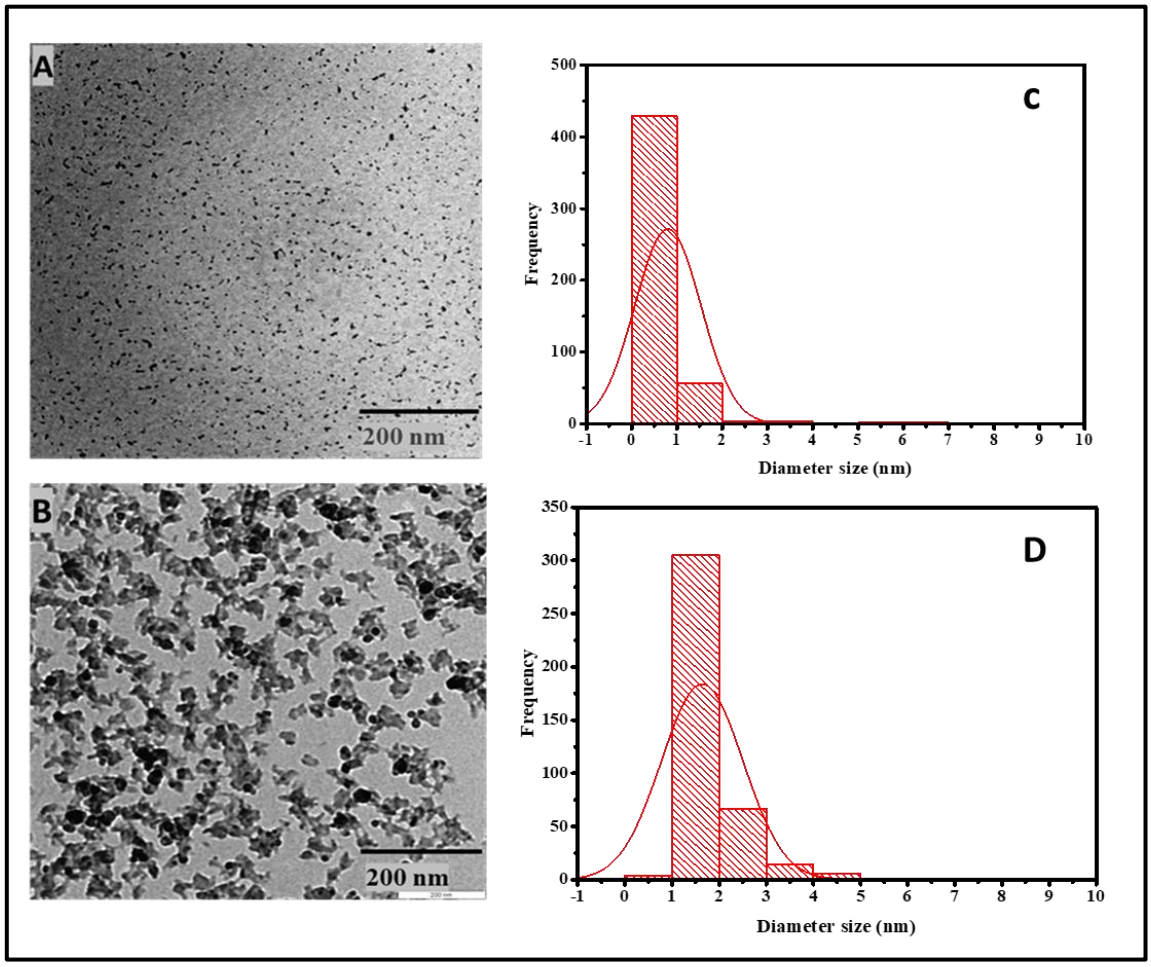

Figure 7: TEM micrographs of GQDs (A) and MA-GQDs (B) dispersed in water with the corresponding particle size distribution histograms (C, D).

3.6 Powder XRD study of GQDs and MA-GQDs

The XRD spectrum in **Figure 8A** exhibits one broad peak for GQDs at 20.8˚ corresponding to the structure reported previously.[20] MA-GQDs (**Figure 8B**) have ten sharp peaks at positions 12.8˚, 18.4˚, 22.0˚, 25.6˚, 28.6˚, 33.6˚, 36.1˚, 44.2˚, 46.1˚and 51.9˚. This increment in the number of peaks implies the successful linking of MA to GQDs, which changed the crystal structure of the resulting material as anticipated because of the introduction of the non-crystalline MA portion present in the MA-GQDs.

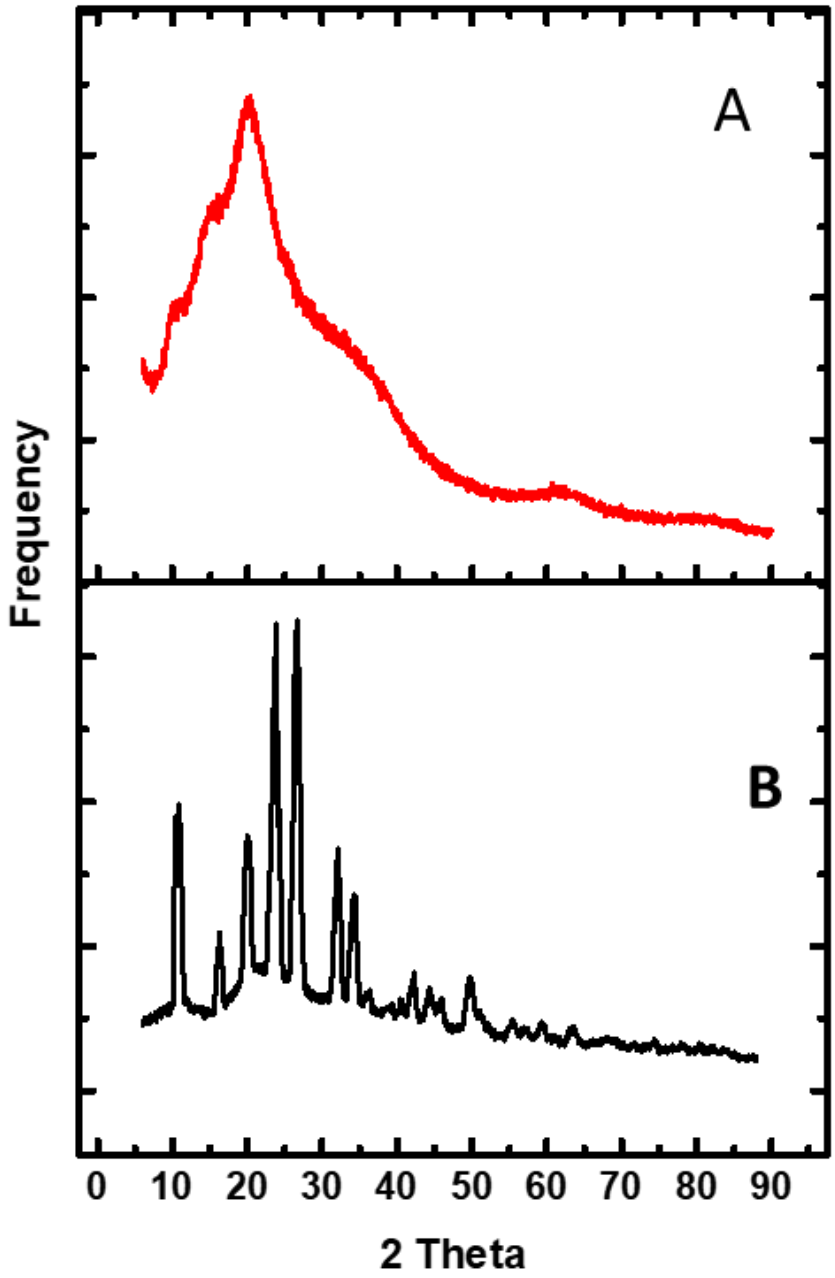

Figure 8: Powder XRD spectra of GQDs (A) and MA-GQDs (B).

3.7 Lateral flow tests of GQDs and MA-GQDs

The lateral flow of GQDs and MA-GQDs was investigated to determine the possible application thereof in the detection of tuberculosis biomarkers which are anti-MA antibodies. **Figure 9** shows that GQDs and MA-GQDs were able to flow through the strips of nitrocellulose membrane when using deionized water as eluent. This flow of GQDs and MA-

GQDs was confirmed by the fluorescence emission spectra obtained at 437 and 430 nm, respectively, when the nitrocellulose membrane was excited at 360 nm. The emission spectra of GQDs (435 nm) and MA-GQDs (450 nm) before lateral flow (i.e., at the point where the sample was deposited onto the strip) were also obtained. The intensity of the emission spectra of GQDs and MA-GQDs after the lateral flow was somewhat lower than before the lateral flow. This is expected, as the GQD and MA-GQD particles are dispersed over a wider area after elution. These results show that GQDs and MA-GQDs are water-dispersable materials that can flow through a lateral flow test membrane, and thus MA-GQDs have the potential to detect anti-MA antibodies via the nitrocellulose membrane flow technique. It can be deduced that the MA-GQDs were more dispersable in water as compared to the coupled material prepared with semiconductor QDs reported in our previous work.[19] As can be seen in the inset shown in **Figure 9**, all the sample at the spotting point eluted up the strip, while for the semiconductor-based MA-QDs, some spotted sample remained at the initial spotting point. Good solubility in water and low toxicity thus makes MA-GQDs the preferred material to potentially detect anti-MA antibodies and diagnosis of tuberculosis using the nitrocellulose membrane flow technique.

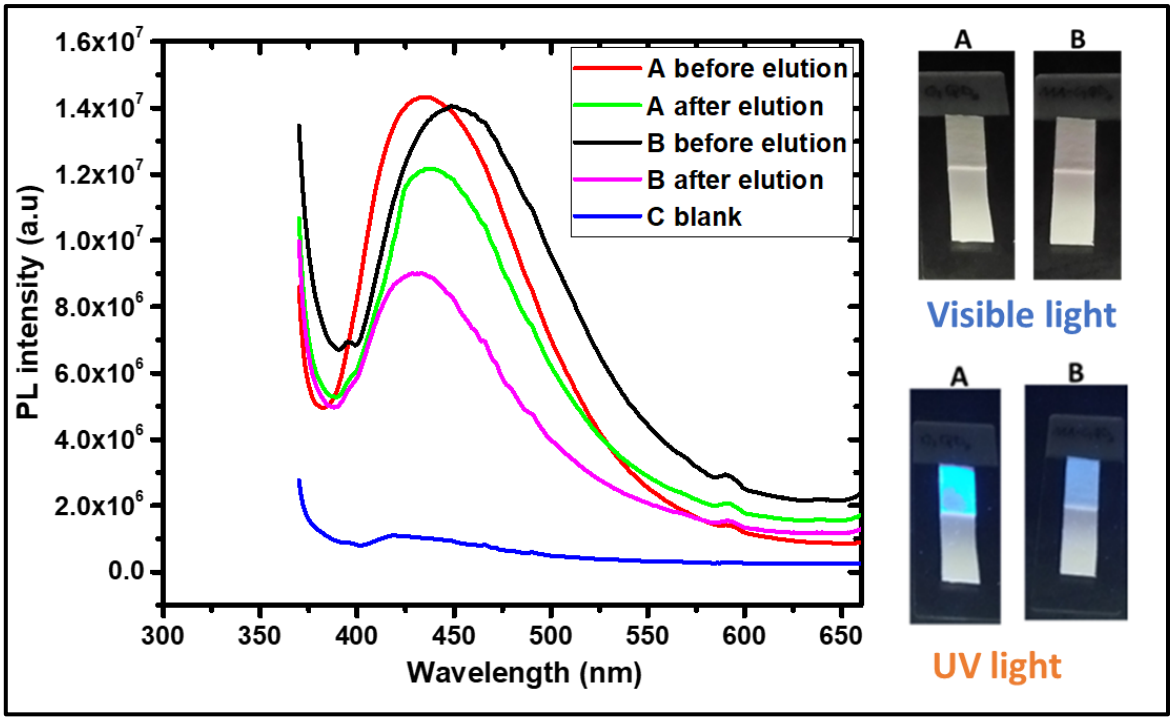

Figure 9: PL fluorescence spectra of GQDs (A) and MA-GQDs (B) dried on nitrocellulose membrane strips before elution (5 mm above the bottom edge) and after elution (5 mm below the upper edge). The excitation wavelength used was 360 nm. The inset shows GQDs (A) and MA-GQDS (B) under visible light and UV light after lateral flow.

Conclusion

GQDs were synthesized using a well-established hydrothermal method and were successfully linked to MAs to form MA-GQDs. The synthesized GQDs and linked MA-GQDs were characterized by fluorescence, UV-vis, FT-IR, XRD spectroscopy, and TEM analysis. The absorption results showed that both GQDs and MA-GQDs exhibit a wide range of absorption wavelengths between 420 to 200 nm, which enables changes of excitation wavelength used in fluorescence sensing applications. Fluorescence results showed that GQDs have a narrow emission spectrum (FWHM of 57.7 nm), with a fluorescence quantum yield of 69.0% with the highest fluorescence emission wavelength at 440 nm, while MA-GQDs have a somewhat broader spectrum (FWHM of 97.2 nm) and the highest emission wavelength at 470 nm after

exciting at 360 nm, with a fluorescence quantum yield of 21.6%. The appearance of -N-C=O peaks between 2450-2790 cm^{-1} in the FT-IR spectrum of the MA-GQDs indicates the appearance of the peptide bond (amide linkage), which confirms the covalent linking of MAs to GQDs. TEM results exhibited an average approximate particle size distribution of GQDs of 0.8 ± 0.3 nm and 1.6 ± 0.8 nm for MA-GQDs. The powder XRD results showed an increment in the number of peaks for MA-GQDs compared to one broad peak for GQDs. This suggests that the covalent linking of MAs to GQDs changed the crystal structure of the resulting material. Nitrocellulose membrane lateral flow experiments confirmed the elution of MA-GQDs with deionized water as eluent.

In view of the simplicity of the process, low toxicity of the material, as well as the good dispersibility of the highly fluorescent MA-GQDs in water, enabling their lateral flow through a nitrocellulose membrane, the novel MA-GQDs have the potential to be used in the detection of anti-MA antibodies and in point of care TB diagnosis. Furthermore, the use of GQDs in this study showed some competitive advantages over our previous work, where cadmium based QDs were used as a proof of concept for the development of a MA-coupled QD sensor. The use of GQDs has not only averted the potential toxicity concerns of cadmium, but also resulted in improved dispersibility in water which makes it ideal for lateral flow experiments. This study paves the way towards a simple, quick, and cost-effective method for TB detection.

Declaration of conflicts of interest

The authors declare no conflict of interest.

Acknowledgements

Funding for this work was provided by NRF-TWAS scholarship and a postgraduate student bursary from the University of Pretoria (KK). We thank the Microanalysis and Microscopy Laboratory of the University of Pretoria for their help with TEM analysis.

References

[1] Y.R. Kumar, K. Deshmukh, K.K. Sadasivuni, S.K. Pasha, Graphene quantum dot based materials for sensing, bio-imaging and energy storage applications: a review, *RSC Adv.*, 2020, *10*, 23861-23898.

[2] C. Zhao, X. Song, Y. Liu, Y. Fu, L. Ye, N. Wang, F. Wang, L. Li, M. Mohammadniaei, M. Zhang, Synthesis of graphene quantum dots and their applications in drug delivery, *J. Nanobiotechnol.*, 2020, 18, 1-32.

[3] P. Tian, L. Tang, K. Teng, S. Lau, Graphene quantum dots from chemistry to applications, *Mater. Today Chem.*, 2018, 10, 221-258.

[4] W. Chen, G. Lv, W. Hu, D. Li, S. Chen, Z. Dai, Synthesis and applications of graphene quantum dots: a review, *Nanotechnol. Rev.*, 2018, 7, 157-185.

[5] B.D. Mansuriya, Z. Altintas, Applications of graphene quantum dots in biomedical sensors, *Sensors*, 2020, 20, 1072.

[6] E.J. North, M. Jackson, R.E. Lee, New approaches to target the mycolic acid biosynthesis pathway for the development of tuberculosis therapeutics, *Curr. Pharm. Des.*, 2014, 20, 4357-4378.

[7] J. Madacki, F. Laval, A. Grzegorzewicz, A. Lemassu, M. Záhorszká, M. Arand, M. McNeil, M. Daffé, M. Jackson, M.-A. Lanéelle, Impact of the epoxide hydrolase EphD on the metabolism of mycolic acids in mycobacteria, *J. Biol. Chem.*, 2018, 293, 5172-5184.

[8] M. Beukesa, Y. Lemmera, M. Deysela, J.a.R. Al Dulayymid, M.S. Bairdd, G. Kozad, M.M. Iglesiasd, R.R. Rowlesd, C. Theunissend, J. Grootene, Structure–function relationships of the antigenicity of mycolic acids in tuberculosis patients, *Chem. Phys. Lipids*, 2011, 163, 1800–1808.

[9] F.L. Ndlandla, V. Ejoh, A.C. Stoltz, B. Naicker, A.D. Cromarty, S. van Wyngaardt, M. Khati, L.S. Rotherham, Y. Lemmer, J. Niebuhr, C.R. Baumeister, J.R. Al Dulayymi, H. Swai,

M.S. Baird, J.A. Verschoor, Standardization of natural mycolic acid antigen composition and production for use in biomarker antibody detection to diagnose active tuberculosis, *J. Immunol. Methods*, 2016, 435, 50-59.

[10] M. Watanabe, Y. Aoyagi, M. Ridell, D.E. Minnikin, Separation and characterization of individual mycolic acids in representative mycobacteria, *Microbiology*, 2001, 147, 1825-1837.

[11] Y. Lemmer, L. Kalombo, R.-D. Pietersen, A.T. Jones, B. Semete-Makokotlela, S. Van Wyngaardt, B. Ramalapa, A.C. Stoltz, B. Baker, J.A. Verschoor, Mycolic acids, a promising mycobacterial ligand for targeting of nanoencapsulated drugs in tuberculosis, *J. Control. Release*, 2015, 211, 94-104.

[12] S. Shang, D. Kats, L. Cao, E. Morgun, D. Velluto, Y. He, Q. Xu, C.-R. Wang, E.A. Scott, Induction of *Mycobacterium tuberculosi*s lipid-specific T cell responses by pulmonary delivery of mycolic acid-loaded polymeric micellar Nanocarriers, *Front. Immunol.*, 2018, 9, 2709.

[13] E.B. Bahadır, M.K. Sezgintürk, Lateral flow assays: Principles, designs and labels, *TrAC-Trends Anal. Chem.*, 2016, 82, 286-306.

[14] L. Anfossi, F. Di Nardo, S. Cavalera, C. Giovannoli, G. Spano, E.S. Speranskaya, I.Y. Goryacheva, C. Baggiani, A lateral flow immunoassay for straightforward determination of fumonisin mycotoxins based on the quenching of the fluorescence of CdSe/ZnS quantum dots by gold and silver nanoparticles, *Microchim Acta*, 2018, 185, 94.

[15] M. Sajid, A.-N. Kawde, M. Daud, Designs, formats and applications of lateral flow assay: A literature review, *J. Saudi Chem. Soc.*, 2015, 19, 689-705.

[16] N. Ariffin, N.A. Yusof, J. Abdullah, S.F. Abd Rahman, N.H. Ahmad Raston, N. Kusnin, S. Suraiya, Lateral flow immunoassay for naked eye detection of *Mycobacterium tuberculosis*, *J. Sens.*, 2020, 2020, 1687.

[17] S. Sudha, Tuberculosis diagnosis-an overview to the conventional diagnostic methodology and need for nanodiagnosis, *Int. J. Med. Eng. Inform.*, 2016, 8, 27-40.

[18] D.R. Silva, F.C.d.Q. Mello, G.B. Migliori, Tuberculosis series 2020, *J. Bras. Pneumol.*, 2020, 46, 1806-3756.

[19] K. P. Kabwe, S. A. Nsibande, Y. Lemmer, L. A. Pilcher, P. B.C. Forbes, Synthesis and characterisation of quantum dots coupled to mycolic acids as a water-soluble fluorescent probe for potential lateral flow detection of antibodies and diagnosis of tuberculosis, *Luminescence,* 2022, 37, 278.

[20] H. Safardoust-Hojaghan, M. Salavati-Niasari, O. Amiri, M. Hassanpour, Preparation of highly luminescent nitrogen doped graphene quantum dots and their application as a probe for detection of *Staphylococcus aureus* and *E. coli*, *J. Mol. Liq.*, 2017, 241, 1114-1119.

[21] D. Magde, R. Wong, P.G. Seybold, Fluorescence quantum yields and their relation to lifetimes of rhodamine 6G and fluorescein in nine solvents: Improved absolute standards for quantum yields, *Photochem. Photobiol.*, 2002, 75, 327-334.

CHAPTER FIVE: The binding interaction of MA-QDs to anti-MA antibodies (Gallibodies, Gb)

This chapter discusses the detection of the binding interaction of MA-QDs to anti-MA antibodies using the Enzyme-linked Immunosorbent Assay, lateral flow assay, and fluorescence techniques.

5.0 Introduction

Pure mycolic acid (MA) is a proven antigen and has been shown to bind specifically to a few selected gallibodies and there are other gallibodies that are specific to cholesterol. There are also some gallibodies that bind to both MA and cholesterol (less specific) [1]. Therefore, this chapter presents the findings on the binding of MA-QDs (modified antigen) to anti-MA antibodies (gallibodies) to determine whether the modification of the MA affects its antigenicity. The confirmation on the binding of MA-QDs (modified antigen) to anti-MA antibodies was tested using the Enzyme-linked Immunosorbent Assay (ELISA), the lateral flow method, and fluorescence techniques.

5.1 Materials

The synthesis of the fluorophores (CdSe/ZnS QDs, GQDs, MA-CdSe/ZnS QDs, 4MA-CdSe/ZnS QDs, MA-GQDs and stearic acid-CdSe/ZnS QDs (StA-CdSe/ZnS QDs)) was described in Chapters three and four. Stearic acid (StA), hexane and dichloromethane (DCM) were purchased from Radchem Laboratory Chemicals and Consumables (South Africa). Mycolic acid used to prepare fluorophores for the lateral flow test was purchased from Sigma-Aldrich (Germany). Deionised water (9.2 $\mu S/cm^3$) was obtained from an in-house Drawell laboratory water purification system (Drawell Scientific Instrument Co, Ltd, USA). Membrane blocking solution (Life Technologies, USA), strips of nitrocellulose membrane (CN95 Sartorius Stedim Biotech, Germany), phosphate-buffered saline (PBS) purchased from Sigma-Aldrich (Germany), wash buffer (0.1% Tween 20 in PBS (0.1 M pH 7.4, blocking buffer (4% oxoid casein in PBS (0.1M)), anti-MA antibodies (gallibodies, Gb, 12+ CH_2-4) [2], immunoglobulin (IgY), bovine serum albumin (BSA), mycolic acid (Sigma-Aldrich, Germany) for ELISA and fluorescence tests, secondary antibodies (BIORAD goat anti-chicken lgG (fc):HRP conjugated to horse radish peroxidase (HRP)), enzyme substrate (tetramethylbenzidine (TMB)) and a light HP Scanjet 2400 flatbed scanner (Hewlett Packard

Company, USA) were all supplied by the Council for Scientific and Industrial Research (CSIR, South Africa). MA was used as positive control, while StA-CdSe/ZnS QDs and StA were used as negative controls.

5.2 Characterization techniques

Absorbance measurements were conducted on SpectraMax-paradigm microplate reader with a multi-mode detection platform (Molecular devices, LLC, USA).

Excitation and emission spectra were obtained using a Horiba Jobin Yvon Fluoromax-4 spectrofluorometer (Horiba Instruments Inc., USA) and a SpectraMax-paradigm microplate reader multi-mode detection platform (Molecular devices, LLC, USA).

5.3 Experimental

5.3.1 Enzyme-linked Immunosorbent Assay (ELISA) test of MA-QDs

The ELISA technique was used to see if MA retained its antigenic properties after being coupled to the quantum dots. The ELISA assay was carried out according to the protocol described by Ranchod [2] as follows: In small vials, 0.25 mg of MA-CdSe/ZnS QDs, stearic acid-CdSe/ZnS QDs (StA- CdSe/ZnS QDs), stearic acids (StAs) and MA were suspended in 1 mL of dichloromethane (DCM) to form a 0.25 mg/mL coating solution. Another 0.25 mg/mL coating solution was prepared by dissolving 0.25 mg of MA in 1 mL of hexane as uncoupled control. 100 µL of 0.25 mg/mL solution of each sample was added to the individual wells of the Maxisorp 96-well plate. The plate was incubated at room temperature overnight. The coating solution was removed by flicking out the 96-well plate, and the plate was washed three times by filling the wells with the wash buffer (0.1% Tween 20 in PBS (0.1 M) pH 7.4). The solution was flicked out of the microtiter plate over a sink, and the remaining drops were removed by patting the plate with tissue. The wells were then blocked with 300 µL blocking buffer (4% oxoid casein in PBS (0.1 M) pH 7.4) and incubated for 2 hr at room temperature.

The blocking buffer coats any unbound surface area in order to minimise non-specific binding. The blocking buffer was flicked out and the wells were washed three times with wash buffer. 50 µL of 1 mg/mL of the primary synthetic gallibodies (anti-MA antibodies) were added to each well and allowed to incubate at room temperature for 1 hr [2]. The wells were washed three times with wash buffer. 50 µL of 1 mg/mL of BIORAD goat anti-chicken immunoglobulin conjugated to horse radish peroxidase (HRP) as secondary antibodies were added per well and incubated at room temperature for 1 hr. Soon after, excess secondary antibodies were flicked out of the wells by tapping the plate on a lint-free tissue, and the wells were washed three times with 300 µL wash buffer. 50 µL of tetramethylbenzidine (TMB) enzyme substrate was dispensed in each well for 4-5 min and changed the color from yellow to blue. To stop the reaction, 50 µL of H_2SO_4 (2 N) solution was added to the solution and the absorption measurements were conducted at 450 nm in three replicates using a SpectraMax-paradigm microplate reader with a multi-mode detection platform. Some individual wells of the Maxisorp 96-well plate used as blanks were only coated with fluorophores and MA without anti-MA antibodies. These blanks did not stick on the wells of the plates. As a result, they only gave a yellow color without changing to blue.

5.3.2 Fluorescence binding of MA-CdSe/ZnS QDs to anti-MA antibodies

The sensing probe MA-CdSe/ZnS QDs (0.2 mg/mL), pure CdSe/ZnS QDs (0.2 mg/mL) and antibody solutions were prepared by suspending them in phosphate buffered saline (PBS, 0.1M) with a pH of 7.4. The concentration of 0.025 mg/mL of the specific anti-MA antibodies (gallibodies, Gb), an antibody not specific to MA (immunoglobulin (IgY) and a non-antibody protein bovine serum albumin (BSA) was used. To 100 µL of each of the buffered antibodies, 100 µL of 0.2 mg/mL of the fluorescence probe MA-CdSe/ZnS QDs and CdSe/ZnS QDs were added on the microtiter 96-well plate and allowed to incubate for 30 min before fluorescence measurements were taken in three replicates for each well. This was done to allow the binding

of MA-CdSe/ZnS QDs with anti-MA antibodies. 100 µL of 0.1 M PBS was also added to 0.2 mg/ml of the MA-CdSe/ZnS QDs and CdSe/ZnS QDs on the individual wells of the microtiter 96-well plate to take into consideration the effects of dilution. CdSe/ZnS QDs, IgY antibody and protein BSA were used as negative controls. The fluorescence measurements were obtained using a SpectraMax-paradigm microplate reader with a multi-mode detection platform, with excitation at 390 nm.

5.3.3 Membrane lateral flow binding of MA-CdSe/ZnS QDs, 4MA-CdSe/ZnS QDs and MA-GQDs to anti-MA antibodies (gallibodies)

In small vials, 0.01 mg of each of the fluorophores were dispersed in 100 µL of deionized water to form a 0.1 mg/mL solution, while anti-MA antibodies (gallibodies) were diluted to 0.1 mg/mL solution with PBS. 5 µL of 0.1 mg/mL solution of gallibodies were spotted on each strip of nitrocellulose membrane halfway up the membrane and allowed to dry for 30 min at room temperature so that they were fixed on the nitrocellulose membrane. Aliquots (5 µL) of each of the 0.1 mg/mL solutions of the fluorophores were spotted onto the bottom part (below the halfway) of the strips of nitrocellulose membrane. These strips were then dipped vertically into individual test tubes with 200 µL of membrane blocking solution as an eluent and the fluorophores were allowed to flow to the test line via capillary action. Separate nitrocellulose membranes without gallibodies were also prepared. Membrane blocking solution was used as negative controls as well as CdSe/ZnS QDs and GQDs. The resulting nitrocellulose membrane strips were then scanned using a light HP Scanjet 2400 flatbed scanner for visual analysis.

The scanned nitrocellulose membrane strips were each stuck onto 2 x 4 cm glass microscope slides using Sellotape. The slides with and without gallibodies were inserted in the solid sample holder of the Horiba Jobin Yvon Fluoromax-4 spectrofluorometer for fluorescence measurements. The strips on the slides were inserted in such a way that light from the detector passed through the suspected point of interaction (test line). A blank strip of the nitrocellulose

membrane was similarly prepared as a control. All the fluorescence spectra were obtained using an excitation wavelength of 360 nm for graphene-based fluorophores and 390 nm for cadmium-based fluorophores, while emission was recorded from 370 to 800 nm, with slit widths set at 5 nm for both excitation and emission.

5.4 Results and discussion

5.4.1 Enzyme-linked Immunosorbent Assay (ELISA) test of MA-QDs

An indirect ELISA test was conducted with pure MA as positive control, MA-CdSe/ZnS QD as test sample, and CdSe/ZnS QDs as negative control. MA dissolved in hexane was used as a reference because it has been used before and it had been proven that it binds well with gallibodies [2]. This antigen gave the expected results demonstrating that the assay system was functional. However, the solvent for coating the ELISA plate was changed in order to accommodate the MA-QDs that were insoluble in hexane. The solvent was therefore changed from hexane to dichloromethane and stearic acid was included as an additional negative control. The indirect ELISA test results indicated the interaction between the anti-MA antibodies (gallibodies, Gb) and the sensing probe: MA-CdSe/ZnS QDs, StA-CdSe/ZnS QDs, StAs dissolved in DCM, and pure MAs dissolved in both DCM and hexane for comparison. The diluents were used as the blank controls in the assay. The results show that the MA-CdSe/ZnS QDs probe, StA-CdSe/ZnS QDs, StAs, and pure MAs all produced absorbance signals. The MA/hexane signal produced was significantly higher than its control signal, as has been reported previously [2]. However, the MA/DCM was not, indicating that DCM as solvent either did not allow the MA to stick onto the surface of the plate or that the residual DCM on the plate increased the non-specific binding of the gallibodies onto the plate. This can also be concluded from the other test samples where the control stearic acid groups showed non-specific binding towards the gallibodies. The absorbance signals of the test and blank correspond to the blue and red bars in **Figure 5.1,** respectively**.**

Repeat experiments showed that MA results were not reproducible in DCM. These variations in results were most probably due to the use of DCM as the solvent, hence this method may not be used to successfully test the binding of MA-QDs to anti-MA antibodies (gallibodies).

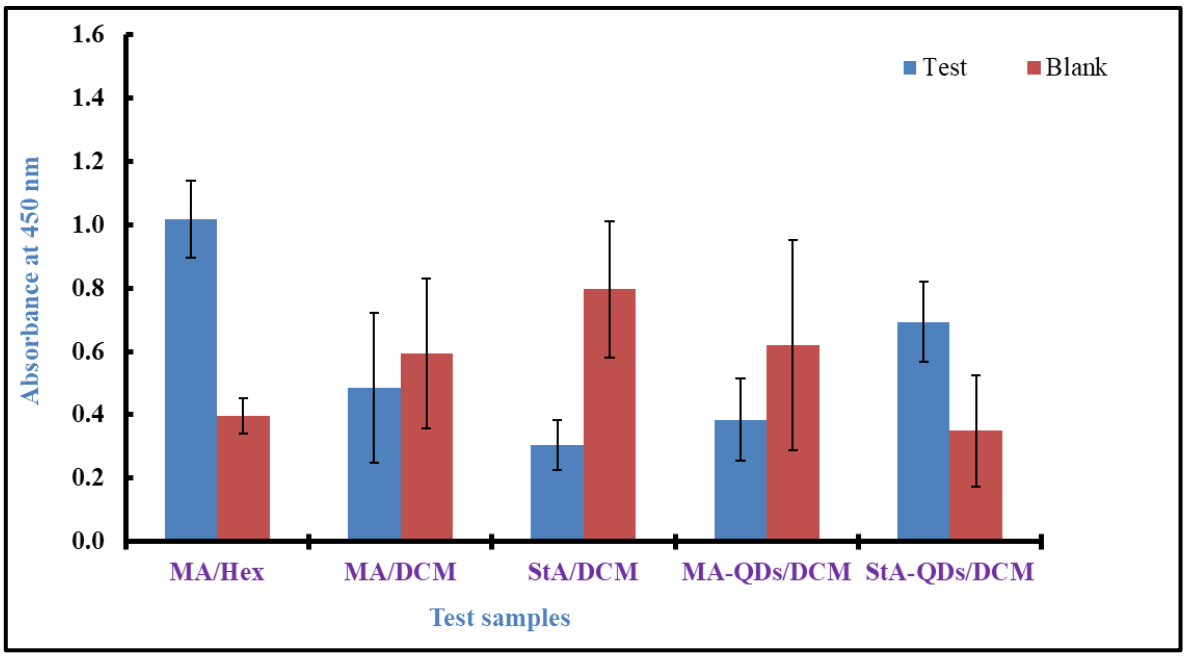

Figure 5.1: Indirect ELISA test results for MA-CdSe/ZnS QDs denoted as MA-QDs, StA-CdSe/ZnS QDs (StA-QDs), StA in DCM, and pure MAs in hexane and DCM (Error bars indicate standard deviation, (n = 3).

Limitation of this ELISA test.

This ELISA test was designed based on the proven binding between MA dissolved in hexane and anti-MA antibodies. Due to difficulties in solubilities of MA-QDs in hexane, DCM was used instead. It was discovered that DCM partially dissolved the wells of the Maxisorp 96-well plate. This could have affected the binding between the sensing probe and the anti-MA antibodies. An attempt was made to switch to glass microwell plates, unfortunately, MA and the MA-QDs did not stick to the surface by hydrophobic interaction and were removed in the

washing steps. Hence, it was concluded that the ELISA for this particular test was not reliable thus an alternative strategy was needed.

The alternative strategy was to use the fluorescence method. This method relies on the size tunability of the QDs and their high fluorescence quantum yields, hence binding of MA-QD to anti-MA antibodies should induce a measurable change in fluorescence. In this fluorescence method presented in Section 5.4.2, the specific binding between the MA-QDs and anti-MA antibodies, antibody IgY and protein BSA was explored.

5.4.2 Fluorescence binding of MA-QDs to anti-MA antibodies (Gallibodies, Gb)

Figure 5.2 shows the interaction of MA-CdSe/ZnS QDs and CdSe/ZnS QDs with gallibodies (specific), immunoglobulin (IgY) (non-specific antibodies), bovine serum albumin (BSA) (non-specific protein) and phosphate buffered saline (PBS) in the wells of microtiter 96-well plate. The results showed that the fluorescence intensity decreased upon the addition of 100 µL of 0.025 mg/mL Gb, IgY, BSA and PBS (**Figure 5.2(A)**). Phosphate buffered saline (PBS) was used to as the diluent. The decrease in intensity observed in **Figure 5.2 (A)** may be attributed to the interaction between the MA-CdSe/ZnS QD probe and the antibodies/proteins. The results showed that interaction with BSA decreased the signal the most, followed by Gb, whilst IgY decreased the least, while maintaining the same emission wavelength. These results indicated that BSA interacted more with MA-CdSe/ZnS QDs than Gb and IgY. The type of interaction observed in **Figure 5.2 (A)** appears to be non-specific because even non-specific antibodies and protein BSA also showed some interactions.

Similar results were observed when 0.2 mg/ml of CdSe/ZnS QDs without bound MA were used with the same concentration of the antibodies (0.025 mg/mL), as shown in **Figure 5.2 (B).** These results clearly showed that specific antibodies (Gb), non-specific antibodies (IgY) and protein (BSA) interacted with CdSe/ZnS QDs. More interactions were observed in IgY and

BSA. Non-specific binding towards all the test molecules were observed. It might be the cysteine coated on the surface of the QDs that is responsible for this non-specific interaction.

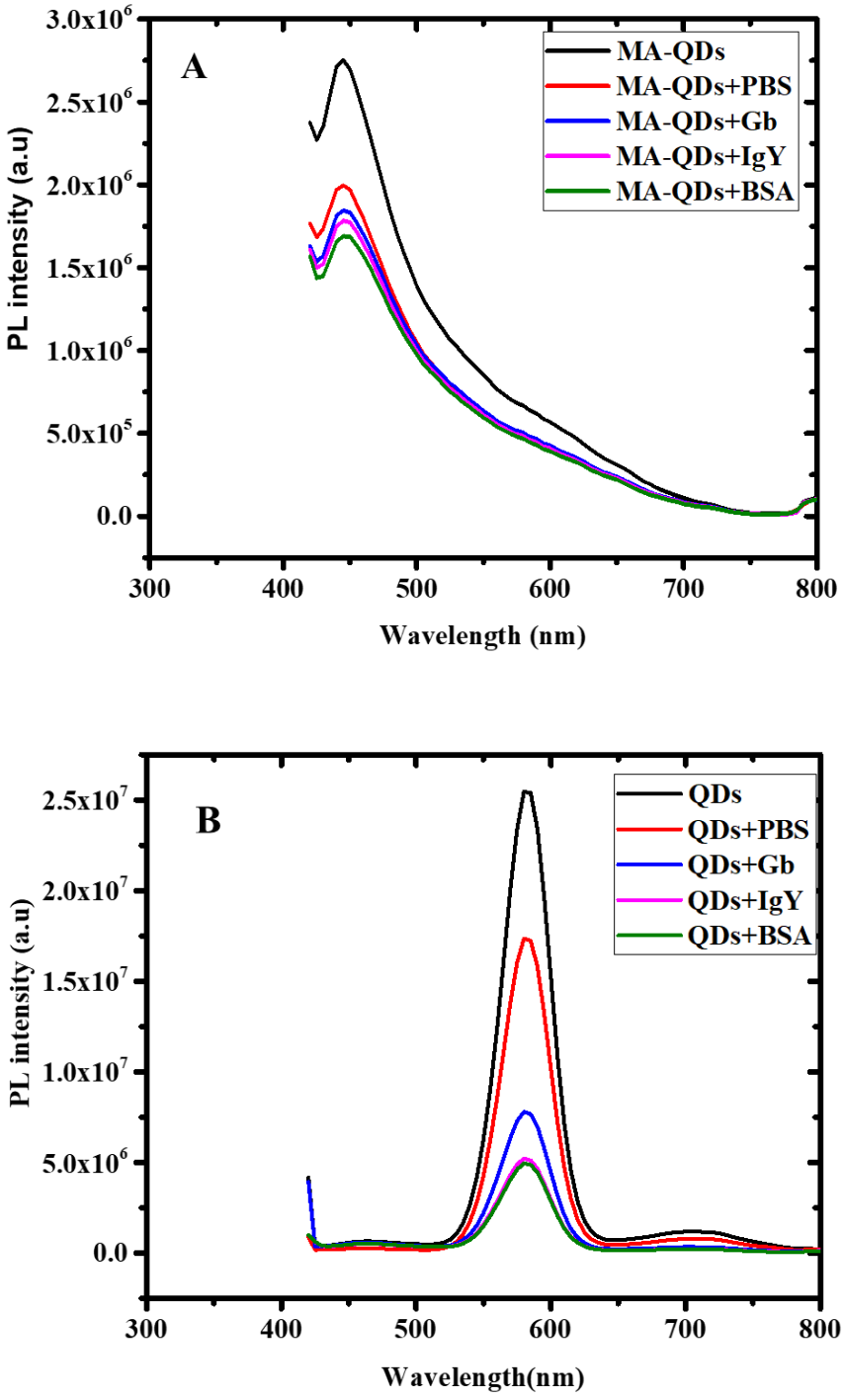

Figure 5.2: Fluorescence detection of the binding of specific (Gb) and nonspecific (IgY) antibodies and protein BSA at 0.025 mg/mL with 0.2 mg/mL of MA-CdSe/ZnS QDs probe (A) and 0.2 mg/mL of CdSe/ZnS QDs (B) suspended in phosphate buffered saline (PBS).

5.4.3 Membrane lateral flow binding of MA-CdSe/ZnS QDs, 4MA-CdSe/ZnS QDs and MA-GQDs to anti-MA antibodies (Gallibodies, Gb)

The fluorescence method revealed that the interaction between MA-CdSe/ZnS QDs and anti-MA antibodies was non-specific. This may be due to the small amount of MAs coupled to the surface of the QDs and the nature of the QDs (cadmium based) which are semiconductors. In this section, therefore, two new coupled fluorophores (fluorescence probes) are presented, namely 4MA-CdSe/ZnS QDs and MA-GQDs. In the synthesis of these probes, a four-fold amount of MA (4 mg) was used in an attempt to increase the loading, hence the four in front of MA-CdSe/ZnS QDs to differentiate it from the one used for the ELISA test in Section 5.3.1 and the fluorescence method in Section 5.3.2, where 1 mg of MA was used. The details about the synthesis of these probes are presented in Chapters three and four respectively. In this section, a membrane lateral flow test was explored to show the interaction between the new fluorescence probes (4MA-CdSe/ZnS QDs and MA-GQDs) and anti-MA antibodies (gallibodies). The previously tested fluorescence probe (MA-CdSe/ZnS QDs) was also used for comparison, while GQDs (from Chapter four) were used as negative control. The fluorescence probes were loaded onto lateral flow nitrocellulose membranes and eluted with an aqueous membrane blocking solution. The gallibodies were pre-loaded and immobilized halfway up the nitrocellulose membranes.

The flow of the MAs linked to quantum dots and the detection of their binding to anti-MA gallibodies on nitrocellulose membranes is demonstrated in **Figure 5.3 (A).** The results showed that CdSe/ZnS QDs and MA-CdSe/ZnS QDs were able to visually flow and showed clear interaction with gallibodies as indicated by the green box. GQDs and MA-GQDs also visually flowed and showed faint interaction with the gallibodies as indicated by the red box in **Figure 5.3 (A)**, with the interaction of GQDs in the absence of MA appearing to be visibly lower.

Although there were some interactions with all the fluorophores, this type of interaction appears to be non-specific as CdSe/ZnS QDs and GQDs which did not have MA as an antigen for the gallibodies also showed similar interactions.

Since the MA-GQDs appeared to have a stronger interaction than the GQDs alone, it was important to accurately quantify the fluorescence at the test line. **Figure 5.3 (B)** shows the fluorescence properties of scanned nitrocellulose membrane strips onto which CdSe/ZnS QDs, MA-CdSe/ZnS QDs, 4MA-CdSe/ZnS QDs, CdSe/ZnS QDs + Gb, MA-CdSe/ZnS QDs + Gb, and 4MA-CdSe/ZnS QDs + Gb had been spotted, which were studied using photoluminescence (PL) spectroscopy with excitation at 390 nm. The fluorescence results showed that there was a significant difference between the fluorescence emission spectrum of CdSe/ZnS QDs (maximum wavelength at 572 nm) and CdSe/ZnS QDs + Gb (maximum wavelength at 450 nm). This difference in emission spectrum confirmed that there was an interaction between CdSe/ZnS QDs and Gb which changed the PL properties of the CdSe/ZnS QDs + Gb. The fluorescence results also showed that the intensity of the emission spectra of MA-CdSe/ZnS QDs and 4MA-CdSe/ZnS QDs were somewhat higher than the intensity of MA-QDs + Gb and 4MA-QDs + Gb. This was another indication that MA-QDs and 4MA-QDs interacted with Gb. A plain nitrocellulose membrane strip was used as a blank.

Figure 5.3 (c) shows the fluorescence properties of scanned nitrocellulose membrane strips onto which GQDs, MA-GQDs, GQDs + Gb and MA-GQDs + Gb had been spotted, which were studied using PL spectroscopy with 360 nm excitation. A plain nitrocellulose membrane strip was used as a blank. It was observed that all the fluorophores had the same emission wavelength (330 nm) but the intensity of the GQDs + Gb and MA-GQDs + Gb were higher than GQDs and MA-GQDs. This change in intensity indicates that Gb interacted with GQDs and MA-GQDs and changed the PL properties of the GQDs + Gb and MA-GQDs + Gb.

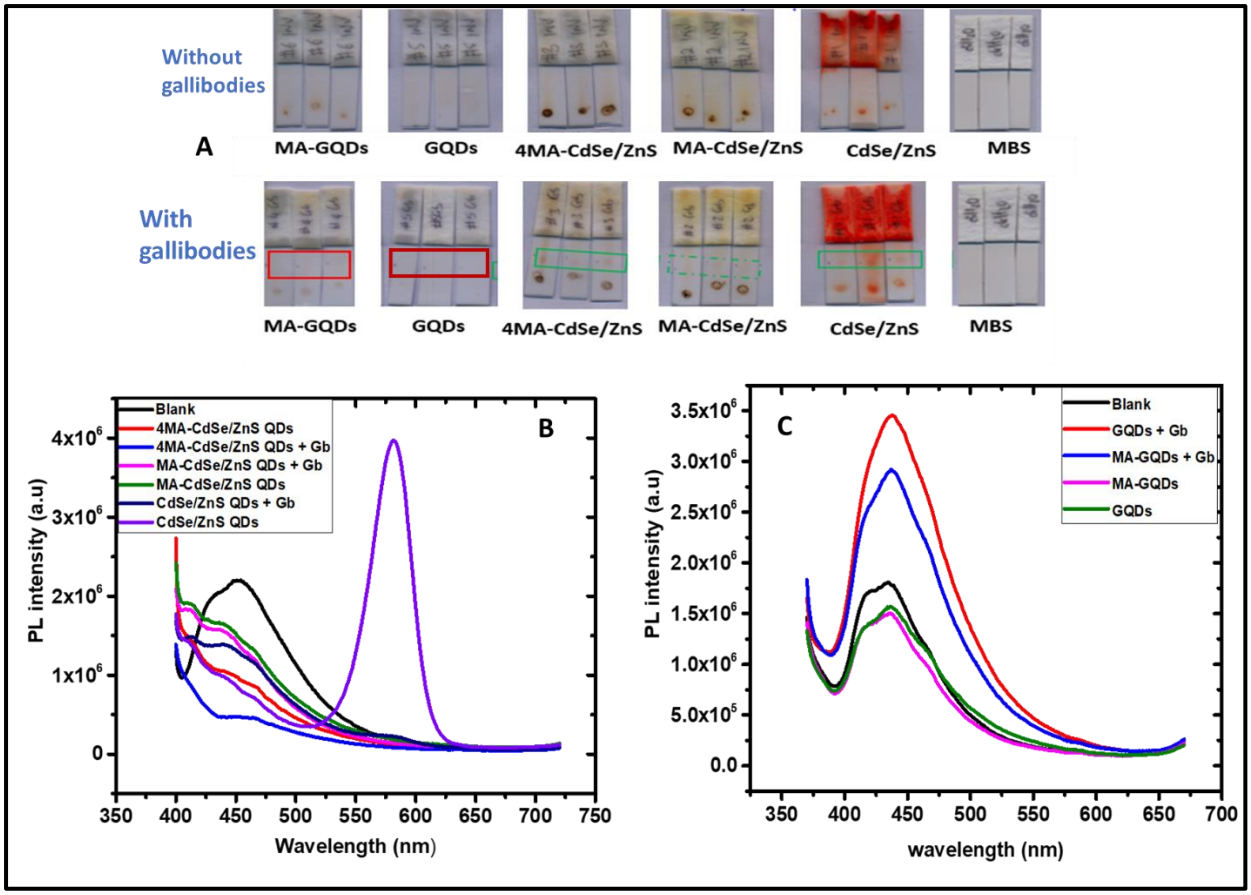

Figure 5.3: (A) Images of the scanned nitrocellulose membrane strips without and with gallibodies. Green boxes show the suspected interaction between gallibodies and CdSe/ZnS QDs, MA-CdSe/ZnS QDs, 4MA-CdSe/ZnS QDs, CdSe/ZnS QDs + Gb, MA-CdSe/ZnS QDs + Gb, and 4MA-CdSe/ZnS QDs + Gb where the red box shows suspected interaction between gallibodies and GQDs, GQDs + Gb, MA-GQDs and MA-GQDs + Gb. (B) Fluorescence spectra of scanned nitrocellulose membrane strips of CdSe/ZnS QDs, MA-CdSe/ZnS QDs, 4MA-CdSe/ZnS QDs, CdSe/ZnS QDs + Gb, MA-CdSe/ZnS QDs + Gb, and 4MA-CdSe/ZnS QDs + Gb, when exciting at 390 nm. (c) Fluorescence spectra of GQDs, GQDs + Gb, MA-GQDs and MA-GQDs + Gb, when exciting at 360 nm.

5.5 Conclusion

All the synthesized fluorophores appeared to interact with the anti-MA antibodies (gallibodies), even those without the antigen mycolic acid. The type of interaction observed for all the fluorophores upon the introduction of gallibodies appeared to be non-specific and thus cannot be used in this manner as a sensor for the detection of anti-mycolic acid antibodies (gallibodies) for the detection of active TB.

From the results obtained, it appears that the non-specific binding of the MA-QDs to the anti-MA gallibodies can be attributed to non-specific interaction with the QD component. Compared to the CdSe/ZnS QDs, the GQDs seem to have a lower binding to the gallibodies. It has been proposed that the antigenicity of MAs is not due to the interaction between a single MA molecule and the antibody, but rather due to an aggregate of MA molecules forming a surface [3]. The high aqueous solubility of the MA-QDs suggests that the loading of MA on each QD was insufficient to form the required antigenic surface. In the case of MA bonded to Fluorescein [1], the antigenicity of MA was maintained presumably because aggregation to form the antigenic surface was still possible. In the case of the MA-QDs, the small size (< 10 nm) of the fluorophores, measured by transmission electron microscope (TEM) and described in Chapters three and four, indicates that there is no formation of much needed MA aggregates that can help maintain their antigenicity.

5.6 References

[1] M. Beukes, Y. Lemmer, M. Deysel, J.a.R. Al Dulayymi, M.S. Baird, G. Koza, M.M. Iglesias, R.R. Rowles, C. Theunissen, J. Grooten, G. Toschi, V.V. Roberts, L. Pilcher, S. Van Wyngaardt, N. Mathebula, M. Balogun, A.C. Stoltz, J.A. Verschoor, Structure–function relationships of the antigenicity of mycolic acids in tuberculosis patients, *Chemistry and Physics of Lipids* 163, (2010), 800-808.

[2] H. Ranchod, F. Ndlandla, Y. Lemmer, M. Beukes, J. Niebuhr, J. Al-Dulayymi, S. Wemmer, J. Fehrsen, M. Baird, J. Verschoor, The antigenicity and cholesteroid nature of mycolic acids determined by recombinant chicken antibodies, *PloS One* 13, (2018), e0200298.

[3] Y. Benadie, M. Deysel, D.G.R. Siko, V.V. Roberts, S. Van Wyngaardt, S.T. Thanyani, G. Sekanka, A.M. Ten Bokum, L.A. Collett, J. Grooten, Cholesteroid nature of free mycolic acids from M. tuberculosis, *Chemistry and Physics of Lipids* 152, (2008), 95-103.

CHAPTER SIX: Overall conclusion and future work

This chapter provides the overall conclusion for the work done and gives suggestions for future work.

6.1 Overall conclusion

Water-soluble core/shell CdSe/ZnS QDs capped with L-cysteine and graphene QDs (GQDs) have been successfully synthesized. ZnS was used as shell material to provide efficient confinement of electrons inside the nanocrystals and does not easily form defects. ZnS also improves physical and chemical properties and allows for easy biofunctionalization. It provides stability to the CdSe (core) by protecting it from the surrounding environment and can prevent, for example, oxidation. L-cysteine was used to cap the CdSe/ZnS QDs and served as a stabilizer and increased their biocompatibility.

L-cys-CdSe/ZnS QDs and GQDs were then coupled to MAs in dry chloroform to form water-soluble fluorescent TB probes, namely MA-CdSe/ZnS QDs, 4MA-CdSe/ZnS QDs, and MA-GQDs respectively. Before coupling of QDs to MAs was achieved, stearic acids and glycine were chosen and used as possible models for MAs and QDs, respectively. Stearic acid was first converted to stearic acid chloride using oxalyl chloride in dry chloroform or dichloromethane and then reacted with glycine in the presence of triethylamine and pyridine as a catalyst to form stearoyl-glycine amide. The structure of the coupled stearoyl-glycine amide was confirmed using ^{1}H and ^{13}C NMR and FT-IR analysis. In MA-CdSe/ZnS QDs, 1 mg of MA was used with 0.06 g of L-cys-CdSe/ZnS QDs while 4 mg of MA was used in the synthesis of 4MA-CdSe/ZnS QDs, and MA-GQDs with the same amount of L-cys-CdSe/ZnS QDs (0.06 g) and 1.50 mg of GQDs in an attempt to increase the loading of MA. The synthesized L-cys-CdSe/ZnS QDs and GQDs plus the coupled MA-CdSe/ZnS QDs, 4MA-CdSe/ZnS QDs, MA-GQDs were characterized by absorption and fluorescence measurements, TEM analysis, FT-IR, and XRD spectroscopy. The Enzyme-linked Immunosorbent Assay (ELISA) test, fluorescence method, and membrane lateral flow method were used to investigate the binding interaction between the fluorescent TB probes and the anti-MA antibodies (gallibodies) in solution.

The absorption results indicate that L-cys-CdSe/ZnS QDs, GQDs, MA-CdSe/ZnS QDs, 4MA-CdSe/ZnS QDs, and MA-GQDs all showed broad absorption bands ranging from 200 to 620 nm which enables variation of excitation wavelength used in fluorescence sensing applications. Fluorescence results show that the L-cys-CdSe/ZnS QDs had a narrow emission spectrum with a full width at half maximum (FWHM) of 40 nm at 590 nm and a quantum yield of 89.9 % when exciting at 410 nm, while MA-CdSe/ZnS QDs and 4MA-CdSe/ZnS QDs had a broader emission peak which was blue-shifted to 474 nm (FWHM=94 nm) and 454 nm (FWHM=81 nm) respectively, with a decrease in PL quantum yield.

Fluorescence results for GQDs showed a narrow emission spectrum (FWHM=57.67 nm) with a maximum emission wavelength at 440 nm and a PL quantum yield of 69.0 % when exciting at 360 nm, while MA-GQDs had a somewhat broader spectrum ((FWHM=97.17 nm), PL quantum yield of 21.6 % with a maximum emission wavelength at 470 nm. The changes in emission spectra and decrease in quantum yields confirmed the formation of the new materials with fluorescence properties similar to the QDs.

The additional peaks between 2450 cm^{-1} and 2790 cm^{-1} in MA-CdSe/ZnS QDs and MA-GQDs FT-IR spectra can be ascribed to -N-C=O modes. The presence of these peaks in MA-CdSe/ZnS QDs and MA-GQDs indicates the appearance of the amide bonds, which confirms the covalent coupling of L-cys-CdSe/ZnS QDs and GQDs to MAs. TEM analysis results showed the average estimated size particle distribution of L-cys-CdSe/ZnS QDs to be 1.0 ± 0.2 nm, 3.1 ± 0.8 nm for MA-CdSe/ZnS QDs, 3.3 ± 0.2 nm for 4MA-CdSe/ZnS QDs, 0.8 ± 0.3 nm for GQDs, and 1.6 ± 0.8 nm for MA-GQDs. TEM analysis also revealed that L-cys-CdSe/ZnS QDs and GQDs dispersed well in water while coupled materials (MA-CdSe/ZnS QDs, 4MA-CdSe/ZnS QDs, and MA-GQDs) showed some particle aggregation. These TEM results implied that the presence of MAs in the coupled materials caused particle aggregation, which is not the case in uncoupled materials (L-cys-CdSe/ZnS QDs and GQDs).

The powder XRD results showed a shift and an increase in the number of peaks for MA-CdSe/ZnS QDs, 4MA-CdSe/ZnS QDs, and MA-GQDs relative to the CdSe/ZnS QDs and GQDs. This suggests that the coupling of MAs to L-cys-CdSe/ZnS QDs and GQDs changed the crystal structure of the coupled material. Sharp peak positions observed in MA-CdSe/ZnS QDs, 4MA-CdSe/ZnS QDs, and MA-GQDs confirm that changing the amounts of MAs does not negatively affect the crystallinity of the material. Membrane lateral-flow experiments confirmed visually the flow of L-cys-CdSe/ZnS QDs, GQDs, MA-CdSe/ZnS QDs, 4MA-CdSe/ZnS QDs, and MA-GQDs through the nitrocellulose membrane with water and membrane blocking solution as eluents. Water and membrane blocking solutions were the preferred eluents to move the fluorophores through the nitrocellulose membrane due to the high affinity for moving through the membrane. They also keep the sample components in solution whilst moving, control the flow speed, and are easily disposed of after use.

Results from all the three different methods (ELISA test, fluorescence, and membrane lateral flow) used to detect the interaction between fluorescent TB probes and anti-mycolic acid antibodies (gallibodies) showed that all the synthesized fluorophores (L-cys-CdSe/ZnS QDs, GQDs, MA-CdSe/ZnS QDs, 4MA-CdSe/ZnS QDs, and MA-GQDs) appeared to interact with the gallibodies, even those without the mycolic acid antigen. The type of interaction observed for all the fluorophores upon the introduction of gallibodies appeared to be non-specific and thus cannot be used directly as a sensor for the detection of anti-mycolic acid antibodies for the detection of active TB. In the ELISA test, the results showed that the MA-CdSe/ZnS QDs probe, StA-CdSe/ZnS QDs, StAs (used as negative controls), and pure MAs (as a positive control) dissolved in DCM, all produced absorbance signals and did not match with the results for pure MAs in hexane which was used as a reference. The absorbance signals observed in the ELISA test in DCM for all the fluorophores appeared to be caused by the non-specific interaction with the anti-mycolic acid antibodies. Fluorescence results showed that the

emission intensity decreased upon the addition of specific Gb, nonspecific IgY, and protein BSA. The decrease in emission intensity was more in BSA, followed by Gb, and IgY was the least. This decrease in intensity observed may be attributed to the interaction between the MA-CdSe/ZnS QD probe and the antibodies/proteins. Similar results were observed when L-cys-CdSe/ZnS QDs without bound MA were used with the same concentration of the antibodies/proteins. The results clearly showed that specific antibodies (Gb), non-specific antibodies (IgY) and protein (BSA) interacted with L-cys-CdSe/ZnS QDs.

Membrane lateral flow results showed that L-cys-CdSe/ZnS QDs and MA-CdSe/ZnS QDs were able to visually flow and showed clear interaction with gallibodies. GQDs and MA-GQDs also visually flowed and show faint interaction with the gallibodies, with the interaction of GQDs in the absence of MAs appearing to be visibly lower. Since the MA-GQDs appeared to have a stronger interaction than the GQDs alone, it was important to accurately quantify the fluorescence properties at the test line of the nitrocellulose membrane strips using photoluminescence spectroscopy. The fluorescence results showed that there was a significant difference between the fluorescence emission spectrum of L-cys-CdSe/ZnS QDs and L-cys-CdSe/ZnS QDs + Gb. The intensity of the emission spectra of MA-CdSe/ZnS QDs and 4MA-CdSe/ZnS QDs were somewhat higher than the intensity of MA- CdSe/ZnS QDs + Gb, and 4MA- CdSe/ZnS QDs + Gb. It was also observed that the GQDs, GQDs + Gb, MA-GQDs and MA-GQDs + Gb had the same emission wavelength (330 nm) but the intensity of the GQDs + Gb and MA-GQDs + Gb were higher than GQDs and MA-GQDs. These differences in emission spectrum and intensity confirmed that there were some interactions between the fluorophores and Gb which changed the PL properties of the fluorophores. Although there were some interactions with all the fluorophores, this type of interaction appeared to be non-specific as L-cys-CdSe/ZnS QDs and GQDs which did not have MA as an antigen for the gallibodies also showed similar interactions.

This non-specific binding of the MA-QDs to the anti-MA gallibodies may be attributed to the non-specific interactions with the QD component. It has been proposed that the antigenicity of MAs is not due to the interaction between a single MA molecule and the antibody, but rather due to an aggregate of MA molecules forming a surface [1]. The high aqueous solubility of the MA-QDs suggests that the loading of MA on each QD was insufficient to form the required antigenic surface. The small size (< 10 nm) of the fluorophores also indicates that there was no formation of much needed MA aggregates that can help maintain their antigenicity, hence no specific binding occurred.

Although MA is expensive, if the proposed procedures (ELISA, lateral flow, and fluorescence) are successful, they will allow TB antibodies to be detected quickly at the point of care, allowing TB patients to begin treatment sooner than with X-rays and sputum analysis, which are costly, unavailable in most health facilities, and take time to obtain results [2].

6.2 Future work

Considering the small amounts of MAs (1 mg and 4 mg) used during the covalent coupling to quantum dots (L-cys-CdSe/ZnS QDs and GQDs), there is a call to increase the quantity of MAs to try and improve the antigenic properties of the coupled materials with regards to anti-MA antibodies interaction. MA-GQDs were more soluble than MA-CdSe/ZnS QDs, but their antigenicity properties were not investigated using the ELISA test. Therefore, it is proposed that the ELISA test for MA-GQDs should be investigated and the antigenic properties towards anti-MA antibodies be determined. Quantification of the amount and concentration of MAs loaded onto QDs was the biggest challenge encountered during this work. Therefore, there is a need to develop techniques that will be able to quantify the amount and concentration of MAs loaded onto QDs.

Using molecular beacons (MBs) with M.tb DNA coupled to MA-QDs as a biosensor to detect anti-MA antibodies in solution is another method that could be investigated to enhance the performance of the biosensor. Molecular beacons are stem-looped stranded hairpin-shaped oligonucleotides with a fluorophore at one end and a quencher at the other terminus [3]. The loop hairpin part of the MB is sensitive and complementary to the target analyte, while the stem portion is a physicochemical transducer made up of two self-complementary regions consisting of five to six nucleotides at the opposite ends of the strands.

MB with M.tb DNA containing amine groups can be covalently attached to MA-QDs via a free carboxylic group to increase the antigenic properties of the probe as a result of the combination of M.tb DNA and MA from the MA-QDs [4]. Upon the hybridization of the MB with the target analyte (anti-MA antibodies), the MB changes its conformation by opening its hairpin structure causing the distance between the fluorophore and the quencher to be far apart for energy transfer to occur, resulting in the restoration of the fluorescence and no quenching. In the absence of the target analyte (anti-MA antibodies), the two complementary regions of the stem hybridize together, allowing the formation of the hairpin structure, causing the fluorophore and the quencher to be close to each other. Considering the proximity of the stem structure, the quencher deactivates the fluorophore excited state, resulting in quenching of photoluminescence. MB probes give a signal that allows the detection of the target analyte in a homogeneous solution immediately without any separation of the probe-analyte hybrid and the unbound probe. In addition, MB probes are highly sensitive, selective and specific [5].

6.3 References

[1] Y. Benadie, M. Deysel, D.G.R. Siko, V.V. Roberts, S. Van Wyngaardt, S.T. Thanyani, G. Sekanka, A.M. Ten Bokum, L.A. Collett, J. Grooten, Cholesteroid nature of free mycolic acids from *M. tuberculosis*, Chemistry and Physics of Lipids 152, (2008), 95-103.

[2] F.A. Khan, A. Majidulla, G. Tavaziva, A. Nazish, S.K. Abidi, A. Benedetti, D. Menzies, J.C. Johnston, A.J. Khan, S. Saeed, Chest x-ray analysis with deep learning-based software as a triage test for pulmonary tuberculosis: a prospective study of diagnostic accuracy for culture-confirmed disease, The Lancet Digital Health 2, (2020), e573-e581

[3] S. Tyagi, F.R. Kramer, Molecular beacons in diagnostics, F1000 Medicine Reports 4, (2012), 10.

[4] P.-J.J. Huang, J. Liu, Molecular beacon lighting up on graphene oxide, Analytical Chemistry 84, (2012), 4192-4198.

[5] K. Huang, A.A. Martí, Recent trends in molecular beacon design and applications, Analytical and Bioanalytical Chemistry 402, (2012), 3091-3102.